5-1-2013

Synaptic Zn2+ release during spreading depolarizations : implications for ischemic brain injury

Russell Carter

Russell E. Carter
Candidate

Neurosciences
Department

This dissertation is approved, and it is acceptable in quality and form for publication:

Approved by the Dissertation Committee:

C. William Shuttleworth, Chairperson

Lee Anna Cunningham

C. Fernando Valenzuela

Surojit Paul

Synaptic Zn^{2+} Release during Spreading Depolarizations: Implications for Ischemic Brain Injury

By

Russell Eugene Carter

B.A., Chemistry/Neuroscience, Concordia College Moorhead, MN 2008

Ph.D., Biomedical Sciences, University of New Mexico, 2013

DISSERTATION

Submitted in Partial Fulfillment of the
Requirements for the Degree of

Doctor of Philosophy
Biomedical Sciences

The University of New Mexico
Albuquerque, New Mexico

April 2013

Synaptic Zn^{2+} Release during Spreading Depolarizations:

Implications for Ischemic Brain Injury

By

Russell Eugene Carter

B.A., Chemistry/Neuroscience, Concordia College Moorhead, MN 2008

Ph.D., Biomedical Sciences, University of New Mexico, 2013

Abstract

The expansion of the ischemic core into surrounding penumbral tissue has prompted researchers to finds ways to limit this progression in hopes of providing better outcomes for patients suffering from stroke. Current therapeutic strategies are limited, and new therapies that can be delivered at late time-points are needed. Zn^{2+} has been well documented to contribute to ischemic injury progression, and chelation of Zn^{2+} significantly improves neuronal survival, even when administered hours after the initial insult. However, determining the source of this Zn^{2+} and the toxic mechanisms involved in ischemia remain unclear.

Over the past 10 years, clinical recordings have provided strong evidence that the occurrence of spreading depolarizations (SD) significantly contributes to the progression of numerous forms of brain injuries, including ischemic stroke. As these events occur

repetitively for hours to days following the initial ischemic event, they pose as a prime candidate for the development of new therapeutic targets. These depolarizing events have the potential capability to release large amounts of synaptic Zn^{2+} into the extracellular space.

The dissertation work presented here addresses whether synaptic Zn^{2+} release occurs during SD and if this source of Zn^{2+} is neurotoxic in the post-ischemic period. SD generated by either localized K^+ applications or an *in vitro* model of ischemia (oxygen/glucose deprivation, OGD), resulted in large releases of synaptic Zn^{2+} in both hippocampal and neocortical tissues *in vitro* and led to postsynaptic accumulation. Zn^{2+} chelation was sufficient to delay the onset of OGD-SD, providing a mechanism for the beneficial effects of Zn^{2+} chelation seen previously. Additionally, elevating intracellular Zn^{2+} levels worsened the recovery after SD, likely through impaired metabolic function. Finally, synaptic Zn^{2+} release was detected following SD *in vivo* and this source of Zn^{2+} significantly contributed to ischemic injury.

These results suggest that targeting synaptic Zn^{2+} stores or release during SD events could be a novel approach in treating ischemic brain injury. As SD events continue to occur days following the initial ischemic event, this suggests the ability to target these events at late time-points where current therapeutics are limited.

Table of Contents

List of Figures

Chapter 1: INTRODUCTION

1.1 The Need for New Therapeutic Targets in Treating Ischemic Strokes

Ischemic stroke is the third leading cause of death in the United States (Lloyd-Jones et al., 2009). In addition to high mortality, the aftermath of stroke brings lifelong suffering, functional impairment and substantial economic burdens to stroke survivors and their families (Lloyd-Jones et al., 2009). Ischemic strokes are caused by a sudden loss of blood flow through cerebral vessels, and are typically caused by thrombosis. The disruption in cerebral blood flow can create regions where the tissue can no longer sustain ionic gradients due to lack of continuous supply of metabolic substrates. Such hypoperfused tissue rapidly undergoes sustained depolarization which can lead to cell death and the formation of a so-called "ischemic core". Surrounding tissue can still survive based on collateral blood supply from nearby vessels, however due to the loss of the primary source of metabolic substrates this tissue can lose synaptic activity as cells use remaining available energy stores to simply maintain ionic gradients required for survival. Regions where brain tissue is functionally silent but where no observed damage is present was originally termed the "ischemic penumbra" by Astrup (Astrup et al., 1977). It was originally thought that over the course of hours to days following the initial ischemic event, the ischemic core simply expanded progressively into the surrounding penumbral tissue, thereby increasing the total volume of non-recoverable tissue (Dirnagl et al., 1999). More recently, it has emerged that the penumbra and ischemic core can be highly dynamic (Lo, 2008, del Zoppo et al., 2011), and even in some cases an ischemic stroke can involve multiple mini-cores, surrounded by corresponding mini-penumbras,

which form and coalesce to create the overall infarct (Olivot et al., 2009). Much work in the last two decades has been concentrated on approaches to reduce or prevent the expansion of ischemic injury, however the current clinical therapeutic strategies for stroke remain very limited.

Currently, the only FDA approved treatment for ischemic stroke is the administration of recombinant tissue plasminogen activator (t-PA). The administration of t-PA can facilitate in the breakdown of the thrombotic clot, by converting plasminogen into plasmin, which in turn promotes the digestion of the thrombi to restore proper blood flow to the hypoperfused tissue. This can be a very effective treatment for some ischemic stroke patients, however, extended treatment with t-PA can enhance the breakdown of the blood-brain barrier (BBB) and increase the risk of hemorrhage (Wang et al., 2004). This increased risk has limited the utilization of t-PA to within a short time frame, usually 3-4.5hrs, following the initial ischemic insult (NINDS Study Group, 1997). Many stroke victims cannot be treated with t-PA within this time period due to, in some cases, lack of knowledge of when the initial stroke occurred, but often the length of time from the initial stroke to the time the patient can receive medical care. While t-PA administration has only been shown to be beneficial soon after stroke, many ischemic brain injuries continue to develop in the hours and days following the onset (Baird et al., 1997, Karonen et al., 1999, Parsons et al., 2002). New therapeutic strategies that are effective at later time points following the onset of ischemic insults are likely to have substantial benefit and it is a significant problem that no such agents are approved for clinical use. The work presented here addresses two potential mechanisms that could contribute together to the enlargement of ischemic injury, and could be a target for interventions at

late time points after the initial stroke insult: 1) Zn^{2+} accumulation; and 2) the phenomenon of spreading depolarization.

1.2 Zn^{2+} in the Central Nervous System

In the late 1950s, while studying several curious cases of anemia in Iran potentially linked with iron deficiency, Dr. Ananda Prasad made a profound discovery. The patients were severely malnourished, and consumed mostly bread and small amounts of clay. No animal protein was consumed. The cases presented with classical symptoms of iron deficiency, however, there was no apparent loss of blood in these patients. In addition, there was severe growth retardation and hypogonadism, which were not apparent in animal models of iron deficiency. While investigating further, Dr. Prasad speculated that zinc (Zn^{2+}) deficiency could account for the symptoms presented that iron deficiency could not. This paper was published in the early 1960s and speculated that dietary Zn^{2+} deficiency was very prevalent in the Middle East (Prasad et al., 1961). Shortly after this work, numerous other cases were reported to be linked with Zn^{2+} deficiency throughout the world, all rapidly responding positively with oral Zn^{2+} supplements (Sandstead et al., 1967). From these initial observations demonstrating the importance of Zn^{2+} for human biology, the study of Zn^{2+} has expanded dramatically, and encompasses nearly all aspects of biological function. This rapid expansion has been summarized by Dr. Prasad in a recent review (Prasad, 2012).

Zn^{2+} is now known to be critically important for the function of a vast array of cellular processes, with over 300 proteins (e.g. Zn-fingers) and nearly 2000 transcription factors requiring Zn^{2+} as a co-factor for proper function (Prasad, 2012). While the

importance for Zn^{2+} in proper development and biological function was highlighted by the works of Dr. Prasad and colleagues, significant amounts of brain Zn^{2+} had actually been identified earlier, a serendipitous finding during investigations of Zn^{2+} release from insulin secreting cells of the pancreas (Maske, 1955). At that time, Maske's finding received little attention as Zn^{2+} was not, at the time, thought to be important for CNS functions. However as described below, subsequent studies confirmed Maske's finding, and studies of Zn^{2+} in CNS physiology and pathophysiology have since expanded greatly.

1.2.1 First Evidence of Synaptic Zn^{2+} Release

Several techniques were developed and utilized to visualize Zn^{2+} localization and these methods revealed a broad distribution of Zn^{2+} throughout the brain. One such technique arose with the development of electron microscopy. An enhanced silver-sulfide staining procedure was developed to visualize Zn^{2+} with ultra-structural resolution (Timm, 1958), and was used to detect Zn^{2+} localized in clear synaptic vesicles within the mossy fiber terminals of the hippocampus (Haug, 1967). This Zn^{2+} pool was described as "exchangeable Zn^{2+}", meaning that it was not bound tightly to binding proteins and was therefore available for interactions with the histochemical staining procedure. In addition, the fact that Zn^{2+} staining was seen in synaptic vesicles but not in other subcellular compartments (such as mitochondria), suggested that there was a discrete pool of synaptic Zn^{2+} that is stained by this procedure. The presence of Zn^{2+} in synaptic vesicles also raised the possibility that Zn^{2+} may be released during synaptic vesicle fusion and participates in synaptic physiology.

It was later confirmed that Zn^{2+} can indeed be taken up into presynaptic terminals and subsequently released upon stimulation. The first evidence for Zn^{2+} release from presynaptic terminals was provided by two laboratories at nearly the same time (Assaf and Chung, 1984, Howell et al., 1984). One of these studies utilized hippocampal slices incubated with the radiolabeled Zn^{2+} tracer, $^{65}Zn^{2+}$. Radiolabeled Zn^{2+} was taken up into hippocampal slices and a subsequent brief (60s) electrical stimulation resulted in significant $^{65}Zn^{2+}$ release into the superfusate, indicating activity-dependent release (Howell et al., 1984). Concurrent work by Assaf and Chung reported increased levels of extracellular Zn^{2+}, detected by atomic absorption spectrophotometry, following high K^{+} (23.8mM) depolarization in slice or kainic acid injections *in vivo* to induce seizure-like activity (Assaf and Chung, 1984). It was estimated that total extracellular Zn^{2+} could reach levels as high as 300μM, however the concentration in the synapse could be even higher. These two seminal works were an important next step in suggesting that synaptic Zn^{2+} release may be important for physiological and pathophysiological activity.

1.2.2 Tools to Visualize Synaptic Zn^{2+}

Another useful technique for visualizing Zn^{2+} in the CNS arose with the development of specific fluorescent compounds that were able to detect the "exchangeable Zn^{2+}" described above. The first compound, the quinoline analogue 6-methoxy-8-*p*-toluene sulfonamide quinolone (TSQ) was found to have a distribution of Zn^{2+} labeling similar to Timm's staining throughout the CNS (Frederickson et al., 1987) (see Figure 1.1). However, this technique required the use of either fresh-frozen or fixed tissue sections and could not be used in live tissue. This concern was later addressed

when another fluorescent Zn^{2+} indicator, 2-methyl-8-p-toluenesulphonamido-6-quinolyloxy acetic acid (Zinquin), was identified that could detect Zn^{2+} in live human leukemia lymphocytes (Zalewski et al., 1993). These techniques, along with Timm's staining, greatly added to studying the localization of Zn^{2+}.

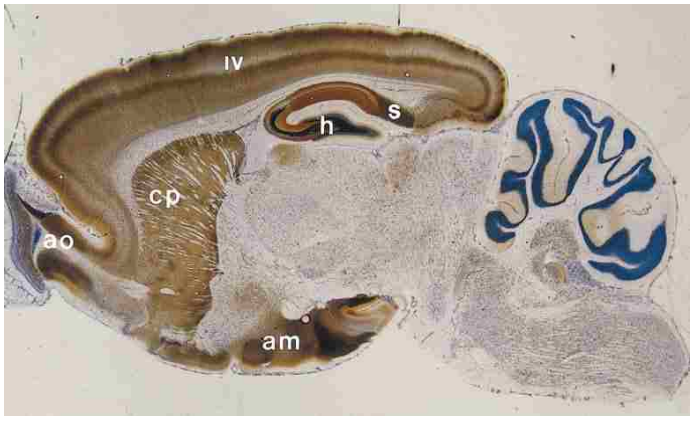

Figure 1.1: Sagittal section of rat brain after Timm's staining technique. The brown staining represents the presence of the "exchangeable pool" of Zn^{2+}. Counter staining was performed with Nissl to indicate cell bodies. Note the dense staining in the subiculum (s), hilus of the dentate gyrus (h), and in the mossy fibers of the hippocampus. Zn^{2+} staining was also prevalent in other brain regions. Accessory olfactory bulb (ao), caudatoputamen (cp), amygdala (am). (Adapted From: Frederickson et al., 2000)

Widely used Ca^{2+} indicators, such as Fura-2, were known to be responsive and more selective to Zn^{2+} than to Ca^{2+}, by almost 100 fold (Grynkiewicz et al., 1985), however until relatively recently, this feature was largely ignored, and signals from the Fura family of indicators were generally ascribed solely to Ca^{2+} dynamics. However, "Ca^{2+}" indicators (such as Fura-2 and MagFura-2) have been exploited to investigate changes in intracellular Zn^{2+} levels in cultured neurons, under conditions that limited intracellular Ca^{2+} changes (Cheng and Reynolds, 1998). In a later report it was suggested that all of the Ca^{2+} response following simulated ischemia and reperfusion in hippocampal slices was mediated by Zn^{2+} (Stork and Li, 2006), suggesting the possibility that the majority of previous reports on intracellular Ca^{2+} could have been contaminated by intracellular Zn^{2+}.

In response to the need for selective Zn^{2+} indicators, a high affinity Zn^{2+} indicator, FluoZin-3, was developed by Molecular Probes to investigate Zn^{2+} release from pancreatic β-cells in the early 2000s (Gee et al., 2002). This indicator has a much higher affinity for Zn^{2+} and signal to noise ratio than previous Zn^{2+} indicators, and was better restricted to the extracellular space. To test whether Zn^{2+} was contributing to the classical Ca^{2+} responses described above, FluoZin-3 was used alongside "Ca^{2+}" indicators to simultaneously detect changes in intracellular Zn^{2+} and Ca^{2+} (Devinney et al., 2005). These authors were able to clearly show and distinguish intracellular Zn^{2+} and Ca^{2+} responses in cortical cultures exposed to glutamate (Devinney et al., 2005), highlighting a role for both ions in excitotoxicity. This technique was further developed in our lab (Dietz et al., 2008, Vander Jagt et al., 2009a), and in a collaborator's lab (Medvedeva et al., 2009), for imaging neurons in brain slices by co-loading single cells with Fura-6F and FluoZin-3. These studies differentiated responses attributed to both Ca^{2+} and Zn^{2+}, and supported that early rises in intracellular Zn^{2+} can contribute subsequent, true, Ca^{2+} increases leading to cellular injury, and suggested that the claims above, made by (Stork and Li, 2006), may have been over exaggerated.

Dr. Noebels' laboratory utilized FluoZin-3 to directly investigate synaptic Zn^{2+} release at the mossy fiber synapse. In an elegant study, they showed that upon single action potential stimulation of the mossy fibers, extracellular fluorescence of FluoZin-3 increased, and these signals were completely lost in animals lacking synaptic Zn^{2+}, ZnT3 KO animals (see below) (Qian and Noebels, 2005). In addition, the degree of Zn^{2+} release, as assessed by extracellular FluoZin-3 fluorescence, positively correlated with the amplitude of the electrophysiological response of the postsynaptic potentials (Qian

and Noebels, 2005), suggesting that imaging synaptic Zn^{2+} release could be used as a surrogate for glutamate release during neuronal activity. In a follow-up study, the same group showed that synaptic Zn^{2+} release could be visualized in the CA1 region of the hippocampus from Schaffer collateral stimulation (Qian and Noebels, 2006). These studies provided strong real-time fluorescence evidence that Zn^{2+} is co-released with glutamate during synaptic stimulation.

However, some controversy arose over the use of high affinity indicators when interpreting the collected data. Alan Kay (Kay, 2003) suggested that Zn^{2+} is associated with proteins in the intraluminal space of synaptic vesicles, and upon fusion, Zn^{2+} is externalized to the extracellular space, but still bound to these proteins. In the presence of a high affinity Zn^{2+} indicator in the extracellular space, such as FluoZin-3, it was hypothesized that Zn^{2+} removed from these binding sites by the indicator gives an artificial signal of synaptic Zn^{2+} release (Kay, 2003). This hypothesis does not appear to fully explain the original works by Assaf and Chung, and Howell et al., in 1984 (Assaf and Chung, 1984, Howell et al., 1984) that did not use high affinity indicators, however this hypothesis does raise an important issue for potential artifacts while using high affinity indicators.

1.2.3 Synaptic Zn^{2+} Transporters

In the 1990s, a Zn^{2+} transporter was identified that facilitates Zn^{2+} accumulation into synaptic vesicles. The transporter, ZnT3, was cloned based on the homology to another recently characterized Zn^{2+} transporter, ZnT2 that was known to be involved in endosomal loading of Zn^{2+} (Palmiter et al., 1996a). The cloned ZnT3 gene had ~52%

base pair homology to ZnT2, and corresponded to a protein of approximately 40kDa (Palmiter et al., 1996b). While the structure of ZnT3 has not been confirmed, it and other ZnTs, are predicted to have six transmembrane domains based on homology to bacterial Zn^{2+} transporters (Gaither and Eide, 2001a). The expression of ZnT3 is restricted to the brain and testis, and within the brain, mRNA and protein staining for ZnT3 mirrored the staining profile for the detection of vesicular Zn^{2+} with Timm's stain (Palmiter et al., 1996b). In addition, a gene with ~86% homology to mouse ZnT3 was cloned from human cDNA, indicating the presence of a similar transporter in humans.

Three years after publication of the ZnT3 sequence, Palmiter's group developed a genetic knockout of ZnT3 (ZnT3 KO) (Cole et al., 1999). The generation of these KO animals, from electroporation of the target vector into embryonic stem cells, results in the absence of the ZnT3 gene throughout life. ZnT3 KO mice were found to have approximately 20% reduction in total Zn^{2+} in the neocortex and hippocampus, two regions normally highly enriched with Zn^{2+} (Cole et al., 1999). The deletion of the ZnT3 transporter corresponded with an elimination of Timm's staining and TSQ fluorescence, implying that ZnT3 regulates the uptake of Zn^{2+} into synaptic vesicles. This suggests that ~20% of the total brain Zn^{2+} is stored in synaptic vesicles. The presence of synaptic Zn^{2+} has been primarily observed in glutamatergic synapses, and a co-targeting mechanism of vesicular glutamate transporter 1 (Vglut1) and ZnT3 was identified in PC12 cells (Salazar et al., 2005), although there is also evidence for synaptic Zn^{2+} present at inhibitory synapses within the spinal cord (Danscher et al., 2001). In PC12 cells, it was found that the levels of both transporters reciprocally influenced the transport capabilities of the other. Interestingly, it was observed that glutamatergic signaling was not affected in

young ZnT3 KO animals as evidenced by the lack of impairment in spatial learning, memory, or sensorimotor functions (Cole et al., 2001). However, it was found that these animals had an increased susceptibility to seizures induced by kainic acid injections (Cole et al., 2001), suggesting that synaptic Zn^{2+} had a physiological role in limiting seizures. Additionally, synaptic Zn^{2+} is required for the induction of long term potentiation (LTP) at the mossy fiber/CA3 synapse (Li et al., 2001). More recent studies have revealed that ZnT3 KO mice have an age-dependent decline in cognitive function (Adlard et al., 2010), further suggesting a physiological role for synaptic Zn^{2+}.

1.2.4 Zinc and Neuronal Injury

Assuf and Chung originally speculated that Zn^{2+} might play a role in neuronal injury following seizures based on previous observations that the CA3 region of the hippocampus was strongly susceptible to seizure-induced injury and from the measurements of elevated Zn^{2+} in the CA3 area following seizure-like activity (Assaf and Chung, 1984). This idea gained some important, but circumstantial support when it was subsequently found that degeneration of CA3 neurons following strong mossy fiber electrical stimulation was accompanied by a loss of vesicular Zn^{2+} shown by a loss of Timm's staining (Sloviter, 1985). These initial studies prompted the idea that synaptic Zn^{2+} release may play a role in neuronal degeneration.

Zn^{2+} was clearly described to be toxic to both neurons and glial in culture by the work of Dr. Denis Choi and colleagues in the late 1980s. They reported that exposures of neuronal cultures to 300μM Zn^{2+} for 15min induced rapid morphological changes, and near-complete cell degeneration 24hrs later (Yokoyama et al., 1986, Choi et al., 1988).

These cellular responses (increased cell swelling and abnormal morphology) shared some similarities with the classical responses to excessive glutamate exposures and subsequent Ca^{2+} excitotoxicity. However, it was noteworthy that the degenerative process in response to Zn^{2+} occurred even in the absence of extracellular Na^{+} and Ca^{2+}, suggesting that Zn^{2+} itself can contribute directly to neuronal injury.

Zn^{2+} can directly affect mitochondrial function and cell survival through several mechanisms. Uptake of cytosolic Zn^{2+} into mitochondria was shown by using a fluorescent probe directed to accumulate into mitochondria, to detect Zn^{2+} signals in cultured cortical neurons (Sensi et al., 2000). It was concluded that mitochondrial Zn^{2+} accumulation, depended on mitochondrial membrane potential, likely via the same mechanisms as utilized by Ca^{2+} (Sensi et al., 2000). Additionally, the increases in fluorescence were abolished upon total Zn^{2+} chelation by a membrane permeable Zn^{2+} chelator, *N,N,N',N'*-tetrakis (2-pyridylmethyl) ethylenediamine (TPEN) (Sensi et al., 2000). Later it was shown that low nM Zn^{2+} (10nM) could induce swelling in isolated mitochondria, and this swelling was due to Zn^{2+} uptake into mitochondria, through the Ca^{2+} uniporter, and subsequent opening of the mitochondrial permeability transition pore (mPTP) (Jiang et al., 2001). Once the mPTP is opened, pro-apoptotic factors such as apoptosis-inducing factor (AIF) and cyctochrome C can be released, leading to apoptotic signaling cascades and cell death (Jiang et al., 2001). It was subsequently found that cytochrome C release from mitochondria was significantly reduced, by selectively chelating extracellular Zn^{2+} with CaEDTA following brief (10min) global ischemia in rats (Calderone et al., 2004), further suggesting that Zn^{2+} disrupts mitochondrial integrity and triggers neuronal injury pathways.

1.2.5 Metabolic Inhibition and Zn^{2+} Accumulation

Zn^{2+} has also been suggested to contribute to neuronal injury as a consequence of inhibition of cellular energy production through several mechanisms. Zn^{2+} can bind directly to and inhibit multiple enzymes in the production of ATP. Inhibition of glycolysis can occur from Zn^{2+} binding to phosphofructokinase (PFK) and glyceraldehyde-3-phosphate dehydrogenase (GAPDH). Inhibition contributing to neuronal injury likely occurs preferentially at GAPDH, as the reported IC_{50}s for Zn^{2+} of the purified enzymes are 1.5μM (Ikeda et al., 1980) and 300nM (Krotkiewska and Banas, 1992), respectively. GAPDH inhibition was supported when it was found that elevated levels of intracellular Zn^{2+} resulted in neuronal death by a buildup of metabolites upstream of GAPDH and depletion of metabolites downstream of GAPDH (Sheline et al., 2000). Importantly, neuronal survival after Zn^{2+} exposures was improved by pyruvate supplementation, which can bypass glycolysis and permit ATP production from oxidative phosphorylation within mitochondira, supporting the hypothesis that Zn^{2+} inhibits glycolysis and contributes to neuronal injury (Sheline et al., 2000). One surprising finding from that study was that intracellular Zn^{2+} accumulation also resulted in a depletion of NAD^+, which is normally reduced by GAPDH, leading the authors to suggest that an unidentified NAD^+-catabolizing enzyme was responsible for this decrease. Later, it was found that Zn^{2+} accumulation lead to activation of poly(ADP-ribose) polymerase-1 (PARP-1) (Kim and Koh, 2002). The activation of PARP-1, in response to DNA strand breaks, results in the activation of the DNA repair processes by the consumption of NAD^+ to create poly(ADP-ribose) moieties (D'Amours et al., 1999).

This process is usually very transient, however with prolonged activation, the decrease in NAD^+ levels can contribute to neuronal injury. Additionally, it was found that a family of NAD^+-catabolizing deacetylaces, the sirtuin family, was activated in response to toxic Zn^{2+} exposures in culture and lead to a decrease in NAD^+ levels (Cai et al., 2006), further implicating NAD^+ depletion, and subsequent energy depletion, as a mechanism of Zn^{2+} toxicity.

Within mitochondria, Zn^{2+} has been shown to disrupt both the tricarboxylic acid (TCA) cycle and the electron transport chain (ETC). Zn^{2+} can interfere with the functions of α-ketoglutarate dehydrogenase complex (KGDHC), with an estimated K_i of around 100nM, thereby inhibiting the TCA cycle (Brown et al., 2000). Zn^{2+} has also been shown to inhibit the mitochondrial ETC. While inhibition at multiple sites within the ETC has been hypothesized, complex III is proposed to be the major site of Zn^{2+} inhibition (Dineley et al., 2005). Under conditions of impaired mitochondrial respiration, cells can usually resort to anaerobic respiration and survive on glycolysis for some time. However, due to the potent effects of Zn^{2+} on both mitochondrial respiration and glycolysis, combined with the substantial energy needed to maintain ionic gradients, neurons and astrocytes are particularly vulnerable to prolonged Zn^{2+} elevations. While tremendous progress has identified several pathways with which Zn^{2+} contributes to neuronal injury, the mechanism(s) underlying Zn^{2+}-dependent neuronal injury in ischemic strokes remains uncertain.

1.2.6 Involvement of Zn^{2+} in Ischemia

It has been well established that cells normally maintain very low levels of free intracellular Zn^{2+} in order to mitigate the toxic effects of this ion (Sensi et al., 2011). However, disruptions in Zn^{2+} homeostasis can be seen in several pathophysiological states of the brain, such as ischemia. The first report linking excess endogenous Zn^{2+} accumulation and poor neuronal outcome following ischemia was shown in the mid-1990s (Koh et al., 1996), expanding on prior studies linking exogenous Zn^{2+} exposures to neuronal injury. Koh and co-workers showed that degenerating neurons in the hippocampus accumulated high levels of intracellular Zn^{2+}, assessed by TSQ staining, following a 10min period of global ischemia in rats. In cultured neurons, excess intracellular Zn^{2+} accumulation contributes to neuronal death, and by utilizing a membrane impermeable Zn^{2+} chelator (CaEDTA), the authors showed a decrease in the number of degenerating neurons in culture. By expanding their work *in vivo*, they showed that intracerebroventricular injections of CaEDTA, prior to the onset of global ischemia, significantly reduced the number of degenerating neurons in the hippocampus (Koh et al., 1996). This seminal work provided the first evidence that endogenous extracellular Zn^{2+} could significantly contribute to ischemic injury. Results from this work were later reproduced (Lee et al., 2002), and more surprisingly and clinically relevant, CaEDTA administration at time points long after the initial ischemic insult (up to 60hrs) prevented neurotoxic Zn^{2+} accumulation and subsequent neuronal injury (Calderone et al., 2004). These findings suggest the potential to target neurotoxic Zn^{2+} at later stages following ischemia when current therapeutic targets are not beneficial.

Some discrepancies exist regarding the time-course of extracellular/intracellular Zn^{2+} accumulation following stroke. Microdialysis studies have revealed a large transient increase in extracellular Zn^{2+} accumulation in the neocortex following transient occlusion of the middle cerebral artery in rats (Kitamura et al., 2006b). This Zn^{2+} accumulation peaked around 30min after the onset of ischemia, and returned to baseline concentrations within 1 hour, suggesting that extracellular Zn^{2+} accumulates rapidly but transiently following ischemia. It was reported that early administration of CaEDTA did not prevent early increases in intracellular Zn^{2+} accumulation, but did block late accumulations (Calderone et al., 2004), suggesting the possibility for a secondary phase of extracellular Zn^{2+} accumulation. It still remains unclear as to what source(s) contribute to the extracellular accumulation and subsequent intracellular accumulation of neurotoxic Zn^{2+}. Determining how and when Zn^{2+} accumulation occurs could help in the development of new strategies and time-courses to decrease ischemic neuronal injury.

1.2.7 Potential Sources and Measurements of Zn^{2+} Accumulation during Ischemia

In neurons, there are two major pools of intracellular Zn^{2+} (see Figure 1.2). The first is bound to a large population of intracellular metal binding proteins (metallothioneins, MT), including MTIII in neurons and astrocytes (Palmiter et al., 1992). While the previous work of Koh and colleagues described above reported a role for toxic effects of extracellular Zn^{2+} accumulation (Koh et al., 1996), evidence exists that intracellular release from MTIII can play a significant role under some conditions. Metallothioneins act as a buffer for intracellular Zn^{2+}, and other metals, to prevent the metals from reaching toxic levels. Under conditions similar to those generated by

ischemia, such as oxidative stress and intracellular pH changes, intracellular Zn^{2+} can be liberated from MTIII (Aizenman et al., 2000). This oxidative-induced release of Zn^{2+} prevents MTIII from sequestering Zn^{2+} until the redox state of the protein has been restored. As these oxidative conditions can persist during ischemia, it is possible that the Zn^{2+}-buffering potential of cells is severely compromised and toxic levels of Zn^{2+} can be achieved rapidly, thus contributing to neuronal degeneration. In agreement with this hypothesis, MTIII-KO mice have significantly larger infarct volumes compared to wild-type controls after transient ischemia followed by reperfusion (Koumura et al., 2009).

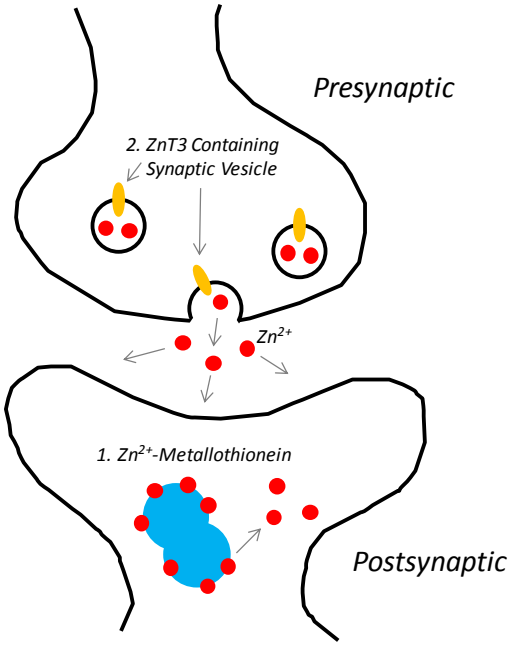

Figure 1.2: Schematic representation of the two major sources of intracellular Zn^{2+}. The first source is bound to intracellular metal binding proteins, metallothioneins (1.). A second source of Zn^{2+} is co-localized with glutamate in synaptic vesicles, via the actions of the Zn^{2+} transporter ZnT3 (2.).

Another potential source of neurotoxic Zn^{2+} may be from the second pool of Zn^{2+}, synaptic Zn^{2+} (see section 1.2.1). Interestingly, the location of the highest enrichment of synaptic Zn^{2+}, the hippocampus, was also the site highly susceptible to ischemia and Zn^{2+} mediated toxicity (Koh et al., 1996). While the levels of synaptic Zn^{2+} only account for approximately 20% of the total Zn^{2+} in the hippocampus and cortex (Cole et al., 1999), levels released into the extracellular space during neuronal activation are estimated to reach significant

levels (up to 300μM) as described above, and could provide toxic levels of Zn^{2+} accumulation.

Ischemia results in the slow depolarization of neurons due to the loss of energy substrates available to maintain ionic gradients across the plasma membrane. This depolarization may result in synaptic vesicle fusion and release and accumulation of synaptic Zn^{2+} in the extracellular space. Synaptic Zn^{2+} release has been suggested to translocate from presynaptic sites to postsynaptic neuronal cell bodies following electrical stimulation (Suh, 2009) and traumatic brain injury (Suh et al., 2006). This "translocation" hypothesis could explain the extracellular accumulation and subsequent intracellular accumulation in postsynaptic cells following ischemia. One adjunct hypothesis for the increased infarct volumes in MTIII KOs described above could be explained by the inability to sufficiently buffer synaptic Zn^{2+} accumulations as opposed to intracellular release. However, there have been very few studies investigating the role of synaptic Zn^{2+} release, by utilizing ZnT3 KO animals, on neuronal injury.

Following the generation of ZnT3 KO mice, it was found that these animals had an increased susceptibility to seizures (Cole et al., 2000) as well as an increase in intracellular Zn^{2+} accumulation in degenerating neurons of the hippocampus following seizures (Lee et al., 2000). The observation of increased intracellular Zn^{2+} accumulation, despite the lack of vesicular Zn^{2+} in the ZnT3 KO animals, argued against the translocation hypothesis. It was further suggested that a different source of Zn^{2+}, other than synaptic Zn^{2+}, was more important for neuronal injury, at least in the context of seizure (Lee et al., 2000). However, in a more recent study, ZnT3 KO animals demonstrated less photoreceptor degeneration in the retina following light-induced retinal

degeneration (Bai et al., 2013), which contrasts against seizure work done above and suggests that synaptic Zn^{2+} is involved in retinal injury. Clearly, the source of neurotoxic Zn^{2+} following numerous pathological states is still debated. Currently, studies of ischemia in ZnT3 KO mice are lacking. One possibility for a recurring source of synaptic Zn^{2+} release following ischemia could be from repetitive waves of depolarization that propagate through neuronal tissue, for many days following the initial ischemic event, termed spreading depolarizations.

1.3 Spreading Depolarization

In 1944 the Brazilian physiologist Aristides Leao was investigating seizure mechanisms following electrical stimulation of the rabbit cortex (Leao, 1944c). While monitoring the spontaneous electrical activity for signs of seizure-like activity following electrical stimulation, he discovered an unusual silencing of spontaneous electrical activity when the brain was strongly stimulated. By using a series of differential electrical recordings of the exposed cortex, Leao noticed that the suppression of activity originated from the site of stimulation and propagated outward from that site, eventually encompassing the entire cortical hemisphere, at a rate calculated to be approximately 2-6mm/min. The suppression of spontaneous electrical activity was transient and recovered fully within several minutes, in a similar manner to that which it was suppressed (Leao, 1944c). He also discovered that this suppression of activity could be elicited in the cortex of cats and pigeons, suggesting that this phenomenon was likely widespread throughout species (Leao, 1944c).

Leao subsequently showed that accompanying the depression of spontaneous cortical activity was a large, slow, potential change recorded from the extracellular space (Leao, 1947). This slow extracellular direct current (DC) potential shift was recorded as a multi-phasic response, starting with a large negative component followed by a recovery and slight overshoot into the positive range with a return to baseline within minutes (see Figure 1.3). This DC shift is now considered as the classical hallmark of spreading depolarization (SD). Subsequent studies by Leao also showed that a similar DC shift occurred following a global ischemia model in rabbits (Leao, 1947), thus establishing the possibility for the occurrence of SD under pathological conditions such as ischemia. The "spreading depression of activity" originally discovered by Leao is now recognized as one of the consequences resulting from the propagation of SD through nervous tissue, as discussed below.

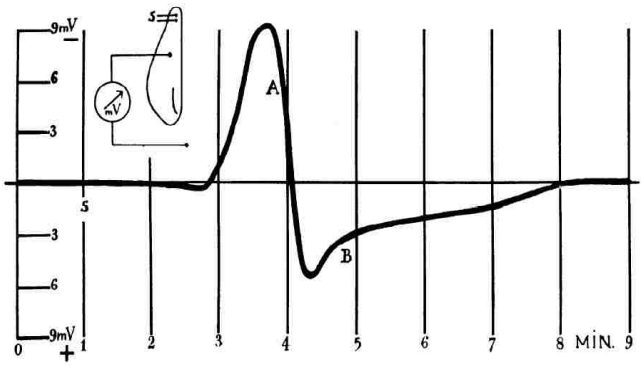

Figure 1.3: Representative recording of the extracellular DC potential shift associated with SD. Following intense electrical stimulation (S), there was an initial slow negative potential change (note that negative is plotted upwards) followed by a rapid recovery (A) and subsequent overshoot (B). The response returned to baseline values approximately 5min following the event. (From: Leao, 1947).

1.3.1 General Mechanisms Underlying Spreading Depolarization

Numerous stimuli can generate SD, including elevated extracellular K^+, simulated *in vitro* models of ischemia (hypoxia or oxygen-glucose deprivation (OGD)), mechanical

stimuli, as well as the intense electrical stimulation and transient ischemia *in vivo* mentioned above (Somjen, 2001). During the passage of SD, there is a near complete depolarization of both neurons and glia. Whole cell recordings during SD have measured the membrane potential to approach near 0mV (Czeh et al., 1992). This prolonged depolarization mirrors the length of the DC shift and is accompanied by dramatic disruptions in ionic gradients. Due to the membrane potential changes, non-selective ion channels open resulting in extracellular increases of $[K^+]$ up to 60mM, along with extracellular decreases in $[Na^+]$, $[Ca^{2+}]$, and $[Cl^-]$ to about 60, 0.08, and 75mM, respectively (Hansen and Zeuthen, 1981, Somjen, 2001). These severe ionic fluxes contribute to the generation of the negative extracellular DC potential shift that can be measured with electrophysiological techniques, as originally described by Leao. The large negative DC shift associated with SD (up to -20mV) is the largest depolarization event recorded in brain tissue, larger than the DC changes seen during brain activity (Somjen, 2001). Additionally, the dramatic changes in ionic gradients result in the corresponding influx of water, generating a marked swelling response.

Once initiated, SD propagates in a feed-forward manner throughout grey matter. The feed-forward nature was originally proposed to arise solely from the effects of extracellular K^+ accumulation caused by SD, which would be sufficient to depolarize neighboring neurons and continue the wave of depolarization (Grafstein, 1956). While there is little doubt that increased extracellular K^+ can lead to neuronal depolarization, this hypothesis did have some inconsistencies. One concern with the K^+ hypothesis was that application of tetrodotoxin (TTX), to prevent voltage-gated Na^+ channels from contributing to full depolarization and neuronal action potential generation, failed to

prevent the propagation of SD, suggesting that depolarization by K^+ alone was not sufficient to drive SD propagation (Tobiasz and Nicholson, 1982). Additionally, extracellular K^+ elevations were not detected immediately prior to the onset of the DC shift (Somjen et al., 1992), as were expected if K^+ were contributing to the propagation of SD. A second hypothesis to explain the feed-forward nature of SD was based on the release and actions of the excitatory neurotransmitter glutamate. This hypothesis was based on the observations that: 1) exogenous application of glutamate could induce SD when applied to the cortical surface; and 2) glutamate release was not suppressed by TTX, suggesting that glutamate can be released in the absence of action potentials (Van Harreveld, 1959). The exact mechanisms underlying SD initiation and propagation under different conditions are still incompletely understood, and a dual hypothesis has emerged for the initiation and propagation of SD that includes contributions of both K^+ and glutamate (Van Harreveld, 1978, Somjen, 2001).

Large amounts of energy are required to restore the ionic gradients after SD, to allow for normal neuronal function to resume. ATP is required to activate ATP-dependent transporters, including the Na^+/K^+-ATPase and Na^+/Ca^{2+}-ATPase. A major role for Na^+/K^+-ATPase function was supported by studies utilizing ouabain, a selective Na^+/K^+-ATPase inhibitor which can generate SD in brain slices. At a high enough concentration to cause complete pump inhibition, ouabain resulted in SD followed by irrecoverable injury. However at a lower concentration that produced only partial pump inhibition, SD was still generated, but neuronal function recovered in only approximately half of these slices (Xiong and Stringer, 2000).

The large energy demand generated by the activation of ATP-dependent transporters requires that neurons have sufficient metabolic substrates to recover fully from SD. Consistent with an increase in metabolism, large increases in glucose utilization (Shinohara et al., 1979) and dramatic decreases in glucose and ATP levels (up to 72% and 54% of baseline, respectively (Mies and Paschen, 1984)) have been measured following the passage of SD. These effects are also accompanied by increases in lactate levels (Selman et al., 2004), presumably due to the conversion of pyruvate to lactate in order to restore NADH levels to continue an increase in glycolytic activity. In support of an increase in glycolysis, Takano and co-workers utilized two-photon imaging during SD to show a heterogeneous distribution of NADH fluorescence with the increased NADH levels associated in close proximity to blood vessels and NADH decreases farther away from blood vessels (Takano et al., 2007). The authors also observed a transient decrease in tissue O_2 levels during the passage of SD, and taken together with the NADH fluorescence observations above, suggest an increase in anaerobic glycolysis following SD (Takano et al., 2007).

Upon neuronal activity, there is an increase in blood flow to provide metabolic substrates to compensate for the increase in metabolism, a process termed neurovascular coupling (Attwell et al., 2010). Based on the substantial neuronal activity during the passage of SD, it seems likely that there would be a corresponding increase in blood flow. The early work of Leao demonstrated dilation of pial vessels and an increase in blood flow following SD under normal healthy conditions (Leao, 1944a). The changes in cerebral blood flow (CBF) following SD are complex, with experimental evidence reporting a hyperemic response occurring initially after the passage of SD followed by a

long-lasting olegemia for up to 1hr (Lauritzen et al., 1982). Yet, despite the large metabolic challenge associated with SD, under normal healthy conditions, SD is fully recoverable and is non-injurious (Nedergaard and Hansen, 1988). However, the consequences of SD may drastically change depending on the current metabolic status of the tissue involved.

1.3.2 Experimental Evidence for Spreading Depolarization in Stroke Injury

As mentioned above, Leao observed a slow negative DC potential shift following electrical stimulation and also after experimental ischemia in the rabbit cortex. While the characteristics of the DC shift recordings with the two different stimuli were somewhat different, Leao postulated that the underlying event, seen during ischemia and that observed during his characterized spreading depression, were likely of the same nature (Leao, 1947). Increases in extracellular K^+ levels, similar to those seen during SD, were subsequently found to spontaneously occur in primate cortex following ischemia (Branston et al., 1977) and were also later observed in the ischemic cortex of the cat (Strong et al., 1983). The occurrence of SD following ischemia prompted investigators to speculate that these events may contribute to the evolution of the ischemic region as more laboratories began to report the occurrence of spontaneous SDs following ischemia (Nedergaard and Astrup, 1986, Back et al., 1994).

In the early 1990s an important study revealed that there was a significant correlation between the number of spontaneous SD events and the total infarct volume following ischemia in rats (Mies et al., 1993). The authors reported a step-wise increase in infarct volume after each SD. The DC shift durations and the recovery of the electrical

activity during the repetitive SDs also grew steadily longer with each depolarizing event. Shortly following that study, it was reported that experimentally inducing SD, by high K^+ applications, following ischemia in rats lead to larger infarct volumes assessed by both histological methods (Back et al., 1996) and diffusion-weighted MRI (Busch et al., 1996). It was also observed that by using a glutamate receptor antagonist (MK-801), the number of spontaneous SDs following ischemia decreased and the infarct area was also smaller in MK-801 treated animals (Iijima et al., 1992). The results of these studies suggested that SDs may be a causative factor in the enlargement of ischemic lesions and by blocking or preventing the occurrence of spontaneous SDs following ischemia could be therapeutically beneficial.

The majority of early animal studies assessing infarct growth with relation to the number of SDs were limited by the time course of the experimental recordings, terminating within a few hours following the induction of ischemia. This presents a problem with trying to develop new therapeutics that could be delivered at late time-points following the initial ischemic event, when infarct enlargement can still occur. In 2003 an important paper addressing this point showed that SDs can occur for many hours following ischemia (Hartings et al., 2003). Rats were subjected to either a 2hr transient (allowing reperfusion) or permanent middle cerebral artery occlusion (MCAO) and DC potential changes were continuously recorded for 24hrs and up to 72hrs in non-anesthetized, freely-moving animals. In the transiently-occluded animals, an initial cluster of SDs was observed during the period of occlusion but ceased following reperfusion. However, around 6hrs after the initial ischemic event (i.e. 4hrs following reperfusion) a secondary phase of SDs was recorded which slowly decreased towards the

end of the recording session (24hrs). Animals undergoing permanent occlusion had SDs occurring throughout the entire 24hr recording period. The secondary phase in the transiently-occluded animals significantly contributed to the overall infarct volume, as blocking SDs in this phase with an NMDA receptor antagonist significantly reduced the infarct volume measured at 24hrs (Hartings et al., 2003). That report was the first evidence that SD events can occur continuously throughout the evolution of MCAO infarcts in rodents and shed new light on the possibility of targeting the occurrence of SDs for new therapeutics at later time-points.

As described above, SD occurring in healthy tissue is typically followed by an increase in blood flow to compensate for the increased metabolic needs of the tissue. However, when SD occurs in compromised brain tissue, surprisingly a rather opposite effect occurs. An inverse neurovascular coupling (i.e. decrease in blood flow in response to intense neuronal activation) was shown to occur during SD in experimental ischemia in rats (Back et al., 1994), and is what is thought to contribute to the deleterious effects of SD in pathological states. In experimental settings, the first SD following ischemia was found to propagate radially outwards in all directions, with subsequent SDs continuously cycling around the ischemic lesion in both rats and cats (Nakamura et al., 2010, Kumagai et al., 2011). Inverse CBF responses were observed following the continuously cycling SDs, and with each cycle around the core, the SD event never propagated through the region of tissue that it previously invaded. This observation suggested that the persistent decrease in blood flow, and therefore the sustained metabolic burden following SD, significantly contributes to the recruitment of surrounding penumbral tissue into the ischemic core.

Despite strong supporting evidence from animal stroke studies, a major problem in the field was that many investigators were hesitant to extrapolate the experimental finding of SD to human patients. This was mainly due to the difficulty of non-invasively electrically detecting the occurrence of these depolarizations in humans. The difficulty was in part due to the high impedance of the skull and dura combined with the small area of tissue undergoing depolarization, and the slow propagation of SD, to be detected by large scalp electroencephalogram (EEG) recordings (Lauritzen et al., 2011). However, in 2002, a significant breakthrough occurred when the first potential evidence for the electrical detection of SD in the acutely injured human brain was reported.

1.3.3 Clinical Relevance of Spreading Depolarizations in Brain Injury

In the 2002 study, 14 patients with intracranial hematomas that required a decompressive craniotomy for recovery were recruited for SD recording. The craniotomy procedure allowed for the placement of a subdural electrode strip with four differential electrical recording channels to monitor ECoG activity, in a similar fashion to that of the original works of Leao, for up to 63hrs. In 5 of the 14 patients (36%) suppression of ECoG activity was recorded that spread from one recording channel to the next in a propagating nature (Strong et al., 2002). The ECoG suppression and the spread of the ECoG suppression to subsequent channels were both similar to the propagation of SD previously reported in animal models. While changes in DC potentials were not able to be recorded in that study, subsequent advancements in the subdural electrode strips and data analysis allowed for simultaneous recording of ECoG and DC potentials. These strips were implemented in numerous subsequent studies and allowed for the further

characterization of SDs in the injured human brain. This prompted the formation of an international research group in 2002 named COSBID (CoOperative Study of Brain Injury Depolarizations), to pool collected data from across the globe to further help understand these events. The first of these studies recorded ECoG and DC potentials from 12 intracranial hematoma patients, in which 6 of those patients showed classical negative DC potential shifts associated with suppression of ECoG activity (Fabricius et al., 2006).

As a result of the COSBID work, in 2008 repetitive SDs were found to occur in humans following ischemic stroke. In that study, the authors recorded an average of ~100hrs in each of 16 patients who had middle cerebral artery occlusions (Dohmen et al., 2008). SDs were recorded in 14 of the 16 patients, and in the 2 where SDs were not seen, it was found that the electrode strips were placed over tissue that was already infarcted and non-responsive. Repetitive SDs were seen up to 5 days following the electrode placement. Importantly, in some patients it was observed that when an SD event propagated through the tissue it could lead to a permanent irrecoverable suppression of ECoG activity. The spread of permanent electrical silencing matched post-operative MRI and computed tomography (CT) scans showing the enlargement of the infarct (Dohmen et al., 2008). Thus, these results further supported that SD events propagate through penumbral tissue and are likely responsible for the recruitment of partially compromised tissue into the ischemic core.

Most clinical SD recordings have concentrated on recordings in the intensive care unit, but a recent study has demonstrated SD events at earlier time-points during neurosurgical procedures for acute brain injury. Twenty patients with malignant hemispheric stroke, where a craniotomy was required, were monitored with laser speckle

imaging (LSI) to record blood flow changes during a 20min period immediately following the craniotomy procedure (Woitzik et al., 2013). Multiple SDs were observed in 7 of the patients that had spatiotemporal propagation patterns similarly documented in experimental animal models (Nakamura et al., 2010). These and other parallel findings from animal and clinical recordings strongly validate the usefulness for studying SD in animal models and the subsequent consequences following numerous brain injuries.

1.3.4 Therapeutic Potential for Blocking Spreading Depolarizations

Based on early experimental work describing the effectiveness of NMDA receptor antagonists on reducing the number of SDs and subsequently reducing overall infarct expansion (see above), the potential to block these deleterious events in humans and improve outcome was suggested as a new therapeutic strategy (Strong et al., 2007, Dreier, 2011, Lauritzen et al., 2011). This has the potential to become very clinically relevant as SD events occur for many days after the initial insult and would greatly increase the therapeutic window for new interventions. The obvious candidate would be NMDA receptor blockers, as they have already been shown to reduce the number of SD events in animal models as described above. Unfortunately, a competitive NMDA receptor antagonist (Selfotel) failed to provide any beneficial effects in two Phase III clinical trials of severe brain injury where SDs were likely to occur (Morris et al., 1999). While SDs were not directly measured in those patients, there are concerns, however, about the use of competitive NMDA receptor antagonists in the prevention of SDs. First, there is a massive increase in the extracellular levels of glutamate during SD (Fabricius et al., 1993), which could outcompete the antagonist. Secondly, it was found that elevated

levels of extracellular K^+ reduced the ability for NMDA receptor antagonists to prevent SDs (Petzold et al., 2005). As increased levels of extracellular K^+ occur not only in metabolically compromised tissue in the penumbra, but also during SD, NMDA receptor antagonists might not be able to prevent SD. On the other hand, ketamine, a noncompetitive NMDA receptor antagonist used for general anesthesia, has been shown to decrease the number of SDs following brain injury (Sakowitz et al., 2009, Hertle et al., 2012). It is unclear if this ability is due to the noncompetitive nature of inhibition or to some other effect, but the results are promising.

Another possibility would be to not prevent the occurrence of SD, but to therapeutically target deleterious consequences following the event. Surprisingly, SD has been shown to be neuroprotective when experimentally induced in healthy tissues. If SD is induced 24hrs prior to the induction of ischemia, infarct volumes were significantly smaller in those animals compared to animals not receiving SD beforehand (Matsushima et al., 1998, Yanamoto et al., 1998). It is possible that following ischemia, when SDs propagate out from the infarct and into healthier tissues, the effects of SD are beneficial in normally perfused tissue, preconditioning the tissue making it more resilient to the expansion of the ischemic core. If this were true, then completely blocking SD occurrence could actually contribute to infarct progression. While this has not been experimentally shown in the context of ongoing ischemia, it raises the question of whether deleterious consequences of SD can be targeted. One potential target that might have a large impact on the expansion of the ischemic infarct could be the release and accumulation of synaptic Zn^{2+} following SD.

1.3.5 Potential for Synaptic Zn^{2+} Release during Spreading Depolarizations

As mentioned above, glutamate release is thought to contribute to SD (Van Harreveld, 1959). Microdialysis studies have shown that extracellular levels of glutamate significantly increase following SD (Fabricius et al., 1993). As a major source for glutamate release from nerve terminals is from synaptic vesicles, one hypothesis is that SD results in large amounts of synaptic glutamate release. Consistent with this is the requirement for both the presence of extracellular Ca^{2+} and NMDA receptor activation for the initiation and propagation of SD. One requirement for synaptic vesicle fusion and release of neurotransmitters is the influx of Ca^{2+} into the presynaptic terminal to activate the final vesicle fusion machinery. Inhibition of presynaptic Ca^{2+} channels (P/Q-type Ca^{2+} channels) blocks SD generated in organotypic hippocampal slice cultures (Kunkler and Kraig, 2004), supporting the idea that synaptic glutamate release contributes to SD. Additionally, by utilizing a different approach that allows glutamate release but blocks postsynaptic NDMA receptors, SD can also be blocked in experimental settings (Lauritzen and Hansen, 1992), and in some clinical settings (Sakowitz et al., 2009).

As described above in section *1.2.3*, Zn^{2+} is co-stored with glutamate in synaptic vesicles, via the actions of the ZnT3 transporter. While the exact mechanism underlying Zn^{2+} uptake through this transporter remains unclear, the concentration of Zn^{2+} in these vesicles has been estimated to be in the millimolar range with accumulations of up to 300μM in the extracellular space following intense depolarization (Assaf and Chung, 1984). Similar glutamate signaling is present in young ZnT3 knockout (KO) mice (Cole et al., 2001), suggesting that glutamate filling appears to not be affected by the lack of vesicular Zn^{2+}. As Zn^{2+} is co-stored with glutamate, and synaptic Zn^{2+} has been detected

following direct electrical stimulation of nerve fibers, it seems reasonable to propose that significant synaptic Zn^{2+} would be released during SD events.

SD events occur repetitively for up to several days following ischemia (Dohmen et al., 2008). If synaptic Zn^{2+} release occurs during SD, this may provide a source of repetitive extracellular Zn^{2+} accumulations following ischemia which could contribute to the toxic Zn^{2+} described above. Previous work in our lab has demonstrated for the first time that Zn^{2+} may be involved in the generation of SD (Dietz et al., 2008). Intracellular Zn^{2+} increases, in single neurons, were found to occur prior to the onset of SD, and this accumulation significantly contributed to the initiation of SD induced by ouabain and OGD (Dietz et al., 2008). Furthermore, a large increase in extracellular FluoZin-3 fluorescence was observed following ouabain-induced SD (Dietz et al., 2008), suggesting the possibility for SD to result in extracellular Zn^{2+} accumulation. Currently, investigations into the potential contributions of synaptic Zn^{2+} release, with the use of ZnT3 KO animals, following SD is lacking. Synaptic Zn^{2+} release during repetitive SDs following ischemia could help explain not only the beneficial effects of chelating extracellular Zn^{2+} during the initial ischemic event (Lee et al., 2002), but also at much later time-points (Calderone et al., 2004), where SDs can occur.

1.4 Goals and Summary of the Presented Work

The goal of the dissertation work presented here was to test the overall hypothesis that synaptic Zn^{2+} release during repetitive SD episodes is a major source of neurotoxic Zn^{2+} in the post-ischemic period. Studies in Chapter 2 examined the mechanisms of Zn^{2+} accumulation following SD in the hippocampus of the brain slice model. These studies

tested whether synaptic Zn^{2+} release could be detected extracellularly by the selective Zn^{2+} fluorescent indicator, FluoZin-3, following SD generated by either microinjections of KCl (high K^+-SD) or oxygen/glucose deprivation (OGD-SD). This study provided real-time fluorescence visualization of Zn^{2+} release during SD the first verification of its synaptic source, and also demonstrated postsynaptic accumulation of Zn^{2+} from a synaptic origin.

Experiments found in Chapters 3 and 4 examined consequences of Zn^{2+} accumulation on SD. In Chapter 3, the goal was to elucidate the mechanism behind the protective effect of total (intracellular and extracellular) Zn^{2+} chelation previously reported in the OGD model of ischemia in brain slices (Medvedeva et al., 2009). Under conditions of Zn^{2+} chelation, complete recovery was seen following a period of OGD when SD was not initiated, however irrecoverable injury still occurred if OGD-SD was generated, suggesting that the major contributor to neuronal injury following OGD was the generation of SD, and the beneficial effect of Zn^{2+} chelation was in delaying the onset of SD, in agreement with our previous work (Dietz et al., 2008).

Studies in Chapter 4 investigated whether Zn^{2+} accumulation can worsen the outcome of SD. The results showed that intracellular Zn^{2+} accumulation prior to the onset of SD significantly delayed the recovery of neuronal activity in brain slices. The effects of Zn^{2+} accumulation were consistent with an increased metabolic burden following SD, providing a potential mechanism of how Zn^{2+} and SD might contribute together in worsening neuronal injury following metabolic compromise.

Chapters 2-4 concentrated on *in vitro* studies in hippocampal slice preparations. Experiments in Chapter 5 expanded these investigations to neocortical tissues more

relevant for clinical studies of ischemic strokes, and also provided the first visual evidence of synaptic Zn^{2+} release *in vivo*. Technical aspects of *in vivo* fluorescence imaging are also examined. Finally, this study also provided evidence that synaptic Zn^{2+} release occurs during ischemia following SD *in vivo*, and significantly contributes to ischemic infarction.

Overall, these studies provide evidence that targeting either the release or postsynaptic accumulation of synaptic Zn^{2+} in the postischemic period could lead to the development of new therapeutics for the treatment of stroke which could be delivered at late time-points. This is encouraging as current therapeutic strategies are limited in most patients to a relatively short time window following initial stroke insults.

Chapter 2: Spreading Depression and Related Events are Significant Sources of Neuronal Zn^{2+} Release and Accumulation

Russell E. Carter[1], Isamu Aiba[1], Robert M. Dietz[1],

Christian T. Sheline[2] & C. William Shuttleworth[1]

[1]Department of Neurosciences

University of New Mexico, Albuquerque, NM, USA

[2]LSU Health Sciences Center

Department of Ophthalmology and the Neurosciences Center of Excellence,

New Orleans, LA, USA

(Published in Journal of Cerebral Blood Flow & Metabolism (2011)31:1073-1084)

2.1 Abstract

Spreading depression (SD) involves coordinated depolarizations of neurons and glia that propagate through brain tissue. Repetitive SD-like events are common following human ischemic strokes, and are thought to contribute to the enlargement of infarct volume. Accumulation of Zn^{2+} is also implicated in ischemic neuronal injury. Synaptic glutamate release contributes to SD propagation, and since Zn^{2+} is co-stored with glutamate in some synaptic vesicles, we examined whether Zn^{2+} is released by SD and may therefore provide a significant source of Zn^{2+} in the post-ischemic period. SD-like events were generated in acutely-prepared murine hippocampal slices by depletion of oxygen and glucose (OGD) and Zn^{2+} release was detected extracellularly by a Zn^{2+}-selective indicator FluoZin-3. OGD-SD produced large FluoZin-3 increases which propagated with the event, and signals were abolished in tissues from ZnT3 KO animals lacking synaptic Zn^{2+}. Synaptic Zn^{2+} release was also maintained with repetitive SDs generated by microinjections of KCl under normoxic conditions. Intracellular Zn^{2+} accumulation in CA1 neurons, assessed using microinjection of FluoZin-3, showed significant increases following SD that was attributed to synaptic Zn^{2+} release. These results suggest that Zn^{2+} is released during SDs and could provide a significant source of Zn^{2+} that contributes to neurodegeneration in the post-ischemic period.

2.2 Introduction

The phenomenon of spreading depression (SD) involves a wave of coordinated neuronal and glial depolarization that spreads in a regenerative manner across brain tissue (Leao, 1944b, Somjen, 2001). SD does not generally cause injury to healthy brain, as

ionic gradients are restored by the action of ATP-dependent transporters. However SD can cause irreversible loss of membrane potential and neuronal injury if metabolic substrates are not sufficient for timely repolarization (Hossmann, 1996, Somjen, 2001). Spreading waves of depolarization that are very similar to SD are observed in animal models of stroke, and accumulating evidence suggests that these SD-like events play a causative role in the evolution of ischemic brain injury (Strong et al., 2000, Hartings et al., 2003). Recent long-term recording in ischemic stroke patients has revealed that SD-like events occur repetitively for many hours and days following stroke onset (Dohmen et al., 2008), suggesting that approaches to limit the onset or consequences of these events may be of benefit at quite late time points.

We recently examined factors contributing to the onset of SD in brain slices, and found that Zn^{2+} accumulation can contribute to initiation of forms of SD that are relevant for ischemia. Chelation of Zn^{2+} could delay or prevent SD-like events generated by either combined oxygen and glucose deprivation (OGD-SD) or by the Na^{+}/K^{+}/ATPase inhibitor ouabain (ouabain-SD), and these effects were more prominent when adenosine A1 receptor activation was enhanced (Dietz et al., 2008). Zn^{2+} is present at high levels in the brain, located in intracellular binding proteins and also concentrated into many nerve terminals via the activity of the ZnT3 transporter (Palmiter et al., 1996b, Frederickson et al., 2005). A large body of literature has shown that disruption of Zn^{2+} homeostasis can cause neuronal injury, via disruption of both glycolytic and mitochondrial function, and actions on a range of other intracellular targets (Choi and Koh, 1998, Dineley et al., 2003, Galasso and Dyck, 2007, Sensi et al., 2009). Reducing Zn^{2+} accumulation has also been shown to limit neuronal injury in animal focal and global ischemia models (Koh et al.,

1996, Lee et al., 2002, Calderone et al., 2004, Galasso and Dyck, 2007). In addition to preventing a number of deleterious intracellular signaling cascades, it is possible that limiting the onset of SD-like events could contribute to beneficial effects of Zn^{2+} chelation in some stroke models.

Previous work has identified glutamate release as a contributor to SD propagation, based on the effectiveness of glutamate receptor blockers and microdialysis measurements of extracellular glutamate accumulation (Fabricius et al., 1993, Somjen, 2001). Although the regulation of glutamate release during SD is not well understood, it is likely that depolarization of nerve terminals due to K^+ elevations contributes. In the present study we have examined whether significant amounts of Zn^{2+} may be released from nerve terminals during SD. Zn^{2+} is co-stored with glutamate in many hippocampal and neocortical synaptic vesicles (Frederickson et al., 2005). High levels of Zn^{2+} can be visualized in nerve terminals by using histochemical staining methods and Zn^{2+} release can be detected following nerve stimulation (Frederickson et al., 2005, Sensi et al., 2009), including studies using the Zn^{2+}-sensitive indicator FluoZin-3 (Qian and Noebels, 2005, 2006), but see also (Kay, 2003)). Knockout of ZnT3 prevents accumulation of Zn^{2+} in synaptic terminals without influencing other essential Zn^{2+} stores (Cole et al., 1999), and prevents fluorescence signals attributed to synaptic Zn^{2+} release (Qian and Noebels, 2006).

We have used fluorescence imaging of Zn^{2+} and ZnT3 knockout (ZnT3 KO) tissues to show here that SD and related events indeed cause large Zn^{2+} releases that appear due to release from synaptic vesicles, and that this source of Zn^{2+} contributes to accumulation in postsynaptic neurons. Releasable Zn^{2+} stores were not readily depleted

with repetitive SD trials, and these results therefore identify SD and related spreading depolarizations as new and potentially significant sources of Zn^{2+} for neuronal injury in the post-ischemic period.

2.3 Materials and Methods

Slice preparation

Acute brain slices were prepared from mice as previously described (Dietz et al., 2008). All procedures were carried out in accordance with the National Institute of Health guidelines for the humane treatment of laboratory animals, and the protocol for these procedures was reviewed annually by the Institutional Animal Care and Use Committee at the University of New Mexico School of Medicine. After cutting in ice-cold solution and then holding for 1 hour at 35^{o}C, artificial cerebrospinal fluid (ACSF) was changed, and slices were held at room temperature until used for recording. Individual slices were then transferred to the recording chamber, and were superfused with oxygenated artificial cerebrospinal fluid (ACSF) at 2 ml/min.

Mice homozygous for deletion of the ZnT3 gene were originally obtained from Dr. Richard Palmiter (Cole et al., 1999) and backcrossed onto C57Bl/6 for >13 generations. A homozygous breeding colony of ZnT3 KO animals was then established at the University of New Mexico. Initial studies of intracellular and extracellular Zn^{2+} transients were made in slices from wild-type FVB/N mice, as were used for previous studies of Zn^{2+} and SD initiation (Dietz et al., 2008). Because no differences were noted in SD-FluoZin-3 responses between wild-type C57Bl/6 and FVB/N mice, responses from ZnT3 KO tissues were either compared with responses from populations of wild-type

C57Bl/6 tissues, or pooled populations of C57Bl/6 and FVB/N tissues, as noted in figure legends. Wild-type animals were obtained from Harlan Laboratories (Bar Harbor, ME) and all animals were housed in standard conditions (12hr/12hr light/dark cycle) before sacrifice at 4-6 weeks of age.

SD initiation and recording

Extracellular measurements of DC potentials were made using borosilicate glass microelectrodes, filled with ACSF (~5MΩ) and placed in stratum radiatum ~50 μm below the surface of the slice. SD was generated by localized microinjection of KCl, delivered by using brief pressure pulses (10-40psi, 100-250ms, 1M solution) from a conventional patch electrode (3-5ΩM) placed under the surface of the slice, ~350μm from the recording electrode. Oxygen-glucose deprivation (OGD) was used to generate the closely-related propagating event (OGD-SD). In both cases (SD and OGD-SD), the passage of the coordinated, spreading depolarization was identified as a sharp drop in DC potential, as previously described (Somjen, 2001). In some experiments, the spread of SD or OGD-SD was monitored by using intrinsic optical signals, generated by transmission of red (>575nm) light.

Zn^{2+} indicator measurements

Extracellular Zn^{2+} measurements were made using the charged form of the Zn^{2+}-sensitive indicator FluoZin-3, using approaches developed by (Kay, 2003, Qian and Noebels, 2005, 2006) and utilized in our recent work (Dietz et al., 2008). FluoZin-3 was dissolved in ACSF at 1.5-2μM and superfused over the slice at 35^{o}C. Background

fluorescence was then reduced by addition of CaEDTA (1mM) in all experiments, except where indicated otherwise. Responses are reported as ($\%\Delta F/F_0$), as Zn^{2+} binds to multiple components of the recording buffer (Rumschik et al., 2009), making absolute calibration from addition of exogenous Zn^{2+} standards problematic. Fluorescence increases due to addition of FluoZin-3 were very similar in wild-type and ZnT3 KO slices, and addition of CaEDTA reduced fluorescence to very similar levels in both wild-type and ZnT3 KO tissues (see Supplemental Figure 1). FluoZin-3 was excited at 495nm, and emission was detected at 535/50nm using a monochromator-based imaging system (Till Photonics).

Intracellular Zn^{2+} measurements were made from single CA1 pyramidal neurons. The procedures for intracellular recording/indicator injection were as described previously (Dietz et al., 2008) using electrodes tip-filled with 1mM FluoZin-3 for recordings from slices superfused at 32^{o}C. Since high resistance intracellular electrodes were used, a lower final indicator concentration was achieved by loading into neurons with passage of hyperpolarizing current (300-800pA, 20 min), and the recording/filling electrode was then slowly withdrawn in 0.5μm steps from the neuron (Dietz et al., 2008). Because high resistance intracellular recording/filling electrodes were used, this withdrawal procedure did not result in significant indicator leak or extracellular accumulation of FluoZin-3. Signals from cell bodies were background subtracted using adjacent regions in the cell body layer, to take into account changes in autofluorescence caused by SD events.

Reagents and solutions

Slice cutting solution contained (in mM): 3 KCl, 1.25 NaH_2PO_4, 6 $MgSO_4$, 26 $NaHCO_3$, 0.2 $CaCl_2$, 10 glucose, 220 sucrose and 0.43 ketamine. ACSF contained (in mM): 126 NaCl, 3 KCl, 1.25 NaH_2PO_4, 1 $MgSO_4$, 26 $NaHCO_3$, 2 $CaCl_2$, and 10 glucose and was equilibrated with 95%O_2 / 5%CO_2. Cutting and recording solutions were both 315-320 mOsm. In oxygen/glucose deprivation (OGD) experiments, ACSF was modified by equimolar replacement of glucose with sucrose, and extensively equilibrated with 95%N_2 / 5%CO_2. FluoZin-3 was obtained from Invitrogen (Carlsbad, CA), and all other reagents were obtained from Sigma (St. Louis, MO).

Statistical Analysis

Data are reported as mean ± standard error of the mean (S.E.M.). Significant differences between group data were evaluated using unpaired or paired Student's t-tests, with correction for multiple comparisons where appropriate.

2.4 Results

Synaptic Zn^{2+} release following OGD-SD

Figure 1A shows a representative example of Zn^{2+} increases associated with SD-like events in the OGD model (OGD-SD). OGD-SD was detected as a sharp DC shift after about 10 min OGD exposure, and was accompanied by a large increase in fluorescence of extracellular FluoZin-3.

Extracellular Zn^{2+} accumulation was detected by using the charged form of FluoZin-3 (1.5-2μM), which is confined to the extracellular space. As described

previously (Qian and Noebels, 2005, 2006) a Zn^{2+} chelator with high affinity but slow Zn^{2+} binding kinetics (CaEDTA, 1mM) was also included to improve signal/noise in the initial measurements. This chelator is effective for these studies because it does not reduce extracellular Ca^{2+} concentrations, but effectively reduces the large background extracellular Zn^{2+} fluorescence signal, due to the higher affinity of this cation than the pre-bound Ca^{2+} ($KD_{Zn}=10^{-16}M$, $KD_{Ca}=10^{-10}M$) (see Supplemental Fig 1). Because of the time taken for exchange of Zn^{2+} with Ca^{2+} on the EDTA molecule (Kay, 2004), extracellular Zn^{2+} is readily detected as FluoZin-3 transients before sequestration by CaEDTA.

In order to test the hypothesis that Zn^{2+} is synaptically released during OGD-SD, mice lacking synaptic Zn^{2+} (ZnT3 KO mice, (see Cole et al., 1999)) were used. ZnT3 is a Zn^{2+} transporter localized selectively to synaptic vesicles (Palmiter et al., 1996b, Cole et al., 1999), which is responsible for transporting cytosolic Zn^{2+} into synaptic vesicles. We previously showed that Zn^{2+} accumulation can contribute to the onset of OGD-SD, and described conditions of high adenosine A1 receptor activation where chelation of Zn^{2+} was sufficient to completely prevent the onset of SD (Dietz et al., 2008). In the present experiments, exogenous A1 receptor agonists were not applied, to ensure that OGD-SD was still generated and allow consequences of these events on Zn^{2+} release to be determined. Under these conditions, OGD-SD was generated in all wild-type and ZnT3 KO tissues (mean onset time 10.09 ± 1.01 min in ZnT3 KO, vs. 8.97 ± 0.50 min in wild-type, p=0.37), however Figure 1B shows that FluoZin-3 increases were abolished in a paired slice from a ZnT3 KO animal. Figure 1C shows mean data from a group of such experiments. Instead of fluorescence increases, small decreases were observed following

the propagation of OGD-SD in ZnT3 KO tissues that were due to changes in autofluorescence and/or tissue swelling (see below).

During OGD exposures, small decreases in FluoZin-3 fluorescence were observed prior to the onset of OGD-SD but these were not significantly different between wild-type and ZnT3 KO preparations (-5.45±1.52 vs. -6.83±1.53 % $\Delta F/F_0$ respectively, p=0.54, n=6 each). As CaEDTA was present throughout these studies, it is unlikely that this is caused by decreases in extracellular Zn2+ levels, as is likely caused by small, uniform changes in tissue optical properties before the onset of OGD-SD (see below). No FluoZin-3 fluorescence increases were observed before the onset of OGD-SD, regardless of whether CaEDTA was present or not (n=17 and n=5, respectively).

Figure 2 illustrates the wave-like spread of the FluoZin-3 increases, and examines the relationship with the onset of OGD-SD. A movie file demonstrating the spread of fluorescence increases is available in the Supplementary Data. Figure 2A shows that the fluorescence increase propagated slowly across the slice (mean 3.68±0.55 mm/min, n=11). This rate was very similar to the propagation rate of OGD-SD observed in this model with intrinsic optical methods in a separate population of slices (4.82±0.70 mm/min, n=9, p=0.22), and consistent with many previous reports for the propagation rate of SD and related events generated in hypoxia or ischemia models (see Somjen, 2001). FluoZin-3 increases were also largest in stratum radiatum (Fig 2B), a region which is expected to contain high concentrations of Zn^{2+}-containing excitatory synaptic inputs (Qian and Noebels, 2006) and be the site of initial current sink during SD initiation (Kunkler et al., 2005). Figure 2C shows that the onset of Zn^{2+} increases was coincident with the onset of OGD-SD measured in the same slices, suggesting that Zn^{2+} increases

occur together with the spread of OGD-SD, rather than significantly leading or following the response.

Relative Amplitude of Signals

As noted above, the methods used to evaluate Zn^{2+} release follow previously published work, where a Zn^{2+} chelator with high affinity but slow Zn^{2+} binding kinetics (CaEDTA) was used to improve signal/noise (Qian and Noebels, 2005). We tested the hypothesis that this chelator greatly reduced the time course of FluoZin-3 transients from OGD-SD by comparing results from parallel studies in the absence of CaEDTA. Figures 3A and B illustrate the greatly enhanced background FluoZin-3 fluorescence in the absence of CaEDTA, and shows fluorescence transients generated by OGD-SD superimposed on these different background fluorescence levels. Figure 3C shows mean data from a set of such experiments, and shows a substantial increase in mean time constant of decay of transients (0.61 ± 0.11 min vs. 2.03 ± 0.25 min, with and without CaEDTA, respectively, n=5, p=0.0023). The peak amplitude of average raw fluorescence transients was increased without CaEDTA (136.46 ± 23.12 vs. 82.43 ± 18.47 arbitrary fluorescence units, 0mM vs. 1mM CaEDTA respectively, p>0.10, n=5 each), but because of the very different background fluorescence levels, the signal/noise ratio of these signals was substantially less than in experiments with CaEDTA (86.13 ± 35.43 (0mM CaEDTA) vs. 241.28 ± 41.04 (1mM CaEDTA) ($\%\Delta F/F_0$), p=0.022, n=5 each). As described previously (Dietz et al., 2008) CaEDTA did not interfere with OGD-SD initiation, with the event occurring at 7.38 ± 0.93 min, compared with 7.80 ± 0.34

without CaEDTA (n=5 for both groups, p=0.65), or propagation (2.86 ± 0.62 vs. 3.68 ± 0.94 mm/min, respectively, p=0.49, n=5 each).

Figure 4A compares extracellular FluoZin-3 responses to electrical stimulation of synaptic inputs with OGD-SD in the same 6 preparations. Responses to relatively short trains of high frequency stimulation (50Hz, up to 200ms trains) were not reliably detected with the CCD methods used in this study, but Figure 3C shows robust extracellular FluoZin-3 transients with 1s trains (50Hz). After recovery from synaptic stimulation (10 min), the same slices demonstrated much larger extracellular FluoZin-3 increases during OGD-SD. When the areas under the curve were compared, FluoZin-3 signals were ~50 fold larger following OGD-SD (1.6±0.71 vs. 85.77±12.36 (%$\Delta F/F_0$)*min, n=6).

As has been noted by others, autofluorescence signals could interfere with FluoZin-3 signals (Kay, 2003, Qian and Noebels, 2005). However Figure 4B shows that differences in background autofluorescence changes are identical in wild-type and ZnT3 KO tissues, and as such cannot be responsible for the conclusions concerning synaptic Zn^{2+} release made above. Figure 4B shows the time courses of autofluorescence signals recorded in paired sets of wild-type and ZnT3 KO slices that were not bathed in FluoZin-3. These signals are recorded at the same wavelength as used for FluoZin-3 studies (495nm), and show small decreases that are due to a combination of flavoprotein autofluorescence changes (Shuttleworth et al., 2003) and tissue swelling that accompanies SD. If differences in baseline fluorescence between unloaded tissues and FluoZin-3 fluorescence are taken into account, the decrease in autofluorescence is calculated to lead to an average underestimation of Fluozin-3 transients of 28.08 ± 5.00 % (n=4). Figure 4C shows that tissue swelling responses (assessed by changes in

transmitted light signals, rather than autofluorescence) were also identical in wild-type and ZnT3 KO tissues.

Taken together, results from Figures 3 and 4 imply that: 1) Zn^{2+} release signals are large, but underestimated due to slow binding to CaEDTA, and by concomitant decreases in background autofluorescence; and 2) differences in autofluorescence changes or tissue swelling do not underlie the difference between wild-type and ZnT3 KO data described above. These results reinforce the idea that FluoZin-3 increases following OGD-SD are indeed due to synaptic Zn^{2+} release.

Responses to High K^+ SD

Repetitive SD-like events have been proposed as an important contributor to the spread of ischemic infarcts in animal models (Hossmann, 1996, Hartings et al., 2003) and recent clinical recordings strongly support this idea for human ischemic stroke (Strong et al., 2002, Dohmen et al., 2008). To determine whether Zn^{2+} release pools are significantly depleted by a single SD event, or alternatively whether significant Zn^{2+} release could occur during repetitive SD events, we examined responses to local microinjections of KCl (high K^+-SD, see Methods). This stimulus produces SD which can be delivered repetitively without neuronal injury in superfused slices.

Figure 5A shows FluoZin-3 measurements in response to a pair of high K^+-SD responses. Similar to the OGD stimulus, K^+-SD induced a large increase in FluoZin-3 fluorescence coincident with electrical SD recordings, that propagated with characteristics consistent with SD (4.05 ± 0.30 mm/min, n=5). The second SD (triggered 15 min after the first) resulted in a very similar electrical SD and FluoZin-3 response. In

a population of 5 slices (Figure 5B) there was no significant decrease in amplitude of FluoZin-3 transients, and no change in the propagation rate of the responses (4.05 ± 0.30 vs. 4.09 ± 0.37 mm/min, p=0.93, respectively).

An additional set of experiments was performed to determine whether additional rounds of SD might lead to some progressive decrement in the amplitude of responses. Five SDs were generated in each slice (15 min interval between trials), and FluoZin-3 was included during the 1st and 5th trials. Intrinsic optical imaging was used to verify that reproducible SDs were generated throughout the series (see Supplemental Figure 2), and also showed that the propagation rate of the events was not altered (4.54 ± 0.16 vs. 4.61 ± 0.22 mm/min for 1st and 5th event, respectively, p=0.77, n=5).

Although there was no demonstrable change in the amplitude of FluoZin-3 transients, it was noted that first transient recovered somewhat more slowly to baseline than in the second trial, although there was not a significant difference in the area of responses (29.36±6.51 vs. 22.20±2.97 (%$\Delta F/F_0$)min, 1st vs. 5th, respectively, p=0.25, n=5 each). This may suggest some small additional, delayed Zn^{2+} release during the first event, but it may also be due to tissue swelling that does not recover fully following the first SD. The fact that there was no difference in the recovery of the 2nd or 5th SDs (supplemental Figure 2), provides some support for the latter possibility, since otherwise a progressive decline in response area would be expected.

Figure 5B also shows that FluoZin-3 increases generated by high K^+-SD are abolished in ZnT3 KO preparations. As with OGD-SD in ZnT3 KO tissues, a small propagating fluorescence decrease is noted, that is attributed to optical (autofluorescence and swelling) changes that occur coincident with SD (see above). These observations

imply that the first SD event does not deplete available synaptic Zn^{2+} pools, and that repetitive SDs could lead to repetitive, large extracellular Zn^{2+} increases in the post-ischemic period.

Chelator and optical effects on high K^+-SD responses

Figure 6 demonstrates that (like the situation with OGD-SD), the duration of Zn^{2+} accumulation is significantly underestimated due to CaEDTA binding. If CaEDTA is omitted, Zn^{2+} increases persist for ~10min after each SD and the increases also invariably appear biphasic, with a second peak occurring ~4-6 min after the onset of SD. These biphasic signals could be the result of two distinct phases of Zn^{2+} release, but could also be due to interruption of a monophasic Zn^{2+} signal by an optical artifact. Figure 6B provides some support for the second possibility. In these studies, the kinetics of FluoZin-3 signals were directly compared with intrinsic optical signals (IOS), as determined from transmission signals in un-labeled tissue (after FluoZin-3 washout in the same tissues). The IOS is attributed to rapid swelling of neurons associated with propagation of SD and passive accumulation of extracellular K^+ by astrocytes (Zhou et al., 2010b). As can be seen, a large, delayed swelling response occurred at ~ 2min after SD, and corresponded to the time course of the dip in the sustained FluoZin-3 increase. It appeared that the second large peak in IOS interrupted the decay in FluoZin-3 response, and indeed this was observed in all 4 preparations examined, with the delayed IOS peak interrupting (at mean 2.39min, n=4) the decay in FluoZin-3 decline (peaks at 0.11 ± 0.02min and 4.53±0.61 min, n=4) in the same preparations. These findings do not rule out a second delayed phased of Zn^{2+} release, but they are consistent with the possibility

that Zn^{2+} increases following high K^+-SD could involve a single large release event which can be rapidly terminated by CaEDTA. Detection of prolonged increases (without CaEDTA) may be interrupted by tissue swelling before a slow decline to baseline.

Intracellular accumulation of Zn^{2+} following SD

We examined whether Zn^{2+} released following SD is accumulated by postsynaptic CA1 neurons. If this is the case, it could provide a significant source of Zn^{2+} that could contribute to neuronal vulnerability and/or potentially contribute to preconditioning (see Discussion). Postsynaptic Zn^{2+} increases were assessed following single-neuron injection of FluoZin-3 via sharp microelectrodes, rather than by using bulk-loading with membrane-permeable indicators, in order to minimize compartmentalization of indicator and difficulty with effective bulk-loading of slices from 4-6 week old mice. The recording electrode was withdrawn prior to the onset of SD.

Figure 7 shows mean intracellular FluoZin-3 increases from two sets of experiments utilizing high K^+ as a stimulus to trigger SD. In the first set, the recording conditions were identical to that used in Figure 5 where CaEDTA was included in the superfusate to remove contaminating Zn^{2+} and thereby improve signal/noise of extracellular FluoZin-3 increases generated by SD. Here, the same approach was used to test the possible contributions of extracellular contaminating Zn^{2+} to intracellular FluoZin-3 responses following SD. As can be seen, in wild-type preparations, there were robust intracellular Zn^{2+} increases in wild-type neurons. In contrast, there was not a significant intracellular transient in ZnT3 KO slices, implying that the main source of

Zn^{2+} available for entry after SD derived from presynaptic vesicles under these conditions.

Figure 7B shows a parallel set of experiments, conducted without CaEDTA in the superfusate. In these experiments, signals in wild-type preparations were larger than observed without CaEDTA ($p<0.03$, $n=5$) and a significant postsynaptic transient is demonstrable in ZnT3 KO tissues. It is possible that CaEDTA could contribute to depletion of Zn^{2+} that is released intracellularly due to oxidative processes (Frederickson et al., 2002). However as discussed below, an alternative interpretation of these findings is that (if CaEDTA is not included) there is sufficient contaminating Zn^{2+} to cause significant postsynaptic accumulation after SD, even without the additional source of coordinated release of Zn^{2+} from synaptic vesicles.

2.5 Discussion

General

This study provides the first evidence that SD causes a coordinated release of Zn^{2+} from nerve terminals that depolarize as the SD event propagates across a brain region. Zn^{2+} release following OGD or localized high K^+ stimulation propagated with characteristics entirely consistent with SD, with the wavefront of FluoZin-3 increases occurring coincident with the DC potential shift and progressing at ~2-5 mm/min across the slice. Similar release was observed with two different types of initiating stimuli, suggesting that Zn^{2+} release could contribute to consequences of SD associated with diverse conditions including brain ischemia, trauma and migraine aura. A single SD event did not deplete the pool of releasable Zn^{2+}, and Zn^{2+} released during SD was

accumulated in postsynaptic neurons. Thus repetitive SDs that occur following ischemia could provide a major source of Zn^{2+}, that in turn could contribute to the progression of ischemic brain injury.

Synaptic Zn^{2+} release

Zn^{2+} is accumulated in synaptic vesicles via the ZnT3 transporter (Palmiter et al., 1996b), and evidence has accumulated that Zn^{2+} release is observed following electrical stimulation of synaptic inputs (Frederickson et al., 2005, Sensi et al., 2009), including from studies utilizing extracellular FluoZin-3 in hippocampal slices (Qian and Noebels, 2005, 2006). Despite the fact that ZnT3 KO lack synaptic Zn^{2+}, basic aspects of excitatory transmission and brain function appear relatively normal (Cole et al., 1999, Cole et al., 2001), but a recent report has described cognitive loss in aged ZnT3 KO animals (Adlard et al., 2010). In the present study, SD was still generated in ZnT3 KO tissues and appeared indistinguishable from SD in wild-type tissues, consistent with previous conclusions that glutamateric transmission is not substantially impaired in these tissues. The observation that FluoZin-3 increases due to SD were abolished in ZnT3 KO tissues implies that these signals detected by the indicator are due to Zn^{2+} derived from synaptic vesicles. The pattern of release was also consistent with synaptic release, as largest increases were observed in regions involved in SD and with high synaptic density (stratum oriens and radiatum, Fig 2B).

Although detection of Zn^{2+} in the extracellular space is usually interpreted to imply Zn^{2+} is released and serves as a neurotransmitter/modulator (Qian and Noebels, 2005, Sensi et al., 2009), it has also been suggested that Zn^{2+} is not normally released, but

remains loosely bound to extracellular binding sites exposed during stimulation (Kay, 2003). In the latter case, FluoZin-3 increases could occur as the high affinity indicator in the extracellular space artificially removes Zn^{2+} from binding sites within vesicles, to give the appearance of vesicular release. However the experiments in Figure 6 do not utilize extracellular indicators that might interfere with release, and yet, Zn^{2+} increases were detected in postsynaptic neurons following intracellular indicator injections. The fact that intracellular Zn^{2+} transients were abolished in the ZnT3 KO tissues (Fig 6A) strongly suggests that Zn^{2+} moves across the synapse and accumulates postsynaptically. It is noted that SD is an exceptionally strong stimulus, involving coordinated and likely severe depolarization of a large population of nerve terminals, and the conclusions here may not apply to more moderate synaptic stimuli. However similar conclusions of transsynaptic flux of Zn^{2+} have recently been made from bulk-loading of Newport green into area CA1, and electrical stimulation of afferent fibers (Suh, 2009).

Other potential sources for extracellular Zn^{2+} increases during OGD

A previous study has reported that OGD and subsequent reperfusion in rat hippocampal slices produces slowly-developing and sustained extracellular Zn^{2+} increases (Wei et al., 2004), that appear very different from the abrupt transient increases we describe in the present study following the passage of SD. The different kinetics are consistent with different sources of Zn^{2+}, since in the prior study it was concluded that release was not from synaptic vesicles, but rather was due to oxidative release from intracellular binding proteins. The slice preparation methods and recording conditions between the two studies are quite different, and appear sufficient to prevent SD from

being generated in the earlier study. It is also possible that the differences in recording conditions made oxidative release of Zn^{2+} less prominent in our recording conditions, since significant Zn^{2+} increases were not observed prior to SD in the current study, including in experiments where CaEDTA was not included in the recording media. However it seems likely that in intact brain, extracellular Zn^{2+} levels in peri-infarct areas could increase due to a combination of oxidative release from damaged neurons, together with periodic large synaptic Zn^{2+} release events as SDs sweep through a brain region. Zn^{2+} elevations have been reported in microdialysis studies of forebrain ischemia and middle cerebral artery occlusion in rats (Kitamura et al., 2006b, a), however studies with higher temporal resolution will be required to determine whether there is pulsitile Zn^{2+} release (due to SD) superimposed on an elevated Zn^{2+} baseline in different regions surrounding an ischemic infarct.

Contaminating Zn^{2+}

Zn^{2+} is likely present at low levels in most *in vitro* recording solutions, as a contaminant of salts and also leached from glass and possibly stimulating electrodes (Kay, 2004). One approach to remove the contributions of exogenous Zn^{2+} is to use solutions containing CaEDTA, a chelator which binds Zn^{2+} with much higher affinity than Ca^{2+} (Kay, 2004). CaEDTA reduces background FluoZin-3 fluorescence to a similar degree in wild-type and ZnT3 KO tissues (Supplemental Figure 1), suggesting that synaptically-derived Zn^{2+} does not contribute significantly to basal Zn^{2+} levels in the superfusate. Similar to previous descriptions of electrically-evoked FluoZin-3 transients in hippocampal slice (Qian and Noebels, 2005), removing contaminating Zn^{2+} improved

the signal-noise ratio of FluoZin-3 transients following SD, and was therefore used in most of the experiments described in this study. However, some experiments were conducted without CaEDTA to determine the possible contribution of contaminating Zn^{2+} to postsynaptic Zn^{2+} increases after SD (Fig 6B).

Ca^{2+} loading of CA1 pyramidal neurons is expected to occur following SD via reverse operation of sodium-calcium exchangers, multiple voltage-dependent channels, and possibly other non-selective cation channels (Somjen, 2001, Dietz et al., 2008). Many of these pathways will also flux Zn^{2+} (Weiss et al., 2000), and thus any Zn^{2+} that contaminates the recording solutions is likely to enter postsynaptic neurons following SD, together with Zn^{2+} derived from the coordinated release from synaptic vesicles. Results of Figure 6B, support this conclusion. When CaEDTA was present, significant FluoZin-3 increases were observed in wild-type neurons but abolished in ZnT3 KO tissues. This implies that synaptic release leads to accumulation close to influx sites that is rapid enough to lead to significant influx before displacement of Ca^{2+} from the chelator. When CaEDTA was not used, FluoZin-3 increases were larger, and importantly, were also significant in cells from ZnT3 KO animals. This strongly suggests that contaminating Zn^{2+} can enter during the large postsynaptic depolarization accompanying SD, together with Zn^{2+} derived from synaptic vesicles. These observations may have implications for other studies of Zn^{2+} accumulation, if significant amounts of free Zn^{2+} are present in recording solutions and enter during postsynaptic activation.

Possible consequences of synaptic Zn^{2+} release

Repetitive SD events accompany and appear to contribute to enlargement of ischemic infarcts (Strong et al., 2000, Hartings et al., 2003, Dohmen et al., 2008). Zn^{2+} chelation has been demonstrated to reduce injury following global ischemia (Koh et al., 1996, Calderone et al., 2004, Galasso and Dyck, 2007) and a large body of literature has identified mechanisms coupling Zn^{2+} accumulation to neuronal injury (Choi and Koh, 1998, Weiss et al., 2000, Dineley et al., 2003, Sensi et al., 2009). It is therefore tempting to speculate that large Zn^{2+} increases that occur following SD contribute to the progression of ischemic injuries. Zn^{2+} increases could lead to disruption of mitochondrial function and/or glycolysis (Sheline et al., 2000, Sensi et al., 2009) and serve as an upstream trigger of deleterious neuronal Ca^{2+} overload (Medvedeva et al., 2009, Vander Jagt et al., 2009b).

The fact that the vesicular release pool is not depleted by a single SD event implies that there is either small fractional release and/or effective refilling of vesicular Zn^{2+} pools between repetitive SD events. SDs could therefore provide a source for substantial Zn^{2+} release throughout the post-ischemic period, as repetitive SDs have been recorded for 10s of hours, or even days following experimental or clinical strokes (Strong et al., 2002, Hartings et al., 2003, Dohmen et al., 2008).

While most studies have concentrated on deleterious functions of Zn^{2+} elevations, it is also possible that a bolus of Zn^{2+} release could limit neuronal excitability and prevent damage under some circumstances. For example, Zn^{2+} is an effective inhibitor of NMDA-type glutamate receptors (Sensi et al., 2009) and limiting flux through these channels after SD has passed through a brain region could limit activation of excitotoxic

processes. SD is also known to confer ischemic preconditioning, and Zn^{2+} release during the event might contribute to this process, via mechanisms that have recently been described for Zn^{2+} in cultured cortical neurons (Aras et al., 2009).

From these considerations, opposing effects of Zn^{2+} may underlie conflicting reports of the consequences of Zn^{2+} chelation on infarction following focal ischemia, where CaEDTA has been reported to both significant delay (Lee et al., 2002) and aggravate injury (Kitamura et al., 2006c). It is possible SD-dependent Zn^{2+} release close to an infarct core may contribute to injury, whereas important beneficial effects may be derived from Zn^{2+} released as SD sweeps further through peri-infarct tissue. Understanding the relative contribution of Zn^{2+} to injury at different times following stroke should also be helpful to determine whether extracellular Zn^{2+} levels can be effectively targeted to improve stroke outcome.

2.6 Figure Legends

Figure 2.1. Synaptic Zn^{2+} release during OGD-SD. ***A***: OGD-SD generated a substantial extracellular FluoZin-3 increase in a wild-type C57Bl/6 preparation. Representative traces that show FluoZin-3 response from a region of interest in stratum radiatum, aligned to the electrical (DC) recording of SD by use of an extracellular electrode at the same location. OGD was initiated at the arrow and present throughout the remainder of the experiment. ***B:*** Identical recording conditions as in ***A***, except in a slice from a ZnT3 KO animal, which lacks synaptic Zn^{2+}. SD was still generated under these conditions (as indicated by the sharp DC shift), however the FluoZin-3 response was abolished. ***C***: Mean FluoZin-3 responses generated by OGD-SD from wild-type

C57Bl/6 (n=6) and ZnT3 KO slices (n=5) indicating a synaptic origin of Zn^{2+} release during OGD-SD.

Figure 2.2. Propagation of extracellular Zn^{2+} increases following OGD-SD. ***A***: Spread of FluoZin-3 increases across a wild-type C57Bl/6 slice during OGD-SD. The brightfield image (left panel) shows the orientation of the slice (s.o., stratum oriens; s.p., stratum pyramidale; s.r., stratum radiatum; s.l.m., stratum lacunosum-moleculare). The color panels are a series of 25 images taken at 3s intervals from this slice, showing the spread of the event. Scale bar, 200μm. ***B***: Summary data of regional differences in FluoZin-3 increases generated by OGD-SD from the different hippocampal subfields of 4 wild-type C57Bl/6 preparations. Greatest increases were seen in s.r. and s.o. ***C:*** Coincidence between onset of FluoZin-3 increases and SD in the same population of slices from ***B***. FluoZin-3 and DC recordings are each both normalized to peak responses and plotted against the time to SD onset (t=0), identified from the DC shift.

Figure 2.3. Effects of CaEDTA on FluoZin-3 transients. ***A:*** FluoZin-3 transients in the presence of CaEDTA. Representative trace from a wild-type C57Bl/6 slice showing the change in raw fluorescence during FluoZin-3 and CaEDTA wash-in. FluoZin-3 and CaEDTA were added to the extracellular recording solution (indicated by the arrows) and were present throughout the remainder of the experiment. Addition of CaEDTA reduced the fluorescence of FluoZin-3 and enhanced signal/noise. OGD was then administered for the remainder of the experiment and the left side of the plot shows the FluoZin-3 response ~2min prior to the onset of SD. ***B:*** FluoZin-3 transients in the absence of

CaEDTA. Representative trace showing the wash in of FluoZin-3 without CaEDTA. The fluorescence remains elevated and following OGD administration, a similar FluoZin-3 transient is observed during OGD-SD. ***C:*** CaEDTA significantly accelerated the rate of decay of FluoZin-3 transients, and reduced the ΔF of FluoZin-3 transients during OGD-SD in wild-type tissues (n=5each).

Figure 2.4. Factors influencing the amplitude of extracellular FluoZin-3 transients during OGD-SD. **A:** Comparison of extracellular FluoZin-3 signals generated by strong electrical stimulation of Schaffer collateral inputs (50 Hz, 1 sec), followed by OGD-SD in the same preparation. Data collected from wild-type FVB/N slices, and are normalized to OGD-SD peak responses in each slice (n=6). ***B:*** Autofluorescence changes are small and opposite in sign to FluoZin-3 responses. Signals are from unlabeled preparations (n=6, both groups), excited at the same wavelength (495nm) as utilized in FluoZin-3 studies. Error bars are smaller than the symbol size, and are overlapping for wild-type C57Bl/6 (filled circles) and ZnT3-KO tissues (open squares). **C*:*** Tissue swelling associated with SD is not responsible for difference in FluoZin-3 signals between wild-type and ZnT3 KO preparations. Mean intrinsic optical signals (see methods) from 6 wild-type C57Bl/6 and 6 ZnT3 KO preparations.

Figure 2.5. Zn^{2+} release following high K^+-SD. ***A***: Representative images and plots of extracellular FluoZin-3 and DC recordings during two episodes of high K^+-SD in the same wild-type C57Bl/6 preparation. Similar to OGD-SD, a large propagating FluoZin-3 increase was observed with SD. Repetitive SDs could be generated with the high K^+-

stimulus, and little decrement in the peak amplitude of FluoZin-3 increases was observed. The location of the K^+-ejection pipette and the recording sites are indicated in the brightfield image, and the color panels show the spread of FluoZin-3 increases during the two SD events. Arrows on DC recording indicate when the microinjection of high K^+ was administered. Elapsed time of each montages is ~1 min. ***B***: Summary data showing no significant decrease in peak FluoZin-3 increases with pairs of repetitive high K^+-SD trials (wild-type C57Bl/6, n=5), or when comparing the 1^{st} and 5^{th} SDs in a separate series of experiments. Abolition of FluoZin-3 increases was observed in ZnT3 KO tissues indicating synaptic release of Zn^{2+} during high K^+-SD.

Figure 2.6. Factors influencing the amplitude of FluoZin-3 transients during high K^+-SD. ***A***: Like the situation with OGD-SD, omission of CaEDTA resulted in substantially longer-lasting FluoZin-3 transients and revealed an additional component to the decay phase. Responses to pairs of high K^+-SD (15min interval) are shown in 1mM CaEDTA (blue) and 0mM CaEDTA (red). ***B***: Intrinsic optical signal changes are synchronous with the interruption of the FluoZin-3 decay. The figure shows superimposition of responses from a slice exposed to high-K^+ bathed in FluoZin-3, followed by a washout period and a second exposure to high-K^+ measuring the intrinsic optical signal (IOS) from the same slice (in the absence of FluoZin-3, see Methods). A large delayed swelling response reported by the IOS (peak ~2min) appeared to interrupt the slow decay in the FluoZin-3 signal.

Figure 2.7. Intracellular accumulation of synaptically released Zn^{2+} following high K^+-SD. Each plot shows mean intracellular FluoZin-3 increases from single CA1 neurons loaded with FluoZin-3 via sharp microelectrodes (see Methods). SD was generated by localized high K^+ microinjection, as shown in Figs 5 and 6. ***A***: In CaEDTA, a large increase in intracellular Zn^{2+} accumulation can be seen in wild-type tissues (n=5, pooled C57Bl/6 and FVB/N), but not in ZnT3 KO tissues (n=5). ***B***: When experiments were repeated without CaEDTA, intracellular FluoZin-3 increases were observed in both wild-type (n=5, pooled C57Bl/6 and FVB/N) and ZnT3 KO tissues (n=5) indicating that contaminating extracellular Zn^{2+} also accumulates postsynaptically following high K^+-SD.

Supplemental Figure 2.1: Extracellular FluoZin-3 fluorescence levels are virtually identical in wild-type and ZnT3 KO tissues. Plots show FluoZin-3 wash-in in 11 wild type (filled diamonds) and 10 ZnT3 KO slices (open diamonds). After signals reach a plateau level, CaEDTA (1mM) is added to reduce background signals, and results in near-identical reductions in fluorescence in both wild-type and KO slices.

Supplemental Figure 2.2: ***A:*** Optical and electrical (DC) recordings from a representative slice subjected to five rounds of high K^+-SD, where FluoZin-3 was present during the 1st (a) and 5th (e) trial. Following the wash out of FluoZin-3 and CaEDTA, three high K+-SDs were elicited (b-d), confirmed by sharp negative DC shifts. Following the 4th SD, FluoZin-3 and CaEDTA were washed back in, and a 5th high K^+-SD was generated, showing little decrement in the peak response compared to the 1st

FluoZin-3 response. ***B:*** Mean data showing the kinetics of the 1st and 5th FluoZin-3 responses to high K^+-SD (n=5 each). A small, but not significant increase in recovery rate was observed in the 5th response. ***C:*** Mean data from two different experiments comparing the kinetics of the 2nd and 5th responses (n=5 each). A lack of increased recovery was observed when comparing the 5th to the 2nd response, indicating that the kinetics of the response is not increasing with each SD.

Figure 2.1

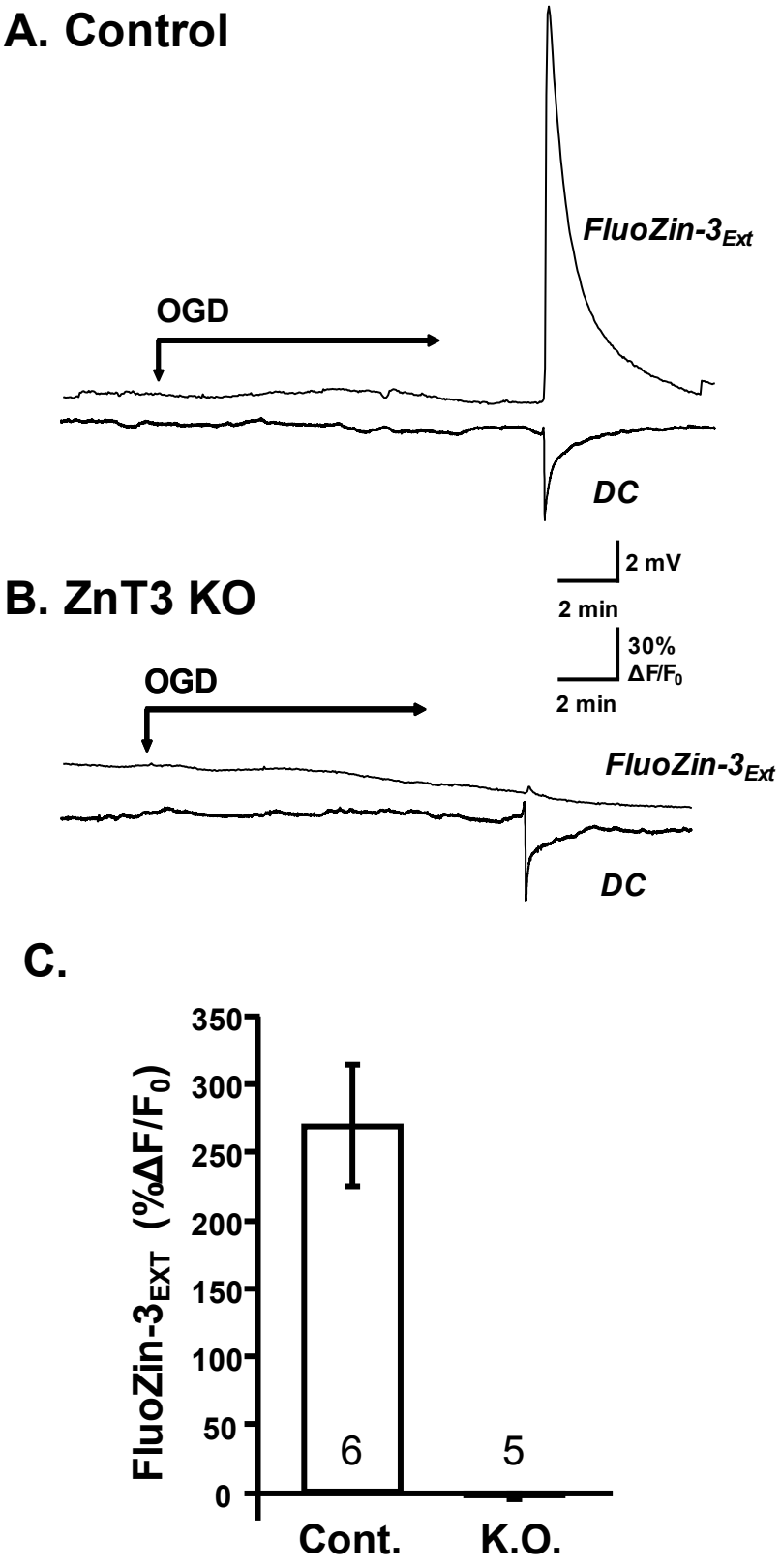
A. Control
FluoZin-3Ext
OGD
DC
2 mV
2 min
B. ZnT3 KO
30%
ΔF/F0
2 min
OGD
FluoZin-3Ext
DC
C.
FluoZin-3EXT (%ΔF/F0)
350
300
250
200
150
100
50
0
6
5
Cont.
K.O.

Figure 2.2

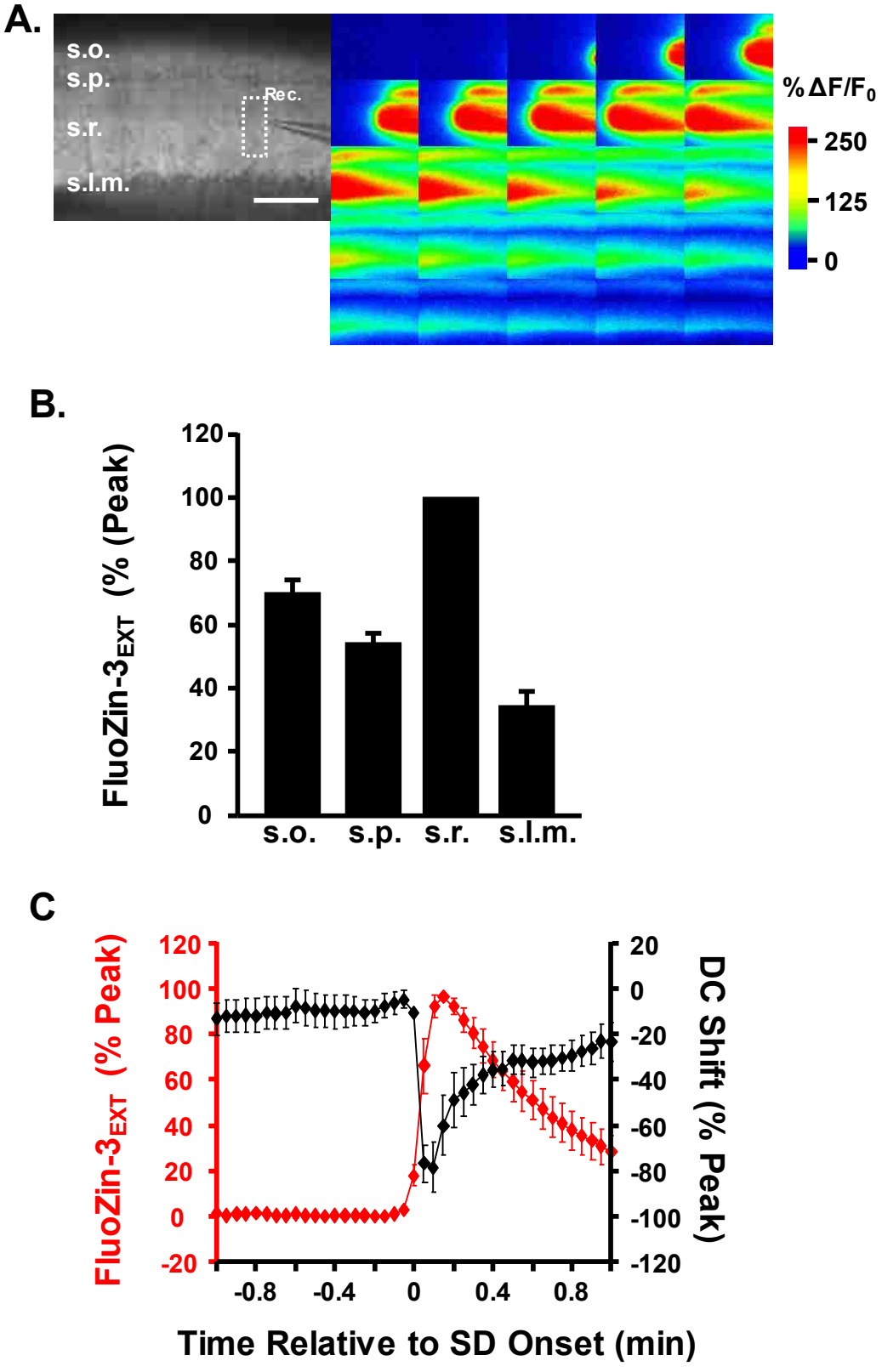
A.
s.o.
s.p.
s.r.
s.l.m.
Rec.
%ΔF/F0
250
125
0
B.
FluoZin-3EXT (% (Peak)
120
100
80
60
40
20
0
s.o.
s.p.
s.r.
s.l.m.
C
FluoZin-3EXT (% Peak)
DC Shift (% Peak)
120
100
80
60
40
20
0
-20
20
0
-20
-40
-60
-80
-100
-120
-0.8
-0.4
0
0.4
0.8
Time Relative to SD Onset (min)

Figure 2.3

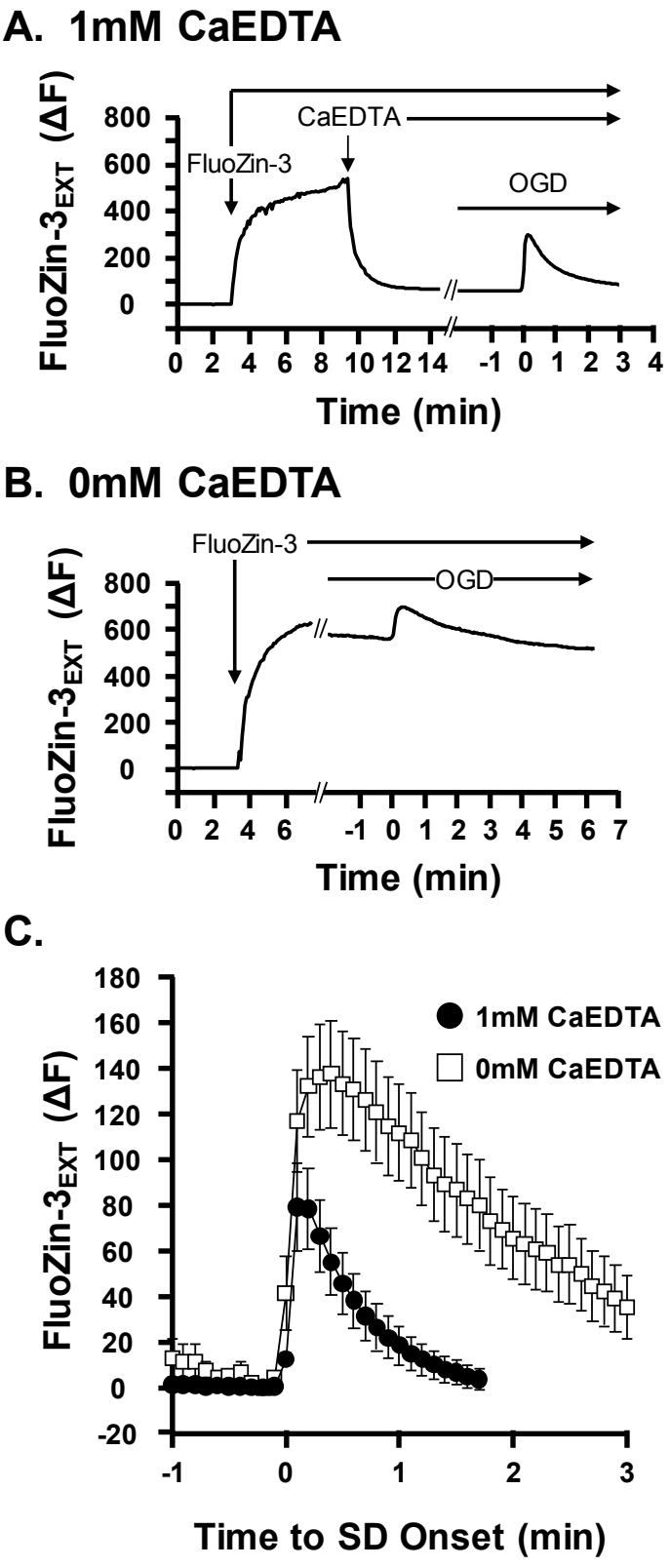
A. 1mM CaEDTA
FluoZin-3
CaEDTA
OGD
FluoZin-3EXT (ΔF)
800
600
400
200
0
0 2 4 6 8 10 12 14 -1 0 1 2 3 4
Time (min)
B. 0mM CaEDTA
FluoZin-3
OGD
FluoZin-3EXT (ΔF)
800
600
400
200
0
0 2 4 6 -1 0 1 2 3 4 5 6 7
Time (min)
C.
1mM CaEDTA
0mM CaEDTA
FluoZin-3EXT (ΔF)
180
160
140
120
100
80
60
40
20
0
-20
-1 0 1 2 3
Time to SD Onset (min)

Figure 2.4

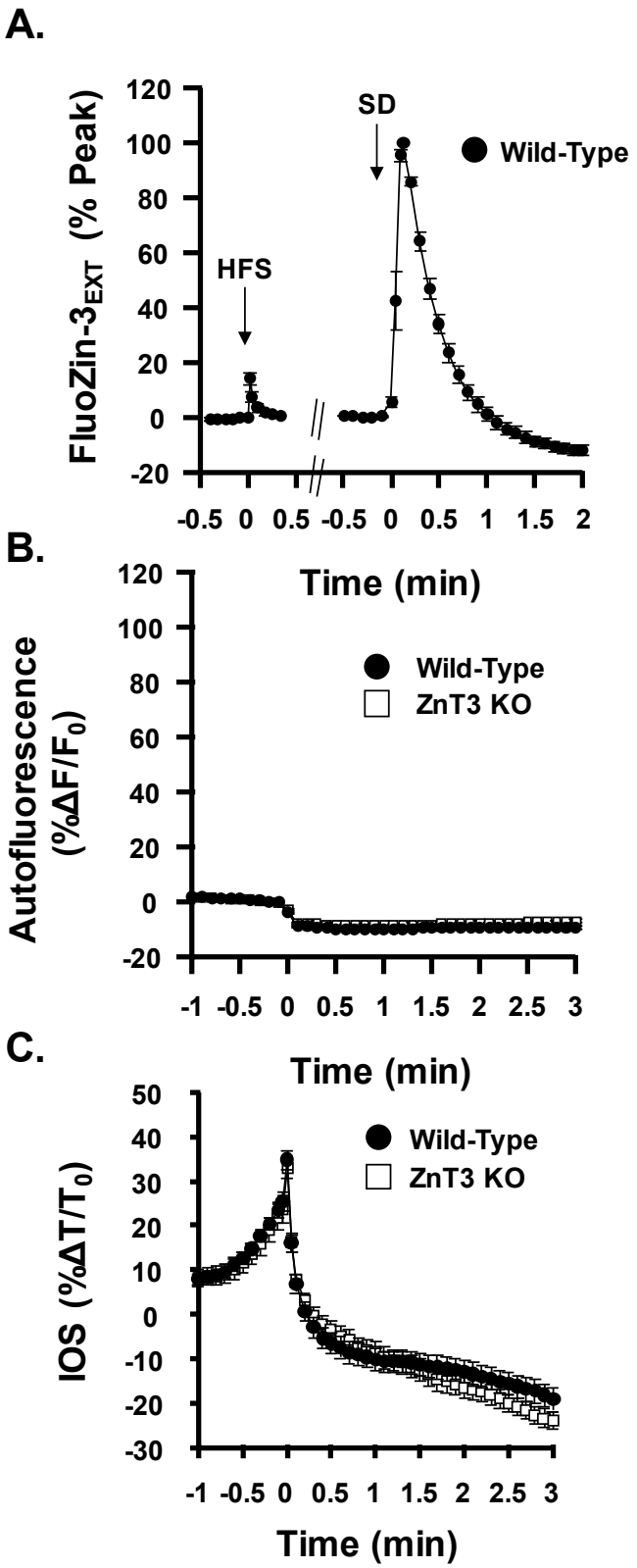
A.
FluoZin-3EXT (% Peak)
HFS
SD
Wild-Type
Time (min)
B.
Autofluorescence (%ΔF/F0)
Wild-Type
ZnT3 KO
Time (min)
C.
IOS (%ΔT/T0)
Wild-Type
ZnT3 KO
Time (min)

Figure 2.5

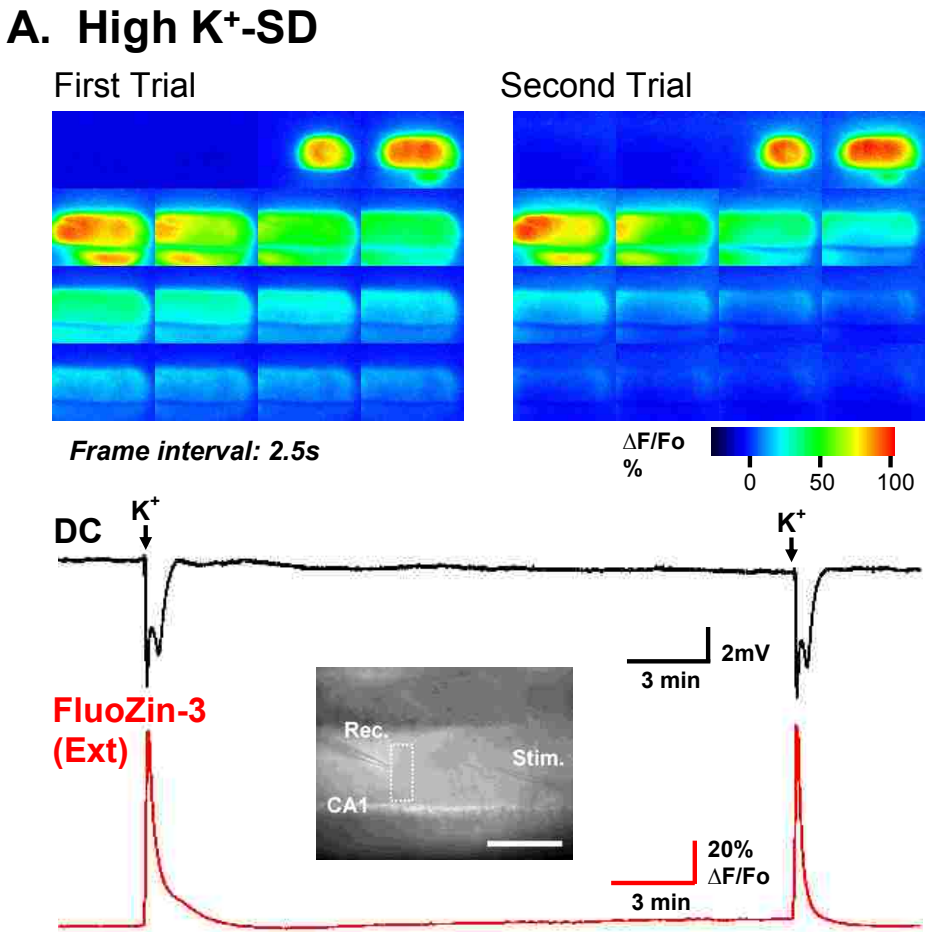
A. High K+-SD
First Trial
Second Trial
Frame interval: 2.5s
ΔF/Fo %
0
50
100
DC
K+
K+
2mV
3 min
FluoZin-3 (Ext)
Rec.
Stim.
CA1
20% ΔF/Fo
3 min

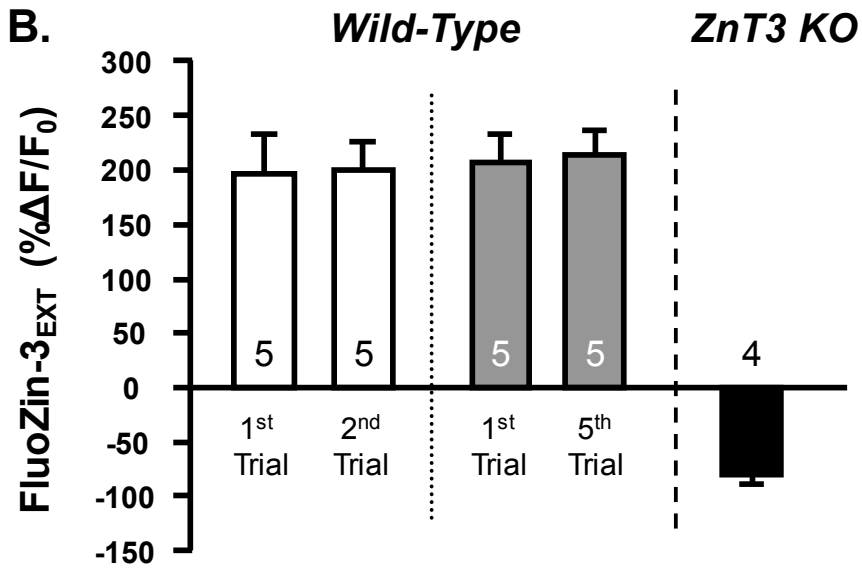
B.
Wild-Type
ZnT3 KO
FluoZin-3EXT (%ΔF/F0)
300
250
200
150
100
50
0
-50
-100
-150
5
5
5
5
4
1st Trial
2nd Trial
1st Trial
5th Trial

Figure 2.6

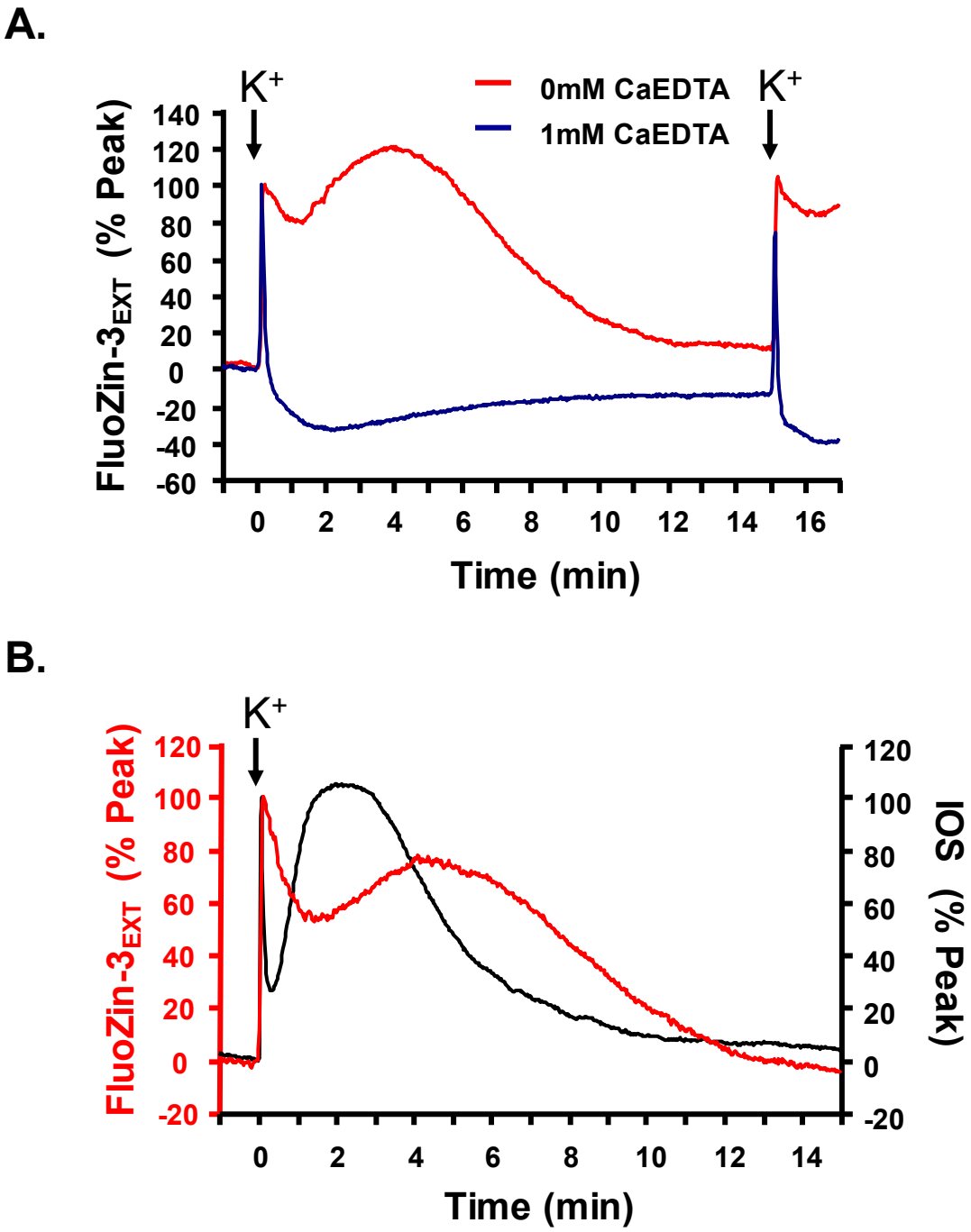
A.
K+
0mM CaEDTA
1mM CaEDTA
K+
FluoZin-3EXT (% Peak)
140
120
100
80
60
40
20
0
-20
-40
-60
0
2
4
6
8
10
12
14
16
Time (min)
B.
K+
FluoZin-3EXT (% Peak)
120
100
80
60
40
20
0
-20
IOS (% Peak)
120
100
80
60
40
20
0
-20
0
2
4
6
8
10
12
14
Time (min)

Figure 2.7

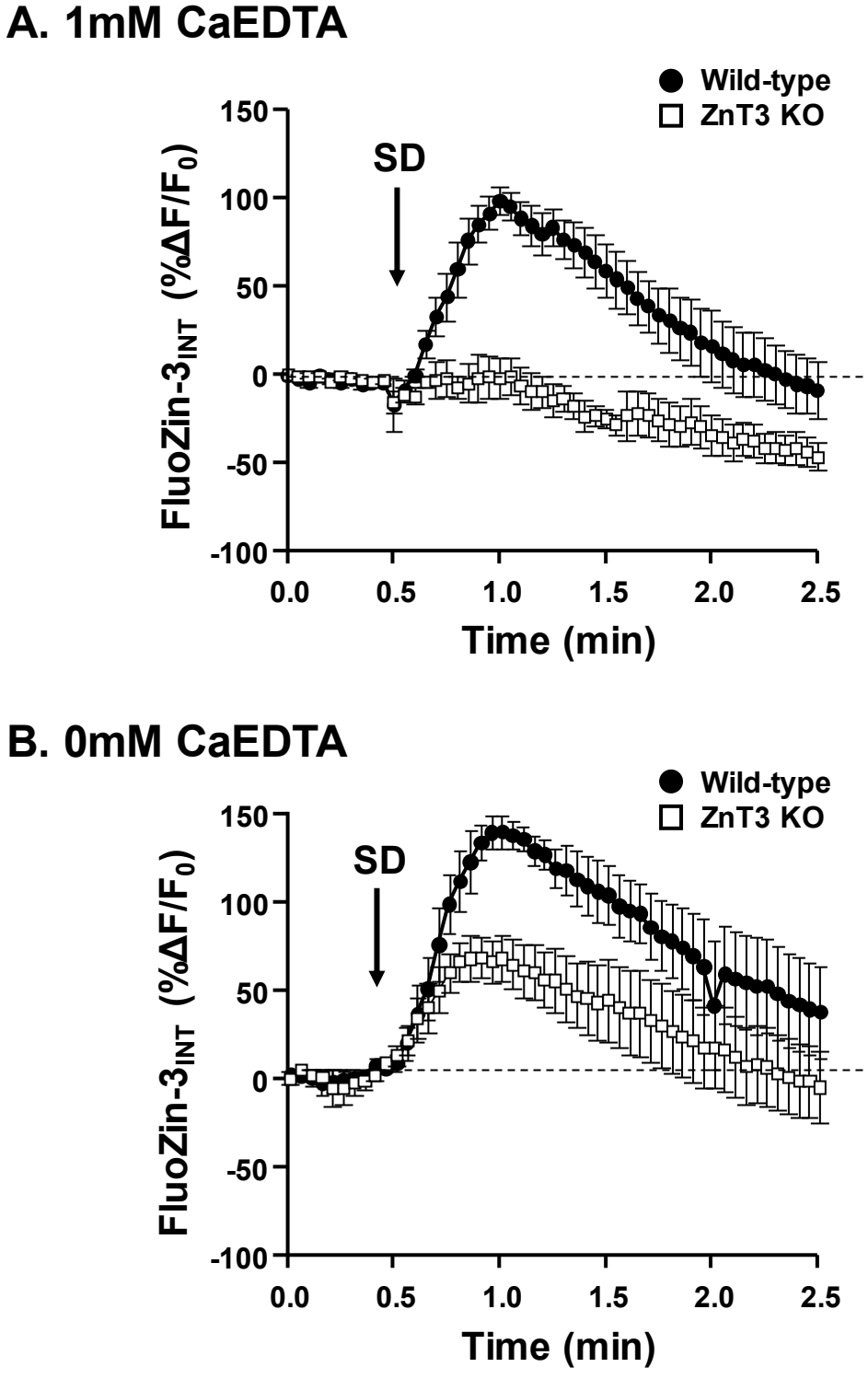
A. 1mM CaEDTA
Wild-type
ZnT3 KO
SD
FluoZin-3INT (%ΔF/F0)
150
100
50
0
-50
-100
0.0
0.5
1.0
1.5
2.0
2.5
Time (min)
B. 0mM CaEDTA
Wild-type
ZnT3 KO
SD
FluoZin-3INT (%ΔF/F0)
150
100
50
0
-50
-100
0.0
0.5
1.0
1.5
2.0
2.5
Time (min)

Supplementary Figure 2.1

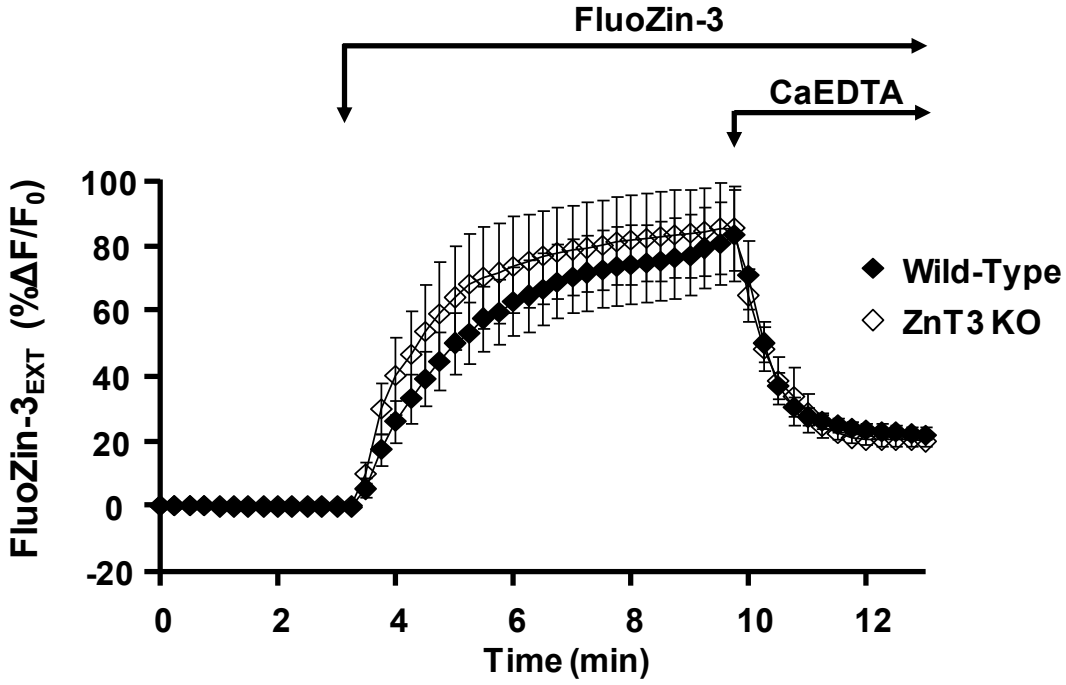

Supplementary Figure 2.2

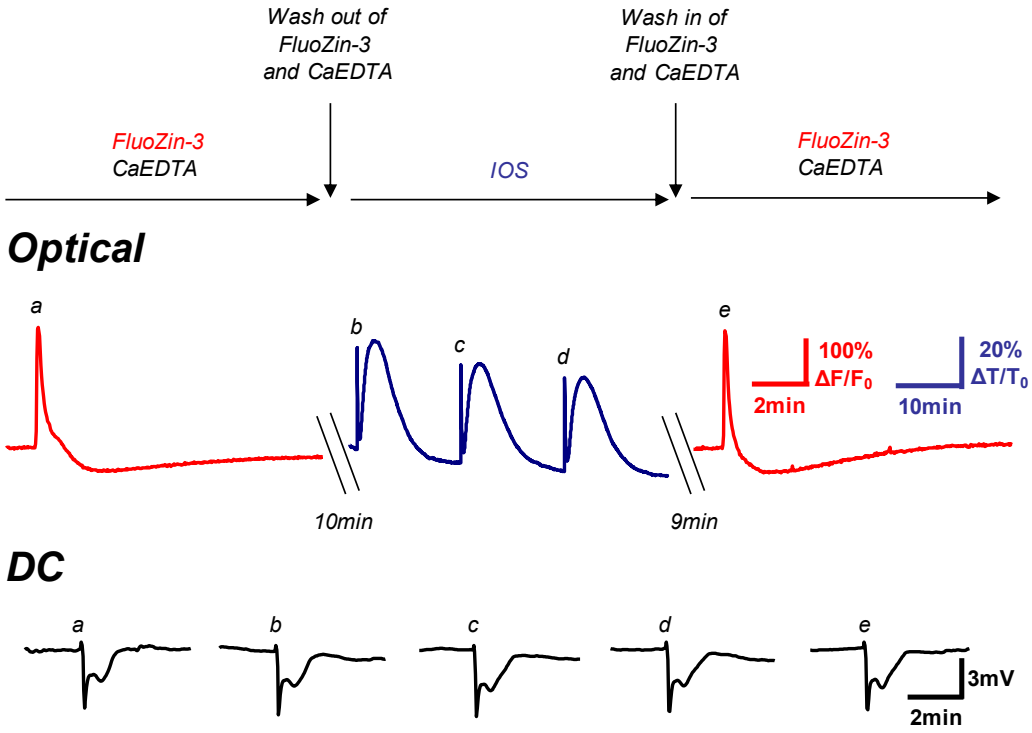

Chapter 3: Zn^{2+} Chelation Improves Recovery by Delaying Spreading Depression-Like Events

Russell E. Carter[1], John H. Weiss[2], C. William Shuttleworth[1]

[1]Department of Neurosciences

University of New Mexico, Albuquerque, NM, USA

[2]Department of Neurology, Anatomy, and Neurobiology

University of California, Irvine, Irvine, CA, USA

(Published in NeuroReport 2010; 21(16):1060-1064)

3.1 Abstract

We previously reported Zn^{2+} chelation improved recovery of synaptic potentials after transient oxygen and glucose deprivation in brain slices. Such an effect could be due to reduced accumulation of Zn^{2+} in postsynaptic neurons, or could also be due to prevention of the onset of spreading depression-like events. A combination of optical and electrical recording was used here to demonstrate that Zn^{2+} chelation is effective because it delays spreading depression-like events. If the duration of oxygen/glucose deprivation was sufficient to generate a spreading depression-like event, irrecoverable Ca^{2+}-dependent loss of synaptic potentials occurred, regardless of Zn^{2+} availability. These results identify a key mechanism underlying protective effects of Zn^{2+} chelation, and emphasize the importance of evaluating spreading depression-like events in studies of neuroprotection.

3.2 Introduction

Transient removal of oxygen and glucose is widely used as an *in vitro* model of aspects of ischemic brain injury (Lipton, 1999). When applied to brain slice preparations, relatively short periods of oxygen and glucose deprivation are used (often 10 min) and neuronal viability can be continuously monitored from the amplitude of evoked excitatory postsynaptic potentials (EPSPs). An initial suppression of EPSPs occurs within minutes due to accumulation of adenosine and A1 receptor activation (Dale and Frenguelli, 2009), however this suppression is readily reversible following restoration of metabolic substrates. Longer periods of substrate removal can lead to persistent loss of EPSPs which is indicative of neuronal injury (Kass and Lipton, 1982).

We recently showed that chelation of Zn^{2+} significantly enhanced recovery of EPSPs after a fixed 10 min period of oxygen and glucose deprivation in the hippocampal CA1 region of murine brain slices (Medvedeva et al., 2009). Other studies have also implicated Zn^{2+} accumulation in injury following substrate removal in rat hippocampal slices (Stork and Li, 2009). The brain contains a large amount of Zn^{2+} (Frederickson et al., 2000) and while levels of this cation are normally tightly regulated within neurons, excessive Zn^{2+} accumulation is toxic to neurons (Choi and Koh, 1998, Bonanni et al., 2006). The beneficial effects of Zn^{2+} chelation could be due to preventing deleterious actions of Zn^{2+} on neuronal mitochondria or other intracellular targets in CA1 neurons (Medvedeva et al., 2009).

An additional possibility is that Zn^{2+} chelation interferes with the onset of spreading depression (SD)-like events in the brain slice model. SD is a coordinated depolarization of neurons and glia that can occur in a variety of experimental and pathological conditions including ischemia (Somjen, 2001), and a form of SD can be readily initiated in brain slices by oxygen and glucose deprivation (Dietz et al., 2008) (termed here OGD-SD). If metabolic substrates are not immediately available to restore ionic gradients, OGD-SD causes rapid neuronal injury (Somjen, 2001), and these responses may therefore be primary causes of neuronal injury in many slice ischemia studies (Obeidat et al., 2000). We recently showed that accumulation of Zn^{2+} can contribute to the initiation of SD-like events in brain slices (Dietz et al., 2008), and in the present study have examined whether delay of these events by Zn^{2+} chelation may be sufficient to explain beneficial effects of this intervention.

3.3 Materials and Methods

All procedures were performed in accordance with the National Institutes of Health guidelines for the humane treatment of laboratory animals and the Institutional Animal Care and Use Committee at the University of New Mexico. Methods for preparation of brain slices (350μm, coronal) were as described previously (Dietz et al., 2008) using C57Bl/6 mice at 4-6 weeks of age of either sex. Experiments were performed on submerged slices, continuously superfused at 2 ml/min at either 32 or 35°C (see Results). OGD-SD was monitored by intrinsic optical signals generated from transmission of >590nm light. Extracellular measurements of slow DC potential shifts or field EPSPs (fEPSPs) evoked by Schaffer collateral stimulation were made from stratum radiatum of hippocampal area CA1. Electrical stimuli (70μs, 0.1Hz) were at a stimulus intensity that generated a response 70% of maximal. The superfusion system allowed for rapid (~0.5min) bath solution exchange after OGD-SD.

Superfusion buffer contained (in mM): 126 NaCl, 3 KCl, 1.25 NaH_2PO_4, 1 $MgSO_4$, 26 $NaHCO_3$, 2 $CaCl_2$, and 10 glucose, equilibrated with 95%O_2/5%CO_2. Ice-cold cutting solution contained (in mM): 3 KCl, 1.25 NaH_2PO_4, 6 $MgSO_4$, 26 $NaHCO_3$, 0.2 $CaCl_2$, 10 glucose, 220 sucrose, and 0.43 ketamine, equilibrated with 95% O_2/ 5% CO_2. For oxygen and glucose deprivation, buffer was modified by equimolar replacement of glucose with sucrose and equilibrated with 95% N_2/ 5% CO_2. Nominally Ca^{2+}-free solutions were prepared by equimolar replacement of Ca^{2+} with Mg^{2+}. *N,N,N',N'*-tetrakis(2-pyridylmethyl)-ethylenediamine (TPEN) was obtained from Invitrogen and all other reagents were obtained from Sigma. TPEN was prepared fresh daily as a 20mM stock in 0.25% DMSO. Data are reported as mean±standard error of the

mean. Significant differences between group data were evaluated using unpaired Student's t-tests.

3.4 Results

Irreversible loss of synaptic potentials following spreading depression-like events

Figure 1A shows the propagation of oxygen/glucose deprivation-induced spreading depression (OGD-SD) as assessed by intrinsic optical imaging. A propagating band of increased light transmission is a consequence of tissue swelling that accompanies the coordinated depolarization (Andrew et al., 1999). In this example, OGD-SD propagated from left to right at 3.03 mm/min and evoked field potentials were abolished coincident with passage of the SD wave front past the recording site. Figure 1B shows mean data from five such experiments. The mean onset time to OGD-SD was 12.7±0.2min and normal buffer was reintroduced into the chamber within 30 seconds of the passage of OGD-SD past the microelectrode recording site. OGD caused an initial loss of fEPSPs (to 7.8±1.0% baseline), and a transient period of recovery then occurred ~4min prior to the onset of OGD-SD (peak response of 51.8±7.3% baseline). This transient recovery of fEPSPs has been described during anoxia and is thought to be due to the accumulation of extracellular K^+ (Sick et al., 1987). Coincident with passage of OGD-SD, fEPSPs were abolished (Fig. 1C), and even though normal buffer was restored quickly following the event, there were no signs of fEPSP recovery within the time frame of these experiments.

In a separate set of experiments (n=7), slices exposed to brief episodes of OGD (7 min) that were not sufficient to produce SD were compared with exposures sufficient to

generate OGD-SD. The short exposures produced a transient loss of fEPSPs (6.5±0.8% baseline) that recovered to near baseline levels (90.1±2.3%) after 15 min restoration of normal buffer. When the same slices were then subjected to OGD-SD (mean onset time of 10.2 ± 0.3min) an irrecoverable loss of fEPSPs (to 3.5±0.5% baseline) was observed, consistent with results shown in Figure 1B. These results are consistent with the hypothesis that the deleterious consequences of SD are responsible for the persistent loss of field potentials following transient OGD exposures.

Delay of spreading depression-like events by Zn^{2+} chelation

We recently showed that chelation of Zn^{2+} with TPEN ($KD_{Zn}=10^{-15.6}M$; $KD_{Ca}=10^{-4.4}M$ (Arslan et al., 1985)) can inhibit the initiation of some forms of spreading depression in hippocampal slices (Dietz et al., 2008). That prior study identified conditions (including activation of A1 receptors with exogenous application of an A1 receptor agonist) where Zn^{2+} chelation was sufficient to prevent the onset of spreading depression generated by the Na^+/K^+/ATPase inhibitor, ouabain. It was also shown that OGD-SD could be delayed or prevented by Zn^{2+} chelation (Dietz et al., 2008). We confirmed a small but significant delay in OGD-SD onset using a combination of intrinsic optical recording and DC recordings of slow potential shifts (Somjen, 2001) under the recording conditions of the current study (no A1 agonists) (12.0±0.5 vs 14.5±0.4 min, control and TPEN, respectively, n=6, $p<0.001$). This difference appeared potentially large enough to explain beneficial effects of Zn^{2+} chelation, depending on the duration of the challenge with oxygen and glucose removal.

Lack of injury if Zn^{2+} chelation prevents OGD-SD during transient challenges

From the results above, a set duration (13min) of oxygen and glucose removal was chosen as a test challenge, to test whether beneficial effects of TPEN were due to preventing OGD-SD onset. With 13 min challenges, OGD-SD should always be generated in vehicle controls, while TPEN-exposed preparations should never experience OGD-SD during these exposures. Indeed, as shown in Figure 2, a 13min oxygen and glucose removal challenge in the presence of TPEN (50μM, 20min pre-exposure, n=5, open triangles) produced only a transient loss of fEPSPs (to 8.9±1.2%), followed by full recovery of fEPSPs to pre-stimulus levels (to 109.9±13.5% baseline). This significant protection was due to TPEN, since in matched vehicle controls, OGD-SD was generated by this 13 min exposure and resulted in irrecoverable loss of synaptic potentials (filled circles).

A separate set of studies was conducted to monitor fEPSP responses to OGD in the presence of TPEN. Figure 2C shows that if SD is allowed to occur, there is no significant benefit from Zn^{2+} chelation. In these experiments, OGD was maintained until SD occurred in the presence of TPEN (onset 14.0±0.4 min, n=5) and rapid restoration of normal buffer did not restore synaptic function (6.0±0.5% at 60 min). Together, these results imply that preventing Zn^{2+} accumulation is not sufficient to prevent neuronal injury following OGD-SD, but Zn^{2+} chelation can completely prevent neuronal injury by preventing the onset of SD during transient OGD exposures.

Contribution of Ca^{2+} to persistent neuronal injury after OGD-SD

A final set of experiments confirmed that excessive Ca^{2+} (rather than Zn^{2+}) accumulation following OGD-SD is the most likely contributor to neuronal injury following OGD-SD in slice (Fig 3). Effects of Ca^{2+} removal were tested by exposure to modified buffer lacking added Ca^{2+} and without addition of any chelators (nominally Ca^{2+}-free, estimated free Ca^{2+} ~ 4μM (Chinopoulos et al., 2007)). Under the recording conditions used in studies above (300μm slices at 32°C), SD could not be generated by OGD in nominally Ca^{2+}-free buffer (n=3), and alternative recording conditions were identified (350μm slices at 35°C) that allowed reliable generation of OGD-SD in nominally Ca^{2+}-free buffer. Ca^{2+} was removed 5min prior to onset of OGD exposures, and Ca^{2+}-free conditions maintained for a further 5 min after OGD exposure. Under these conditions, SD was generated at 5.5±0.4min (n=5), compared with 6.4±0.6min (n=5) in normal buffer. After OGD-SD no recovery of fEPSPs was observed in slices with Ca^{2+} present throughout, but a substantial recovery of fEPSP amplitude (to 69.2±8.2%) was seen in slices where Ca^{2+} was not available during the passage of SD. These results contrast with the lack of effect of Zn^{2+} removal in slices where SD was allowed to occur (Fig 2C), and confirm that Ca^{2+} (rather than Zn^{2+}) is a main contributor to persistent loss of synaptic activity following SD events triggered by OGD.

3.5 Discussion

Zn^{2+} accumulation is strongly implicated in ischemic neuronal injury, and there is significant interest in understanding the cellular and molecular mechanisms underlying Zn^{2+} toxicity (Choi and Koh, 1998, Weiss et al., 2000, Sensi et al., 2009). Studies of

dispersed neuronal cultures have identified pathways that contribute to Zn^{2+} toxicity during excessive glutamate receptor activation or challenge with oxygen and glucose deprivation (OGD) (Sensi et al., 1999, Dineley et al., 2002, Yin et al., 2002, Dineley et al., 2008). When OGD is undertaken in brain slices, deleterious Zn^{2+} dependent mechanisms that have been identified in dispersed cultures may be activated in neurons. However in brain slices, OGD also triggers a profound depolarization event that propagates slowly through the well-organized structure of the slice (Obeidat et al., 2000, Somjen, 2001, Dietz et al., 2008). These events share many similarities with the phenomenon of spreading depression (SD), and cannot be generated in dispersed cultures, as the very large extracellular volume prevents glutamate and K^+ levels accumulating to threshold concentrations for maintaining a feed-forward depolarization. The results of the present study indicate that beneficial effects of Zn^{2+} chelation in the brain slice OGD model can be attributed to prevention of the onset of OGD-SD. Other deleterious effects of intracellular Zn^{2+} accumulation may be activated in CA1 neurons during the OGD exposure, however preventing these effects is not sufficient to prevent the injury caused by massive Ca^{2+} accumulation if SD occurs during this challenge.

It is not fully understood how Zn^{2+} contributes to the onset of OGD-SD, but mitochondrial disruption is one possibility (Dietz et al., 2008, 2009, Medvedeva et al., 2009). As a note, relatively high concentrations (0.4%) of the vehicle used here (DMSO) have been reported to delay the onset of SD induced by hypoxia (Hulsmann et al., 1999). However no delay was observed with the lower DMSO concentrations used here (0.25%, data not shown) and since this vehicle was included all experiments, DMSO effects are not expected to explain the delay of SD and subsequent recovery seen by TPEN.

In previous work, removal of Ca^{2+} following SD induced by OGD restored membrane potential (Tanaka et al., 1999). Consistent with those results, removal of Ca^{2+} during OGD-SD allowed for partial recovery of fEPSPs, indicating that the Ca^{2+} overload during OGD-SD (Dietz et al., 2008) is primarily responsible for the persistent depression of synaptic activity. The residual injury could be due to incomplete removal of Ca^{2+}, but since our previous study showed an enhanced recovery after OGD with combined removal of Zn^{2+} and Ca^{2+} (Medvedeva et al., 2009), we attempted to determine whether the combined removal would enhance synaptic recovery following SD. However under these slice and recording conditions, we were not able to induce OGD-SD with both Ca^{2+} and Zn^{2+} removal, as confirmed by a lack of a DC shift and intrinsic optical signals (n=6, data not shown). This is in agreement with our prior report under different recording conditions and conclusion that both cations contribute to SD initiation (Dietz et al., 2008, 2009). However, because of this block of OGD-SD it is currently unknown whether Zn^{2+} accumulation following SD can contribute with Ca^{2+} to neuronal injury. It is possible that in preparations that do not undergo SD, postsynaptic Zn^{2+} accumulation contributes to different forms of injury.

3.6 Conclusion

These results suggest that delay of the onset of OGD-SD can be sufficient to explain the beneficial effects of Zn^{2+} chelation in a slice model of ischemia. Such effects could be important for limiting the spread of ischemic injury *in vivo*. Additional deleterious effects of Zn^{2+} accumulation may also contribute significantly to injury, in

other ischemia models or conditions where massive ionic disruptions associated with SD events are not the predominant causes of injury.

3.7 Figure Legends

Figure 3.1: Onset of persistent synaptic inhibition coincident with OGD-SD. ***A.*** Monitoring propagation of SD by intrinsic optical imaging. Representative bright-field image (showing placement of electrodes) and montage illustrating OGD-SD propagation across CA1 hippocampal subfield. Scale bar 200μm, image interval 1.5s, advancing wave front indicated by bright band. ***B.*** Loss of fEPSPs during OGD. OGD was continued in each slice until SD was visualized, and then the superfusate was rapidly switched back to normal buffer. A transient recovery of fEPSPs occurred immediately prior to OGD-SD, and was followed by persistent (>1hr) inhibition (n=5). *Inset:* Representative fEPSP traces at time courses depicted on mean data plot. ***C:*** Correlation between OGD-SD onset and loss of fEPSPs ($r^2 = 0.99$).

Figure 3.2: Delay of OGD-SD by TPEN was responsible for recovery of fEPSPs. ***A.*** In these experiments, the duration of OGD was fixed (13 min), so that under vehicle conditions OGD always produced SD (n=5, circles) but the OGD duration was never long enough to generate SD in TPEN slices (50μM, n=5, triangles). fEPSPs were abolished in control, but fully recovered in TPEN. Lower panels show representative traces of fEPSPs during time points indicated in the plot. ***B.*** In contrast, if OGD was maintained until SD was generated in TPEN slices (average 14.03 ± 0.38 min, n=5) no

recovery of fEPSPs was observed. *Inset:* Representative fEPSPs traces at times indicated on mean plot.

Figure 3.3: Ca^{2+} influx was responsible for irrecoverable synaptic loss following OGD-SD. ***A.*** Slices superfused with Ca^{2+}-free buffer during OGD (and 5min pre-, post-exposure) showed partial recovery of fEPSPs even after the generation of OGD-SD (squares), when compared with paired control slices which showed irrecoverable fEPSP loss (n=5, both groups). ***B.*** Representative fEPSP traces taken from time points indicated on mean plot.

Figure 3.1

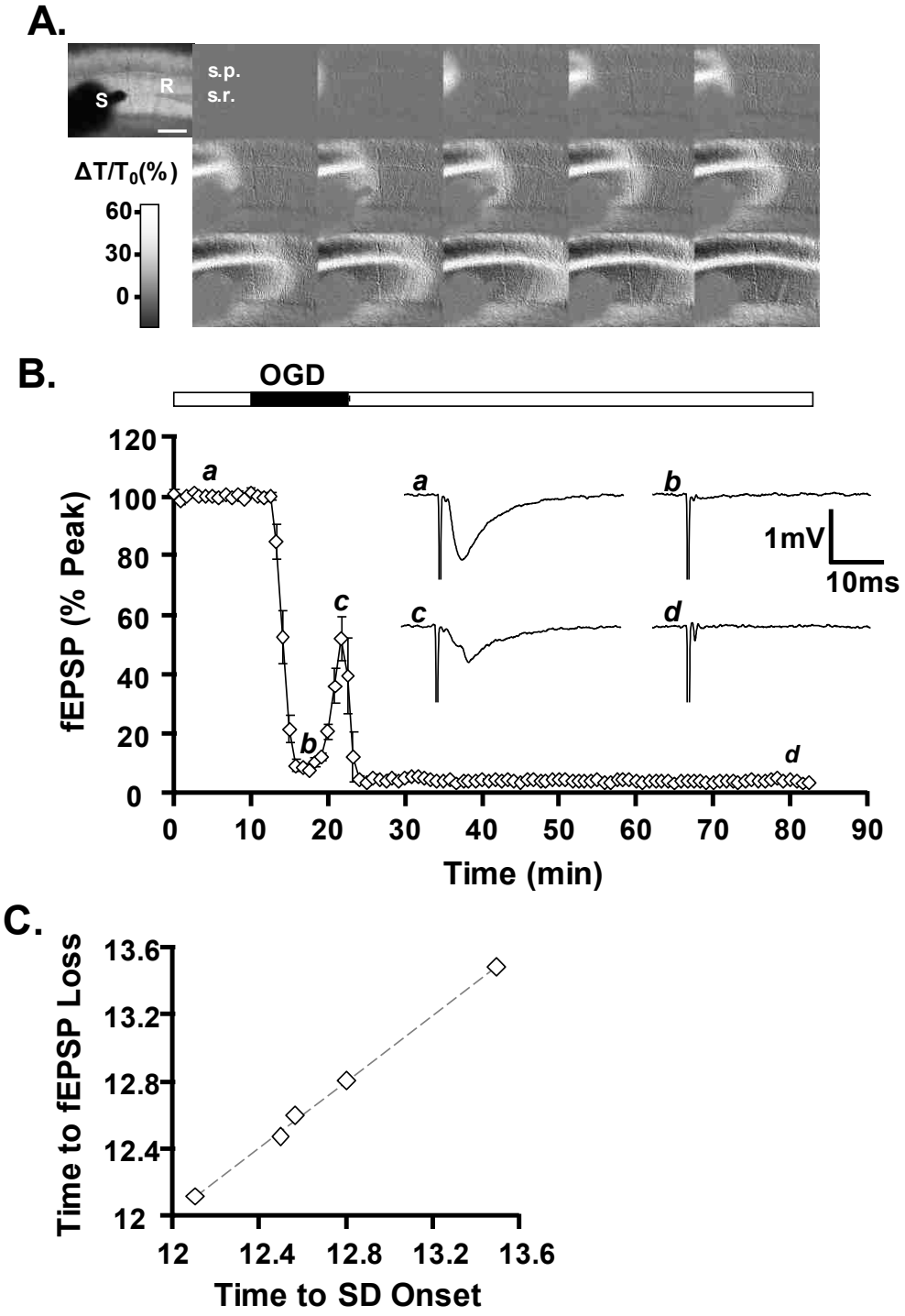
A.
S
R
s.p.
s.r.
ΔT/T0(%)
60
30
0
B.
OGD
fEPSP (% Peak)
120
100
80
60
40
20
0
a
b
c
d
1mV
10ms
0
10
20
30
40
50
60
70
80
90
Time (min)
C.
Time to fEPSP Loss
13.6
13.2
12.8
12.4
12
12
12.4
12.8
13.2
13.6
Time to SD Onset

Figure 3.2

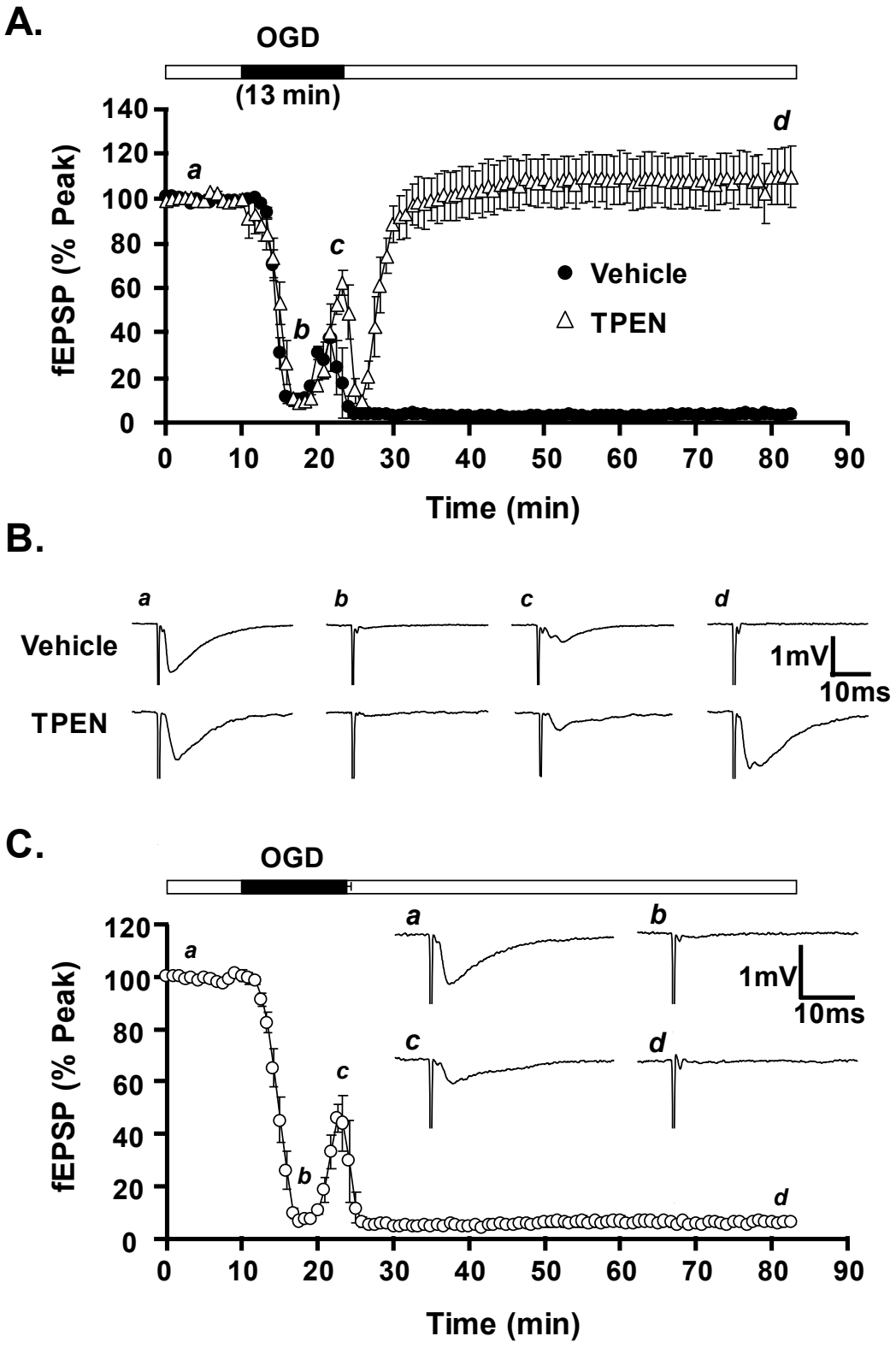
A.
OGD
(13 min)
fEPSP (% Peak)
Time (min)
Vehicle
TPEN
a
b
c
d
B.
Vehicle
TPEN
1mV
10ms
C.
OGD
fEPSP (% Peak)
Time (min)
1mV
10ms

Figure 3.3

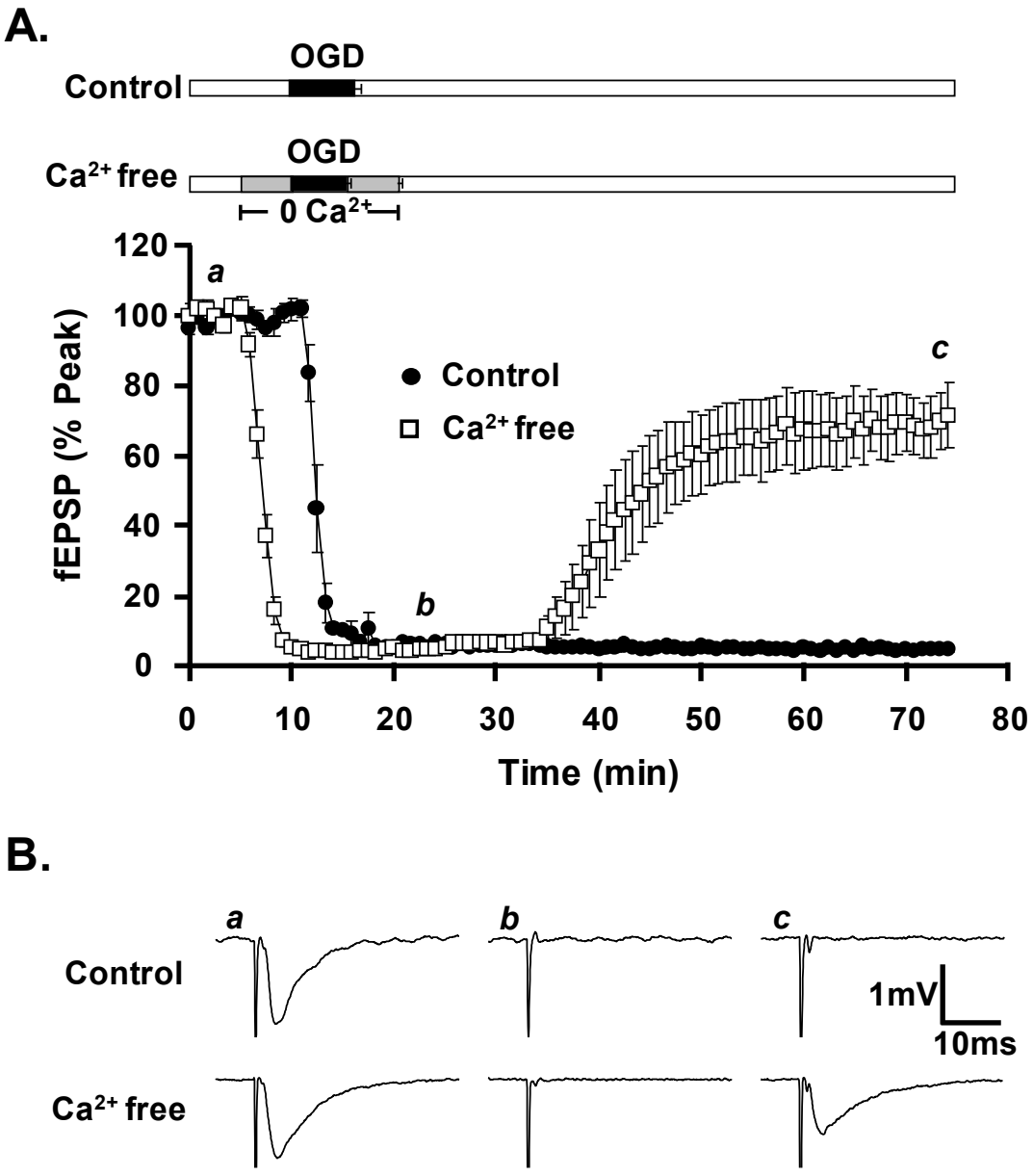
A.
OGD
Control
OGD
Ca2+ free
0 Ca2+
120
100
80
60
40
20
0
fEPSP (% Peak)
a
b
c
Control
Ca2+ free
0
10
20
30
40
50
60
70
80
Time (min)
B.
a
b
c
Control
1mV
10ms
Ca2+ free

Chapter 4: Intracellular Zn^{2+} Accumulation Enhances Suppression of Synaptic Activity Following Spreading Depolarization

Russell E. Carter[1], Jessica L. Seidel[1,3], Britta E. Lindquist[1],

Christian T. Sheline[2], and C. William Shuttleworth[1]

[1]Department of Neurosciences,

University of New Mexico School of Medicine,

Albuquerque, NM, USA

[2]Department of Ophthalmology and the Neuroscience Center of Excellence LSU,

Health Sciences Center, New Orleans, LA, USA

[3]Current Address: Radiology, Stroke and Neurovascular Regulation Laboratory,

Massachusetts General Hospital, Harvard Medical School,

Charlestown, MA, USA

(Published in Journal of Neurochemistry 2013, doi:10.1111/jnc. 12237)

4.1 Abstract

Spreading depolarization (SD) is a feed-forward wave that propagates slowly throughout brain tissue and recovery from SD involves substantial metabolic demand. Presynaptic Zn^{2+} release and intracellular accumulation occurs with SD, and elevated intracellular Zn^{2+} ($[Zn^{2+}]_i$) can impair cellular metabolism through multiple pathways. We tested here whether increased $[Zn^{2+}]_i$ could exacerbate the metabolic challenge of SD, induced by KCl, and delay recovery in acute murine hippocampal slices. $[Zn^{2+}]_i$ loading prior to SD, by transient $ZnCl_2$ application with the Zn^{2+} ionophore pyrithione (Zn/Pyr), delayed recovery of field excitatory post-synaptic potentials (fEPSPs) in a concentration-dependent manner, prolonged DC shifts, and significantly increased extracellular adenosine accumulation. These effects could be due to metabolic inhibition, occurring downstream of pyruvate utilization. Prolonged $[Zn^{2+}]_i$ accumulation prior to SD was required for effects on fEPSP recovery and consistent with this, endogenous synaptic Zn^{2+} release during SD propagation did not delay recovery from SD. The effects of exogenous $[Zn^{2+}]_i$ loading were also lost in slices preconditioned with repetitive SDs, implying a rapid adaptation. Together, these results suggest that $[Zn^{2+}]_i$ loading prior to SD can provide significant additional challenge to brain tissue, and could contribute to deleterious effects of $[Zn^{2+}]_i$ accumulation in a range of brain injury models.

4.2 Introduction

Spreading depolarizations (SD) are waves of neuronal and glial depolarization that propagate slowly throughout brain tissue (Leao, 1944c, Somjen, 2001). SD is commonly recorded as a large extracellular negative direct current (DC) potential shift

and results in a transient suppression of both electrocorticographic activity (Leao, 1947, Somjen, 2001). Large amounts of energy are required to restore ionic gradients before normal function can return, as demonstrated by large reductions in ATP and glucose levels following SD (Shinohara et al., 1979, Mies and Paschen, 1984). Extracellular adenosine accumulation occurs with severe metabolic challenges (Dale et al., 2000, Dunwiddie and Masino, 2001), and can contribute to the transient suppression of field excitatory postsynaptic potentials (fEPSPs) in brain slice models of SD (Lindquist and Shuttleworth, 2012). In healthy brain tissue SD is not injurious (Nedergaard and Hansen, 1988), however under conditions where metabolism is already compromised, such as in ischemic brain tissue, the additional metabolic challenge of repetitive SD events can lead to irrecoverable damage (Busch et al., 1996, Hartings et al., 2003). A growing body of literature from both animal and human recordings suggests that clusters of SDs can be a significant contributing factor to the enlargement of acute brain injuries (Nakamura et al., 2010, Oliveira-Ferreira et al., 2010, Dreier, 2011, Hartings et al., 2011a, Lauritzen et al., 2011).

We have recently demonstrated a significant release of synaptic Zn^{2+} following SD, and subsequent intracellular accumulation (Carter et al., 2011). Zn^{2+} is highly regulated and normally kept at very low intracellular levels, however excessive intracellular Zn^{2+} ($[Zn^{2+}]_i$) accumulation has been associated with a wide range of brain injuries including ischemia and trauma (Sensi et al., 2011, Shuttleworth and Weiss, 2011). It is not yet known whether release and accumulation of Zn^{2+} following SD may be a significant contributor to Zn^{2+} toxicity in a variety of brain injury settings. One mechanism for toxic effects of Zn^{2+} involves disruption of cellular energy production.

Zn^{2+} can directly bind to and inhibit both glyceraldehyde-3-phosphate dehydrogenase (GAPDH, (Sheline et al., 2000)) and the α-ketoglutarate dehydrogenase complex (KGDHC, (Brown et al., 2000)), inhibiting glycolysis and the TCA cycle, respectively. Additionally, Zn^{2+} can inhibit several steps in the mitochondrial electron transport chain (ETC) (Dineley et al., 2003, Sharpley and Hirst, 2006). Indirectly, Zn^{2+} can also inhibit metabolism by activating NAD^+-catabolizing enzymes such as poly(ADP-ribose) polymerase 1 (PARP-1) and the sirtuin family of proteins (Sheline et al., 2000, Cai et al., 2006), depleting NAD^+ levels and inhibiting glycolysis.

The aim of the current study was to determine whether increasing $[Zn^{2+}]_i$ can exacerbate the delay in recovery from SD. The results suggest that when $[Zn^{2+}]_i$ levels are sufficiently elevated prior to the passage of SD, there is a marked additional metabolic challenge, leading to delayed recovery of synaptic transmission.

4.3 Materials and Methods

Slice preparation and recording

All procedures were carried out in accordance with the National Institutes of Health guidelines for the humane treatment of laboratory animals, and the protocol for these procedures was reviewed annually by the Institutional Animal Care and Use Committee (IACUC) at the University of New Mexico School of Medicine. Acute hippocampal brain slices (350μm) were prepared from wild type C57Bl/6J and ZnT3 KO mice of either sex (4-8 weeks old). After cutting in ice-cold cutting solution and then holding for 1hr at 35°C, artificial cerebrospinal fluid (ACSF) was changed, and slices were held at room temperature until used for recording. Individual slices were then

transferred to the recording chamber, and superfused with oxygenated ACSF at 2mL/min at 32^{o}C. Mice homozygous for deletion of the ZnT3 gene were originally obtained from Dr. Richard Palmiter (Cole et al., 1999) and backcrossed onto C57Bl/6J for >13 generations (LSUHSC). A homozygous breeding colony of ZnT3 KO animals was then established at the University of New Mexico.

Extracellular measurements of field excitatory postsynaptic potentials (fEPSPs), were made via stimulation of Schaffer collaterals with a concentric bipolar electrode (CBAEC75, FHC, Bowdoin, ME, USA). Stimulation intensity was set to achieve ~60% maximum response during recording sessions. Extracellular recordings of fEPSPSs and direct current (DC) shifts were made by glass microelectrodes (~2-5MΩ), filled with ACSF and placed in stratum radiatum of CA1 ~50 μm below the surface of the slice. Spreading depolarization (SD) was induced by brief pressure pulses (30psi, 80-100ms) of 1M KCl from a homemade picospritzer (UniBlitz Model D122, Vincent Associates, Rochester, NY, USA; valve: 3-165-900, General Valve Corporation, Fairfield, NY, USA). Onset and propagation of SD was monitored by intrinsic optical signals (IOS), generated by transmission of red light through the tissue (>575nm). Propagation rate and IOS analyses were performed in TillVision (Till Photonics, Rochester, NY, USA). Comparison of fEPSP recovery between groups was defined by the time for fEPSPs to return to 50% pre-SD levels (t_{50}), unless stated otherwise.

Intracellular Zn^{2+} loading

To simulate conditions in which $[Zn^{2+}]_i$ levels were increased, we used a transient exposure (20min) to pyrithione (Pyr, 5μM) in the presence of 0, 30, or 100μM $ZnCl_2$

(Zn/Pyr). This was followed by a 10min washout prior to SD induction to minimize possible contributions of increased extracellular Zn^{2+} during the passage of SD (Aiba et al., 2012). Histidine (His, 200μM) was present during all Zn/Pyr exposures to help solubilize Zn^{2+} and prevent it from precipitating out of solution (Rumschik et al., 2009).

Adenosine measurements

Measurements of extracellular adenosine accumulation were performed as previously described (Lindquist and Shuttleworth, 2012). Briefly, enzyme-coupled electrochemical probes (SBS-ADO-05-50, Sarissa Biomedical, Coventry, UK) generate an amperometric signal proportional to the concentration of adenosine. Measurements reported here are estimates of accumulation at the slice surface, and synaptic levels may be different due to transporter activities within the slice. Calibration of the probes with exogenous adenosine (5-50μM) was performed immediately following individual recording sessions. It is noted that in the present study calibration stocks were made daily, and estimates of adenosine levels following SD are ~10-fold lower than previously reported (Lindquist & Shuttleworth 2012). Adenosine probes were positioned between the bipolar stimulating and recording electrodes in stratum radiatum of CA1.

Reagents and solutions

Slice cutting solution contained (in mM): 3 KCl, 1.25 NaH_2PO_4, 6 $MgSO_4$, 26 $NaHCO_3$, 0.2 $CaCl_2$, 10 glucose, 220 sucrose, and 0.43 ketamine. ACSF contained (in mM): 126 NaCl, 3 KCl, 1.25 NaH_2PO_4, 1 $MgSO_4$, 26 $NaHCO_3$, 2 $CaCl_2$, and 10 glucose, equilibrated with 95%O_2 / 5%CO_2. *N,N,N',N'*-tetrakis(2-pyridylmethyl)-ethylenediamine

(TPEN) was obtained from Intvitrogen (Carlsbad, CA, USA). All other reagents were obtained from Sigma (St. Louis, MO, USA).

Statistical Analysis

Data are reported as mean±standard error of the mean (S.E.M.). Statistical analysis was performed in GraphPad Prism (La Jolla, CA, USA) using paired or unpaired Student's t-test, or analysis of variance (ANOVA), with Bonferroni correction for multiple comparisons where appropriate. Differences were considered significant when $p<.05$.

4.4 Results

Effects of transient $[Zn^{2+}]_i$ loading on fEPSP suppression following SD

Transient loading of $[Zn^{2+}]_i$ (using pyrithione, see methods) prior to SD resulted in significant delay in recovery of fEPSPs after SD. In slices not loaded with Zn^{2+} (5μM Pyr control), SD resulted in fEPSP amplitude suppression that took 11.22±0.95min (n=6) to return to baseline levels (Fig 1A), similar to previously published data (Lindquist and Shuttleworth, 2012). $[Zn^{2+}]_i$ loading produced a concentration-dependent increase in the duration of fEPSP suppression following SD (Fig 1A) and final fEPSP amplitudes remained substantially depressed 25min following SD with the higher Zn^{2+} concentrations (30 & 100μM).

We noted a slight run-down of fEPSP amplitude immediately prior to the onset of SD when slices were loaded with Zn^{2+}. Therefore a set of time-control studies was completed to test whether progressive run-down of fEPSP amplitude alone (without SD)

could have produced the results seen. Thus slices were loaded with 0, 30, or 100μM Zn/Pyr (20min followed by wash out) without inducing SD (Fig 1B). Figures 1C&D compare the effects of $[Zn^{2+}]_i$ loading on final fEPSP amplitudes (assessed at the same time point, i.e. 60min from start of recording) with and without the additional challenge of SD. A concentration-dependent increase in fEPSP run-down was detected even without SD, but the degree of suppression was greatly increased by the combination of Zn^{2+} with SD.

$[Zn^{2+}]_i$ loading increased DC shift duration

We next assessed the characteristics of SDs, generated under the conditions shown in Figure 1A. In Pyr control slices, the waveform and duration of DC shifts were similar to those previously described (Somjen, 2001) and recorded under near-identical conditions without Pyr (Aiba and Shuttleworth, 2012) (Figure 2A). Following $[Zn^{2+}]_i$ loading, the duration of DC shifts were markedly increased (Figure 2B) in a concentration-dependent manner. Propagation rates of SD were assessed using IOS signals (see Methods) and no significant changes in rates were observed (Figure 2C). The effects of $[Zn^{2+}]_i$ loading on DC shift duration are consistent with previous reports that impaired metabolism is associated with increased DC shift duration and worse clinical outcome (Hartings et al., 2011b).

Extracellular adenosine accumulation and A1R activation following SD with $[Zn^{2+}]_i$ loading

Impaired metabolism can lead to increased adenosine accumulation (Dunwiddie and Masino, 2001). It was recently shown in brain slices that secondary fEPSP suppression after SD is mainly mediated by extracellular adenosine accumulation and activation of adenosine A1 receptors (A1Rs) (Lindquist and Shuttleworth, 2012). As shown in Figure 3A, pre-exposure to a selective A1R antagonist (8-cyclopentyl-1,3-dipropylxanthine, DPCPX, 200nM), significantly decreased the duration and degree of fEPSP suppression after SD with $[Zn^{2+}]_i$ loading, compared to the suppression shown in Figure 1. The degree of fEPSP suppression under these different conditions is summarized in Figure 3B. These results are consistent with the effective reversal of secondary fEPSP suppression described previously (Lindquist and Shuttleworth, 2012), and imply that the sustained suppression observed in Figure 1A is largely due to A1 receptor activation rather than neuronal injury.

We next tested whether additional extracellular adenosine accumulation contributed to the A1R-mediated fEPSP suppression seen above. Estimated extracellular adenosine concentration was measured at the slice surface using an enzyme linked probe (see Methods). A test concentration of 30μM Zn/Pyr in combination with SD was chosen as these conditions resulted in a substantial suppression of fEPSPs (see Fig 1A) that was completely mediated by A1R activation (see Fig 3A). Estimated peak extracellular adenosine accumulation during SD was significantly greater when $[Zn^{2+}]_i$ loading was combined with SD (Fig 3C, n=5 each). To test whether exogenous adenosine could replicate the effects of Zn/Pyr exposure, adenosine (50μM) was applied immediately

following the induction of SD in a separate set of experiments (Fig. 3D). The recovery of fEPSPs following SD was significantly decreased by exogenous adenosine, compared with control slices (Fig. 3D). Together, these findings suggest that the enhanced fEPSP suppression by $[Zn^{2+}]_i$ loading with SD was mediated predominantly by increased extracellular adenosine and A1R activation.

Potential intracellular targets for $[Zn^{2+}]_i$ loading effects

We next tested potential mechanisms which could link $[Zn^{2+}]_i$ loading to metabolic inhibition. Enhanced levels of $[Zn^{2+}]_i$ can deplete NAD^+ and thereby inhibit glycolysis either by induction of poly(ADP-ribose) polymerase 1 (PARP-1) or activation of SIRT protein pathways (Sheline et al., 2000, Cai et al., 2006). These possibilities were tested by using selective inhibitors for either PARP-1 (3,4-dihydro-5-[4-(1-piperidinyl)butoxyl]-1(2H)-isoquinolinone DPQ, 25μM) or SIRT (sirtinol, 30μM). As shown in Figure 4, DPQ with 30μM Zn/Pyr did not increase fEPSP recovery compared to vehicle treated slices with 30μM Zn/Pyr ($p=.073$, $n=8$ each). In addition, slices pre-exposed to sirtinol with 30μM Zn/Pyr did not result in a significant recovery of fEPSPs following SD when compared with preparations exposed to Zn/Pyr alone ($p=.8$, $n=3$, data not shown).

In a third set of slices, 5mM pyruvate was superfused for the entire recording session to provide additional TCA metabolic supplementation. In the presence of 5mM pyruvate, fEPSPs suppression following SD was not significantly different compared to slices exposed to 30μM Zn/Pyr alone (Fig 4B, $n=6$ each). Additionally, in slices supplemented with lactate (5mM), fEPSP suppression following 30μM Zn/Pyr with SD

was similar to slices without exogenous lactate (p=.6, n=3, data not shown). Taken together, these results suggest that $[Zn^{2+}]_i$ loading with SD may lead to increased extracellular adenosine accumulation via mechanisms downstream of glycolysis and pyruvate utilization.

Intracellular accumulation prior to SD is required for Zn^{2+} effects

To test whether the enhanced fEPSP suppression (seen in Fig 1A) was indeed a result of $[Zn^{2+}]_i$ accumulation and not a result of an extracellular of Zn^{2+}, a set of slices was exposed to 30μM $ZnCl_2$ in the absence of Pyr. Figure 5A shows full recovery of fEPSPs to pre-SD levels following 30μM $ZnCl_2$ application (n=6), indicating that the enhanced suppression of fEPSPs seen in Figure 1A was due to intracellular accumulation and action of Zn^{2+}. As seen in Figure 1, a small but significant decrease in fEPSP amplitude was also seen upon the addition of 30μM $ZnCl_2$ prior to SD induction (baseline: 101.2±1.62 vs. pre-SD: 89.41±3.05, p<.01).

We next tested whether $[Zn^{2+}]_i$ loading prior to SD was required for the observed effects on fEPSPs (as seen in Fig 1A). To test this, Zn/Pyr application was begun only 5min before SD induction to allow equilibration within the slice prior to the SD challenge. In contrast to the results shown in Figure 1, this exposure resulted in no combined effect of 30μM Zn/Pyr with SD (Fig 5B). Together, these data suggest sufficient time is required (>5min) to allow for $[Zn^{2+}]_i$ accumulation and activation of intracellular targets to generate a significant effect on fEPSP suppression when combined with SD.

Contributions of endogenous Zn^{2+}

We next evaluated whether intracellular accumulation of endogenous Zn^{2+} contributes to the metabolic burden of SD, and prolonged fEPSPs recovery. We first tested whether removal of all chelatable Zn^{2+} with a membrane permeable Zn^{2+} chelator (TPEN, 20μM throughout entire recording session) would influence fEPSP recovery from SD. TPEN pre-exposure resulted in a significant increase in the rate of fEPSP recovery after a single SD challenge (Fig 6A). Interestingly, there also was a significant increase in the fEPSP amplitude following SD in TPEN that was not observed in vehicle slices (TPEN baseline vs. post-SD amplitude: 99.80±1.14 vs. 107.6±1.40, $p<.01$; Vehicle baseline vs. post-SD amplitude: 99.32±0.74 vs. 100.5±1.99, $p=.58$, $n=6$ all groups).

We next tested potential sources of endogenous Zn^{2+} responsible for these effects. Zn^{2+} can be accumulated to high concentrations in many glutamatergic terminals, as a consequence of loading via the transporter ZnT3 (Cole et al., 1999). As terminals depolarize during the propagation of SD, a significant release of synaptic Zn^{2+} occurs and can be visualized as a propagating wave of extracellular Zn^{2+} accumulation (Carter et al., 2011). Since significant postsynaptic $[Zn^{2+}]_i$ accumulation also occurs after SD (Carter et al., 2011), we investigated here whether endogenous synaptic Zn^{2+} release during SD could provide an additional metabolic burden to subsequent SDs. To test this, a series of three SDs were induced at 20min intervals, to allow sufficient time for uptake and activation of intracellular targets following Zn^{2+} release from the first SD (see section 5 above) to influence recovery from prior SDs. However, as shown in Figure 6B, there was no stepwise increase in the duration of fEPSP recovery after multiple SDs, suggesting that synaptic Zn^{2+} release may not be a significant contributor. Figures 6C&D are

consistent with this, as there was no difference in fEPSP recovery after SD in slices from ZnT3 knockout animals, when compared with wild-type animals.

The results shown in Figure 6 were surprising, since we previously showed that there is no evidence of run-down of synaptic Zn^{2+} release during repetitive SDs (Carter et al., 2011), and the figures above suggest that repetitive $[Zn^{2+}]_i$ accumulation in advance of SD should lead to delayed functional recovery. Figure 7 provides an explanation for this apparent discrepancy, showing two consecutive SDs separated by 20min, with similar recovery rates as shown in Figure 6D. We next tested whether exogenous $[Zn^{2+}]_i$ loading with Zn/Pyr was still effective in suppressing fEPSPs in these slices following repetitive SD. Interestingly, the effects of Zn/Pyr on the enhanced fEPSP suppression described above (in SD-naïve slices, Fig 1A) were completely lost under conditions following repetitive SD (Fig 7A, n=6). A set of time-control experiments showed that exogenous $[Zn^{2+}]_i$ loading was still effective in slices where repetitive SDs were not generated (Fig 7B).

Figure 7C shows extracellular adenosine measurements under these conditions of repetitive SD shown in Figure 7A&B. In slices pre-exposed to two SDs, subsequent Zn/Pyr addition did not produce any increase in the amplitude of extracellular adenosine following SD. This is consistent with the lack of effect of Zn/Pyr exposure in Figure 7A. In time-control slices not previously exposed to SDs (matching Fig. 7B), there was still a significant increase in extracellular adenosine accumulation by Zn/Pyr with SD. Exogenous adenosine application (25μM) following the end of the recording session produced similar decreases in fEPSPs under both SD pre-exposed and time-control conditions (final fEPSP amplitudes: 28.29±3.14 vs. 28.16±2.56% baseline, SD pre-

exposed vs. time-control respectively, p=0.97, n=5 each). These results suggest that the loss of effectiveness of Zn/Pyr on fEPSP recovery is likely a consequence of decreased extracellular adenosine accumulation, rather than a change in sensitivity of synaptic transmission to adenosine, or other desensitization mechanisms.

4.5 Discussion

General

This study assessed the contributions of $[Zn^{2+}]_i$ accumulation to the recovery from spreading depolarization (SD) in acute hippocampal brain slices. Transient $[Zn^{2+}]_i$ loading with pyrithione (Zn/Pyr) appeared enhance the metabolic burden following SD, measured by enhanced fEPSP suppression, prolonged extracellular DC shift durations, and increased extracellular adenosine accumulation. Transient $[Zn^{2+}]_i$ loading alone led to a slow run-down of fEPSPs, however when combined with SD, the cumulative metabolic challenge was significantly enhanced. Endogenous Zn^{2+} release and accumulation during SD propagation did not lead to a significant delay in fEPSP recovery. This could be explained by the need for sufficient time prior to SD for $[Zn^{2+}]_i$ accumulation to have significant additive effects, as well as competition with a rapid adaptive mechanism activated following SD that confers resistance to $[Zn^{2+}]_i$ effects during repetitive SDs in the brain slice model.

Additional adenosine accumulation following $[Zn^{2+}]_i$ loading together with SD

Previous work has demonstrated accumulation of extracellular adenosine and suppression of evoked fEPSPs under metabolically compromised conditions (Rudolphi et

al., 1992b, Masino et al., 1999). Such a mechanism appears to explain the additive effect of Zn^{2+} with SD in the current study, as extracellular adenosine accumulation was significantly enhanced by $[Zn^{2+}]_i$ loading, and the A1R antagonist DPCPX improved fEPSP recovery (Fig 3A). The adenosine measurements reported here are estimates of adenosine concentrations at the slice surface, determined by comparison with exogenous adenosine applications (Lindquist and Shuttleworth, 2012). Concentrations of endogenous adenosine at synaptic sites within slices may be quite different, but regardless of absolute levels, the results here show significant functional increases in adenosine accumulation after SD in slices pre-loaded with Zn^{2+}.

A significant run-down of fEPSPs was seen with $[Zn^{2+}]_i$ loading in the 60min time-control experiments where SD was not induced (Fig 1), and suggestions of this run-down could be seen even in the initial 10min washout period prior to SD challenges. It seems likely that A1R suppression also contributes to this slow run-down, and is additive with the metabolic challenge of SD. Curiously, a small transient increase in fEPSPs was seen upon the addition of Zn/Pyr (seen most easily in Fig 4). This increase was present during the addition of either pyrithione or histidine alone (data not shown, n=6 each), which suggests that extracellular or contaminating Zn^{2+} (Carter et al., 2011) may contribute by effects on either excitatory or inhibitory transmission (Xie et al., 1994, Kim et al., 2002, Huang et al., 2008).

Suppression of excitatory neurotransmission by adenosine acting on A1Rs has been widely considered neuroprotective, and following hypoxic challenges, fEPSP recovery was impaired in the presence of DPCPX or in mice lacking A1Rs (Johansson et al., 2001, Sebastiao et al., 2001). However in the current study of SD in normoxic

conditions, we did not detect deleterious effects of DPCPX, and found instead that synaptic recovery was improved under all conditions tested. The majority of fEPSP suppression was mediated by A1R activation following 30μM Zn/Pyr. While fEPSP recovery was significantly improved by DPCPX with the 100μM Zn/Pyr challenge, some sustained fEPSP suppression was still seen (Fig. 3A). This suggests that under conditions of greatly increased metabolic inhibition, SD can result in either irrecoverable injury, out competition of DPCPX by excessive adenosine accumulation, or a combination of both. It remains to be determined whether adenosine accumulation following SD can contribute to delayed neuroprotection under other conditions, for example with clusters of SDs in ischemic conditions.

Mechanisms coupling $[Zn^{2+}]_i$ accumulation to adenosine accumulation

Several possibilities can be considered for mechanisms coupling $[Zn^{2+}]_i$ loading to adenosine accumulation. Sufficient time (many minutes) was required for $[Zn^{2+}]_i$ accumulation to have significant additive effects when combined with SD, consistent with a mechanism involving inhibition of metabolism or depletion of metabolic stores prior to SD. Based on the lack of effectiveness of selective inhibitors, PARP-1 or SIRT protein activation (see Introduction) did not appear to be significant contributors to the delayed fEPSP recovery following $[Zn^{2+}]_i$ loading together with SD (see Section 4). More prolonged Zn^{2+} exposures were utilized in studies which these pathways were identified in toxic Zn^{2+} effects (Sheline et al., 2000, Cai et al., 2006) and it is possible that postsynaptic $[Zn^{2+}]_i$ accumulation here was not sufficiently high enough, or of long enough duration to activate PARP-1 or SIRT pathways. An additional test of PARP-1

and SIRT pathway involvement could involve NAD^+ supplementation (Sheline et al., 2000). However, this possibility was difficult to test experimentally in these slice experiments, as application of NAD^+ alone was sufficient to suppress fEPSPs in a DPCPX-sensitive manner (data not shown). This effect may be due to its ability to mimic adenosine binding at A1Rs (Galarreta et al., 1993).

The lack of effect of pyruvate and lactate supplementation (see Section 4) suggest that any metabolic inhibition caused $[Zn^{2+}]_i$ loading is likely due to actions downstream of pyruvate utilization, within either the TCA cycle (Brown et al., 2000) or the mitochondrial electron transport chain (ETC) (Sharpley and Hirst, 2006). Interestingly, fEPSP recovery was enhanced in the presence of the DMSO vehicle used for both the DPQ and sirtinol studies (compare Figs 4A&B). DMSO has been reported to have antioxidant properties (Sanmartin-Suarez et al., 2011), and it is possible that DMSO reduced reactive oxygen species (ROS) generation by Zn^{2+}. Inhibition of ETC is established to lead to ROS production (Adam-Vizi, 2005) and mitochondrial Zn^{2+} accumulation, impairment of mitochondrial function, and ROS production have all been reported following Zn^{2+} accumulation in neurons (Sensi et al., 1999, Seo et al., 2001, Dineley et al., 2005).

In addition to accumulation due to metabolic depletion, it is possible that other sources of adenosine accumulation could also contribute to effects of Zn^{2+} loading. Higher order metabolic precursors of adenosine, such as ATP release from astrocytes (Halassa and Haydon, 2010) or cAMP release (Rosenberg and Dichter, 1989) can be converted to adenosine extracellularly. It is not yet known whether Zn^{2+} may play a role in either of these, or other, mechanisms of extracellular adenosine accumulation.

Effects of $[Zn^{2+}]_i$ loading on the characteristics of SD

Longer DC shift durations during SD are associated with worse clinical outcomes in a variety of brain injuries that involve impaired metabolism (Dohmen et al., 2008, Hartings et al., 2011b, Lauritzen et al., 2011). Recent work *in vitro* has also shown that longer DC shifts are associated with longer fEPSP suppression in hippocampal slices (Lindquist and Shuttleworth, 2012). We found here that $[Zn^{2+}]_i$ loading prior to SD significantly prolonged the duration of DC shifts (Fig 2), together with the effects on fEPSP recovery and adenosine accumulations discussed above. These results further the notion that longer DC shifts, both *in vitro* and *in vivo*, can be an indicator of larger metabolic challenges, and support a metabolic depletion mechanism for the Zn^{2+} effects described here.

Interestingly, there was no effect of $[Zn^{2+}]_i$ loading on SD propagation rate (Fig 2C), despite the fact that depletion of metabolic substrates can increase SD propagation rates (Seidel and Shuttleworth, 2011). This suggests that either the degree of metabolic inhibition with $[Zn^{2+}]_i$ loading is mild prior to SD, or the nature of metabolic inhibition (i.e.. substrate removal vs. direct metabolic inhibition) determines effects on propagation rate.

Endogenous Zn^{2+} accumulation

We previously showed waves of synaptic Zn^{2+} release and intracellular accumulation following SD propagation (Carter et al., 2011). However, results from the present study suggest that synaptic Zn^{2+} release and subsequent postsynaptic

accumulation does not lead to signs of progressive metabolic depletion, even when SDs were generated repetitively within the same slice (see Fig 6). One explanation for this lack of effect could be that endogenous $[Zn^{2+}]_i$ levels achieved following SD are much lower than those achieved during $[Zn^{2+}]_i$ loading with pyrithione. However, the results of Figure 7 also suggest the potential for a significant and rapid adaptation following SD in brain slices, making the tissue entirely resistant to a subsequent metabolic challenge with Zn^{2+} loading. SD is established to precondition tissues against subsequent ischemic challenges *in vivo*, although this effect has been tested only at relatively late time points (24hrs or greater) following SD induction (Matsushima et al., 1996, Yanamoto et al., 1998). It is not yet known whether the adaptation observed at early time points here shares a similar mechanism with ischemic preconditioning *in vivo*, or with PKC mechanisms linking intracellular Zn^{2+} increases to preconditioning in cultured cortical neurons (Aras et al., 2009).

The small increase in fEPSP recovery seen in the presence of TPEN, together with the lack of effect on fEPSP recovery in ZnT3 KO animals (see Fig 6), suggests that other endogenous, non-synaptic sources of Zn^{2+} can influence fEPSP recovery following SD. Potential contributors could include liberation of $[Zn^{2+}]_i$ from Zn^{2+}-binding proteins (Aizenman et al., 2000) that may occur during conditions generated by SD, or from influx of contaminating Zn^{2+} present in the superfusate (see discussion in Carter et al., 2011). However, the effect of TPEN on fEPSP recovery was quite small, and possibly counteracted by adaptive mechanisms following SD as described above.

Implications for injury

The results here emphasize potentially deleterious effects of intracellular Zn^{2+} accumulation, when combined with SD. Sustained $[Zn^{2+}]_i$ increases are known to occur in the days following stroke injury (Koh et al., 1996), and it seems likely that these sustained increases would make neurons more vulnerable to additional metabolic challenges of SDs that occur in the post-stroke brain (Hartings et al., 2003, Selman et al., 2004, Dreier, 2011, Lauritzen et al., 2011). However, we have also shown that extracellular actions of Zn^{2+} can limit the propagation of SD (Aiba et al., 2012). Therefore, selectively targeting intracellular Zn^{2+} accumulation may be more effective in limiting neuronal injury and improving outcome following several brain injury models, particularly those that involve SD. However it is important to also emphasize that clusters of repetitive SD have been associated with poor clinical outcomes under some conditions (Dreier, 2011, Hartings et al., 2011a, Lauritzen et al., 2011) and a rapid adaptation following SD appears to protect tissues against the additive metabolic burden of intracellular Zn^{2+} (Figure 7). Therefore deleterious metabolic effects of intracellular Zn^{2+} accumulation may not be significant during repetitive SDs clusters, and under such conditions, extracellular effects of Zn^{2+} may dominate and limit the spread of these events (Aiba et al., 2012). These and other divergent actions of intracellular and extracellular Zn^{2+} are likely contributors to different effects of Zn^{2+} chelation that have been reported in experimental injury settings (Lee et al., 2002, Kitamura et al., 2006c).

4.6 Figure Legends

Figure 4.1: Transient $[Zn^{2+}]_i$ loading resulted in increased fEPSP suppression following SD. A: Plots showing the effects of a single SD on fEPSP amplitude. SDs

were generated at the time indicate (arrow), and resulted in a rapid and near-complete initial suppression of fEPSP amplitude. Under control conditions (Pyr), this was followed by recovery over the next ~11min to baseline levels. Slices treated with Zn^{2+} together with the ionphore (Zn/Pyr, applied during time indicated by the black bar), resulted in a concentration-dependent increase in secondary suppression following SD ($p<.0001$, ANOVA with Bonferroni post hoc test, 5μM Pyr vs. 10, 30, and 100μM Zn/Pyr, n=6 each). Circle: Pyr; Square: 30μM Zn/Pyr; Diamond: 100μM Zn/Pyr, n=6 each. **B:** Plots showing effects of Zn/Pyr exposure on fEPSP amplitudes in the absence of SD in a separate set of slices (Circle: Pyr; Square: 30μM Zn/Pyr; Diamond: 100μM Zn/Pyr, n=6 each). **C:** Representative fEPSPs from time points indicated in (A): i-iv, and (B): v-viii. **D:** Mean data showing final fEPSP amplitudes (measured at 60min), determined from experiments shown in (A) & (B) (* $p<.01$unpaired Student's t-test, n=6 each).

Figure 4.2: $[Zn^{2+}]_i$ loading resulted in prolonged DC shifts. **A:** Representative extracellular DC potential shifts recorded during SD in control conditions (Pyr) or 30 and 100μM Zn/Pyr. **B:** Mean data from recordings as shown in (A) showing a concentration-dependent increase in DC duration (measured at 80% recovery, $p<.0001$, ANOVA with Bonferroni post hoc test, n=6 each). **C:** $[Zn^{2+}]_i$ loading had no significant effect on SD propagation rate, as measured from intrinsic optical signals in the same data set as shown in (B) ($p=.15$, ANOVA with Bonferroni post hoc test, 5μM Pyr vs. 30 and 100μM Zn/Pyr, n=6 each).

Figure 4.3: A1R activation and enhanced adenosine accumulation after SD with $[Zn]_i$ loading. **A:** Experiments conducted in the presence of an adenosine A1R antagonist, DPCPX (200nM) showed substantially larger recovery of fEPSPs following SD (arrow) after Zn/Pyr exposure (black bar) (compare with Figure 1, n=6 each). **B:** Comparison of fEPSP suppression under control and DPCPX conditions. Suppression of fEPSP for each preparation was calculated as the area between baseline amplitude and the recovered fEPSP amplitude, from immediately following the onset of SD to the end of the recording (25 min total duration). Suppression was significantly decreased by DPCPX under all conditions tested (*p<.01, **p<.001 unpaired Student's t-test, n=6 each). **C:** Amperometric measurements using an adenosine-sensitive electrochemical probe, showing responses to SD as compared with calibration exposures to exogenous adenosine (5μM) to generate estimated adenosine concentrations at the slice surface (see Methods). Adenosine accumulation during SD (arrow) was significantly enhanced by prior exposure to 30μM Zn/Pyr, compared with Pyr controls (p<.001 at peak, n=5 each). **D:** Application of exogenous adenosine immediately following SD induction (arrow) resulted in a significant reduction in fEPSP recovery that mimicked the effect of Zn/Pyr exposure (n=5 each).

Figure 4.4: Lack of effect of PARP-1 inhibition or pyruvate supplementation on $[Zn^{2+}]_i$ loading effects. **A:** Slices exposed to the PARP-1 inhibitor DPQ (25μM) showed little difference in recovery of fEPSP following SD after 30μM Zn/Pyr compared to slices exposed to 30μM Zn/Pyr alone (p=.13, n=8 each). DMSO (0.1%) was used as a vehicle in these studies. **B:** Addition of 5mM pyruvate together with 30μM Zn/Pyr had

no effect on the recovery of fEPSPs following SD compared to slices exposed to 30μM Zn/Pyr alone (p=.60, n=6 each).

Figure 4.5: Intracellular accumulation and exposure time needed for $[Zn^{2+}]_i$ loading effects. A: Slices exposed to extracellular $ZnCl_2$ alone (black bar, without the ionophore to enhance intracellular accumulation) did not result in slowed recovery of fEPSPs following SD (compare with suppression in Figure 1) (n=6). Representative fEPSPs are shown at times (i-iv) indicated on main plot. **B:** Similarly, no significant delay in fEPSP recovery was observed if $[Zn^{2+}]_i$ loading (Zn/Pyr, black bar) was applied beginning only 5min prior to SD induction (n=6). Representative fEPSPs are shown at times (i-iv) indicated on main plot.

Figure 4.6: Contributions of endogenous Zn^{2+}. A: A small but significant effect of the membrane permeable Zn^{2+} chelator TPEN on fEPSP recovery (20μM TPEN in 0.1% DMSO, 15 min pre-exposure and maintained throughout) (p=.04 for 50% recovery time, Veh vs. TPEN, n=6 each). **B:** Responses to three consecutive SD events in the same slices as (A) (20min intervals, onset indicated by arrows). TPEN exposure (20μM, 15 min pre-exposure and maintained throughout) revealed no cumulative effects due to progressive $[Zn^{2+}]_i$ accumulation on fEPSP recovery rate after repetitive SDs. **C&D:** Lack of effect of synaptically-released Zn^{2+} on fEPSP recovery rate after both single SDs (C) and repetitive SDs (D). Experiments are as described for A&B, but using comparison of wild type and ZnT3 KO slices rather than TPEN. p=.71 for 50% recovery time in C, and n=6 for all traces.

Figure 4.7: Loss of effectiveness of exogenous $[Zn^{2+}]_i$ loading, if slices were first subjected to repetitive SDs. A: In slices exposed to 2 SDs before loading with 30μM Zn/Pyr exposure (black bar), the expected suppression of fEPSP following a subsequent (third) SD challenge was completely lost (n=6, compare with Fig 1A). Representative fEPSPs are shown above at times (i-iv) indicated on main plot. **B:** Mean time control data, showing that exogenous $[Zn^{2+}]_i$ loading was still effective when given in SD-naïve slices, at the same time point as shown in (A) (n=6). Representative fEPSPs are shown above at times (i-iv) indicated on main plot. Note the difference at time point iv compared to the same time point in (A). **C:** Estimated extracellular adenosine accumulation at the surface of slices during SD under conditions shown in panels A & B above, in a separate set of preparations. In slices pre-exposed to two SDs (1^{st} and 2^{nd} SD), subsequent Zn/Pyr addition did not produce any increase in the amplitude of extracellular adenosine following SD (3^{rd} SD). No statistical difference was seen between the three SD challenges in the same slices (repeated measures ANOVA with Bonnferroni's multiple comparison). In time-control slices not previously exposed to SDs (matching Fig. 7B), there was still a significant increase in extracellular adenosine accumulation by Zn/Pyr with SD (see also Fig. 3C). (*$p<0.01$ Student's unpaired t-test, n=5 for each group).

Figure 4.1

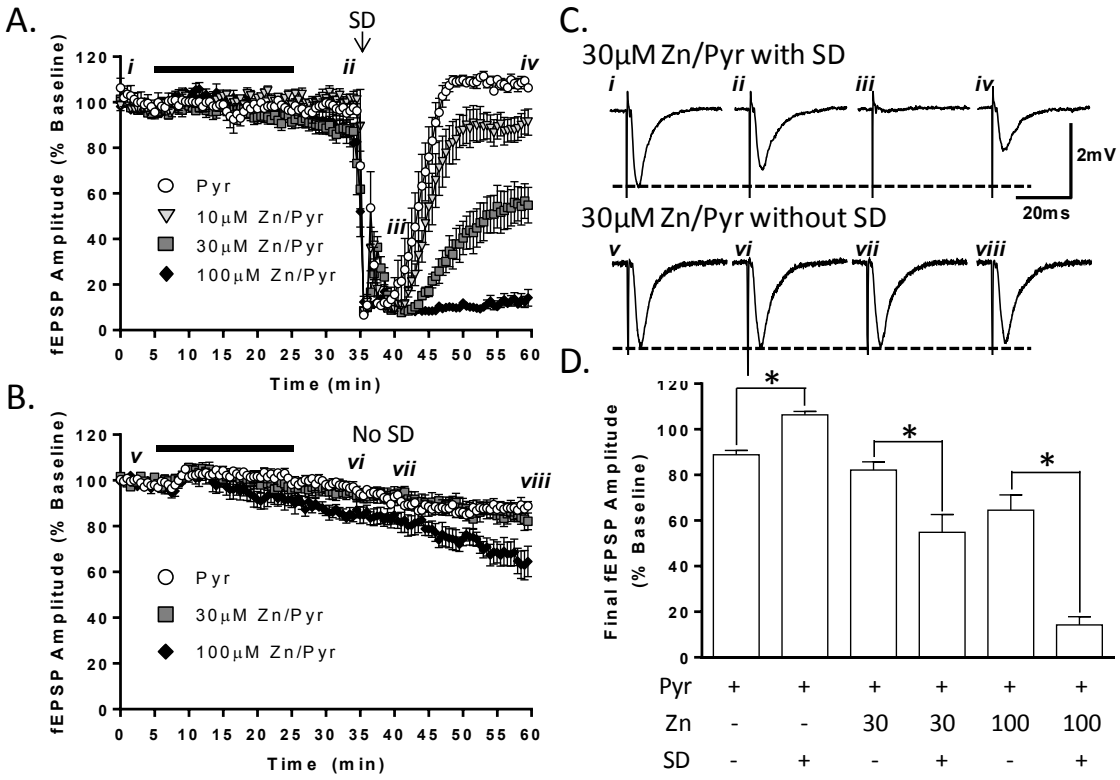
A.
SD
i
ii
iii
iv
fEPSP Amplitude (% Baseline)
Pyr
10μM Zn/Pyr
30μM Zn/Pyr
100μM Zn/Pyr
Time (min)
B.
No SD
v
vi
vii
viii
fEPSP Amplitude (% Baseline)
Pyr
30μM Zn/Pyr
100μM Zn/Pyr
Time (min)
C.
30μM Zn/Pyr with SD
i
ii
iii
iv
2mV
20ms
30μM Zn/Pyr without SD
v
vi
vii
viii
D.
Final fEPSP Amplitude (% Baseline)
Pyr + + + + + +
Zn - - 30 30 100 100
SD - + - + - +

Figure 4.2

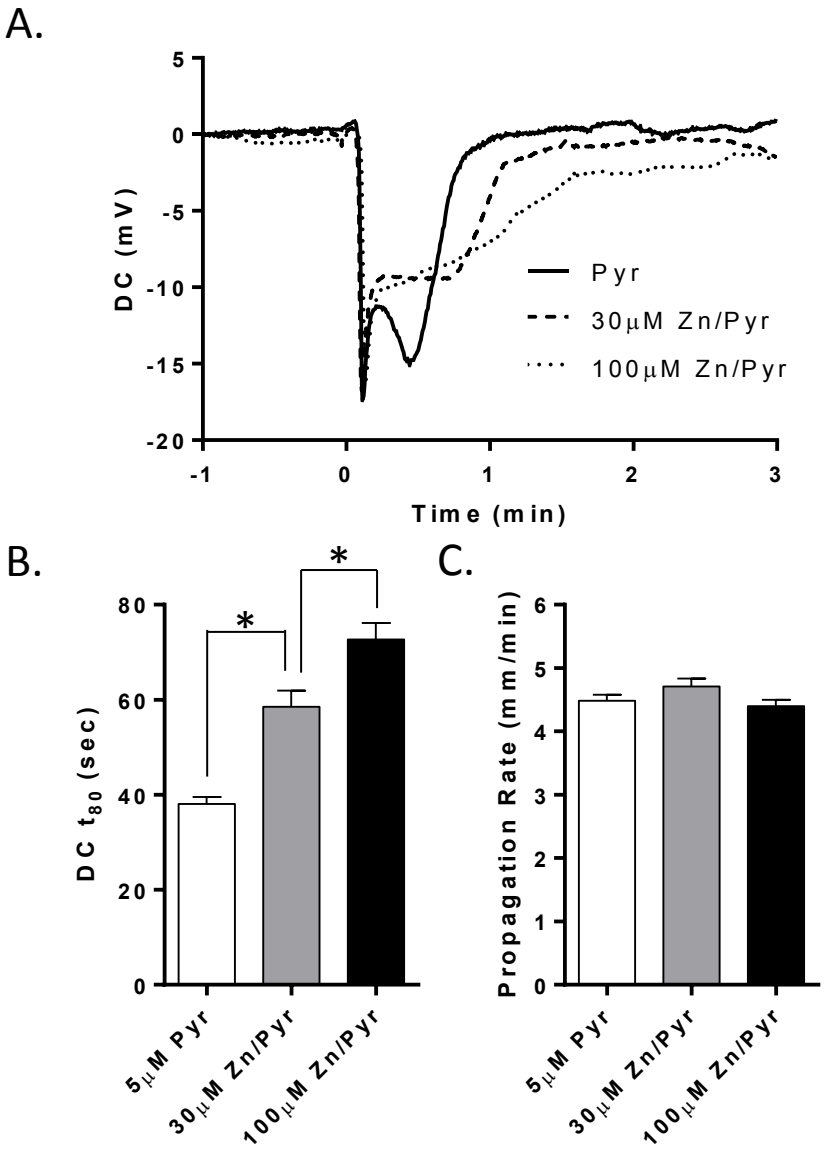
A.
DC (mV)
Time (min)
Pyr
30μM Zn/Pyr
100μM Zn/Pyr
B.
DC t80 (sec)
C.
Propagation Rate (mm/min)
5μM Pyr
30μM Zn/Pyr
100μM Zn/Pyr

Figure 4.3

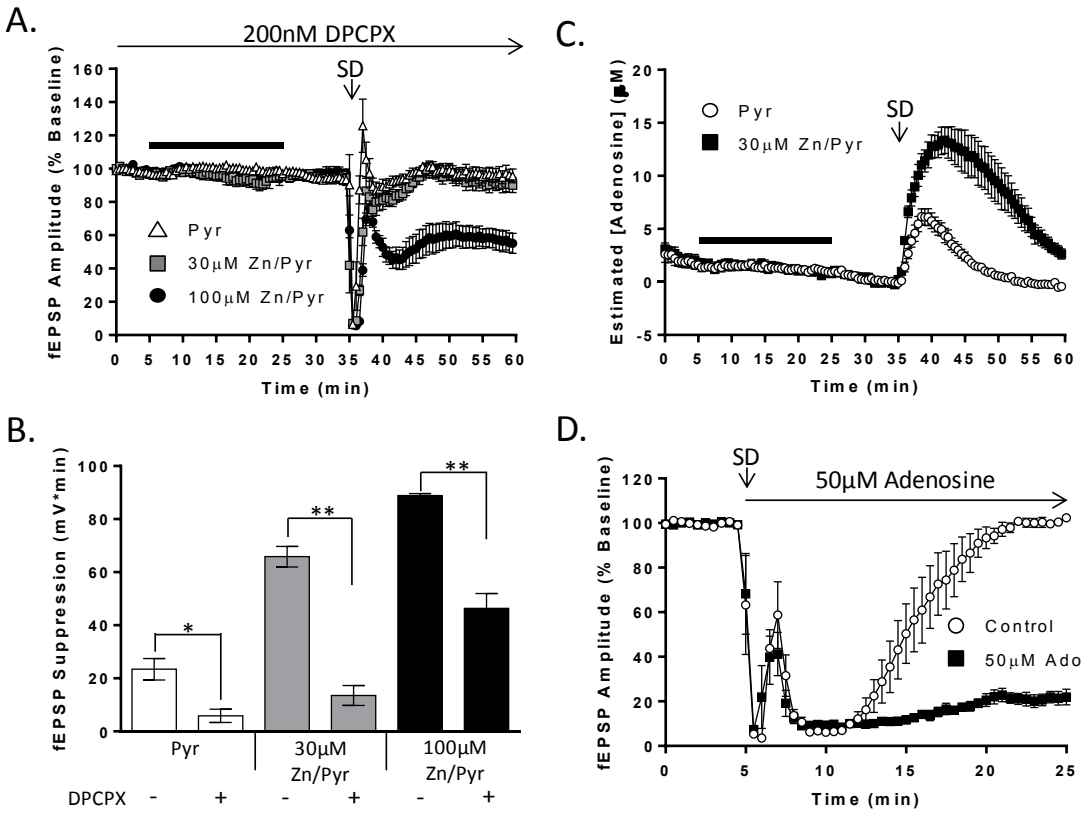
A.
200nM DPCPX
SD
fEPSP Amplitude (% Baseline)
Pyr
30μM Zn/Pyr
100μM Zn/Pyr
Time (min)
C.
Pyr
30μM Zn/Pyr
SD
Estimated [Adenosine] (μM)
Time (min)
B.
fEPSP Suppression (mV*min)
Pyr
30μM Zn/Pyr
100μM Zn/Pyr
DPCPX - + - + - +
D.
SD
50μM Adenosine
fEPSP Amplitude (% Baseline)
Control
50μM Ado
Time (min)

Figure 4.4

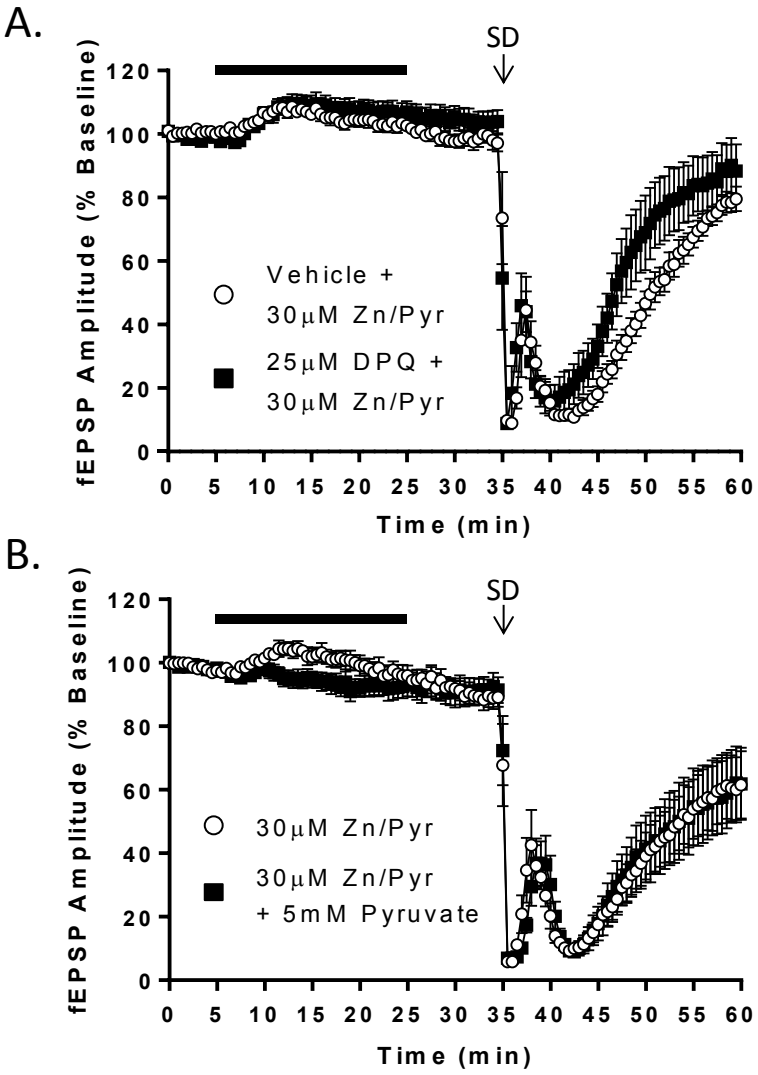
A.
SD
fEPSP Amplitude (% Baseline)
120
100
80
60
40
20
0
Vehicle +
30μM Zn/Pyr
25μM DPQ +
30μM Zn/Pyr
0 5 10 15 20 25 30 35 40 45 50 55 60
Time (min)
B.
SD
fEPSP Amplitude (% Baseline)
120
100
80
60
40
20
0
30μM Zn/Pyr
30μM Zn/Pyr
+ 5mM Pyruvate
0 5 10 15 20 25 30 35 40 45 50 55 60
Time (min)

Figure 4.5

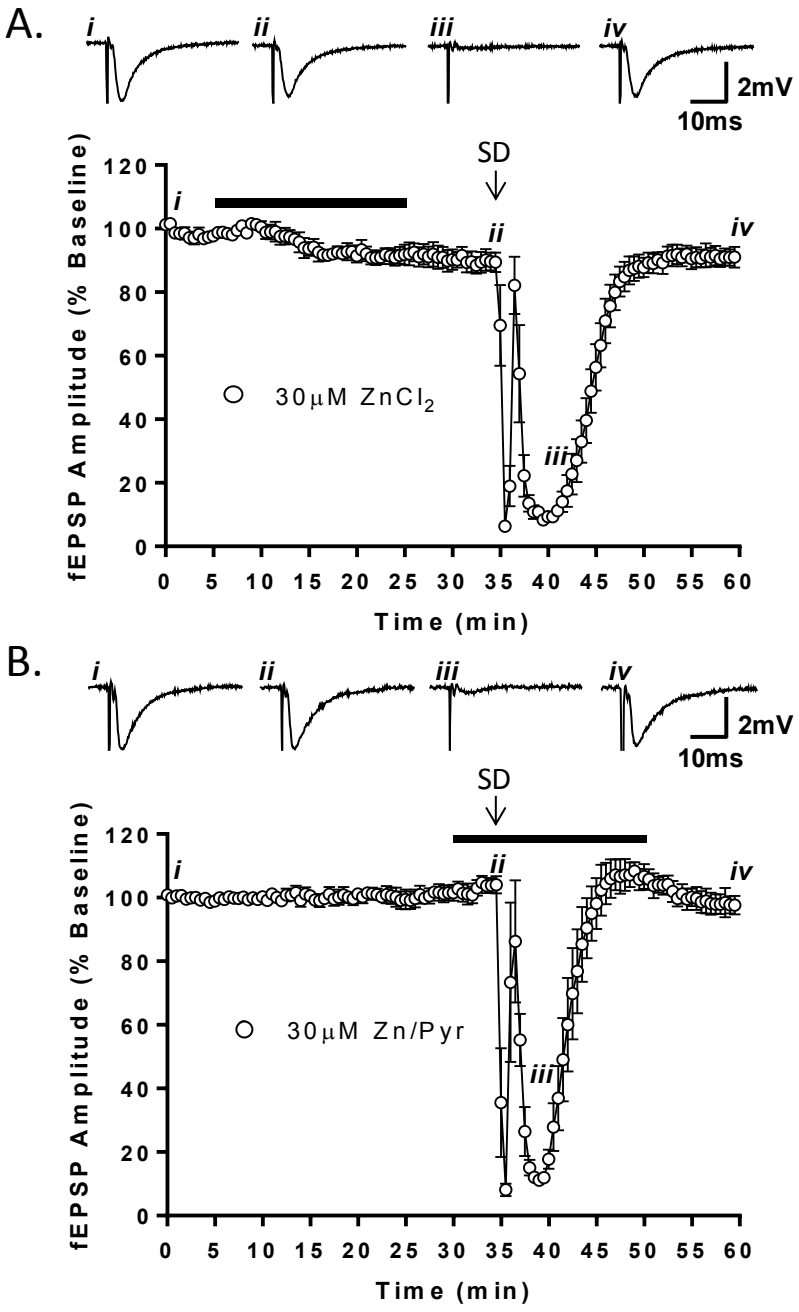
A.
i
ii
iii
iv
2mV
10ms
SD
120
100
80
60
40
20
0
fEPSP Amplitude (% Baseline)
30μM ZnCl2
0 5 10 15 20 25 30 35 40 45 50 55 60
Time (min)
B.
i
ii
iii
iv
2mV
10ms
SD
120
100
80
60
40
20
0
fEPSP Amplitude (% Baseline)
30μM Zn/Pyr
0 5 10 15 20 25 30 35 40 45 50 55 60
Time (min)

Figure 4.6

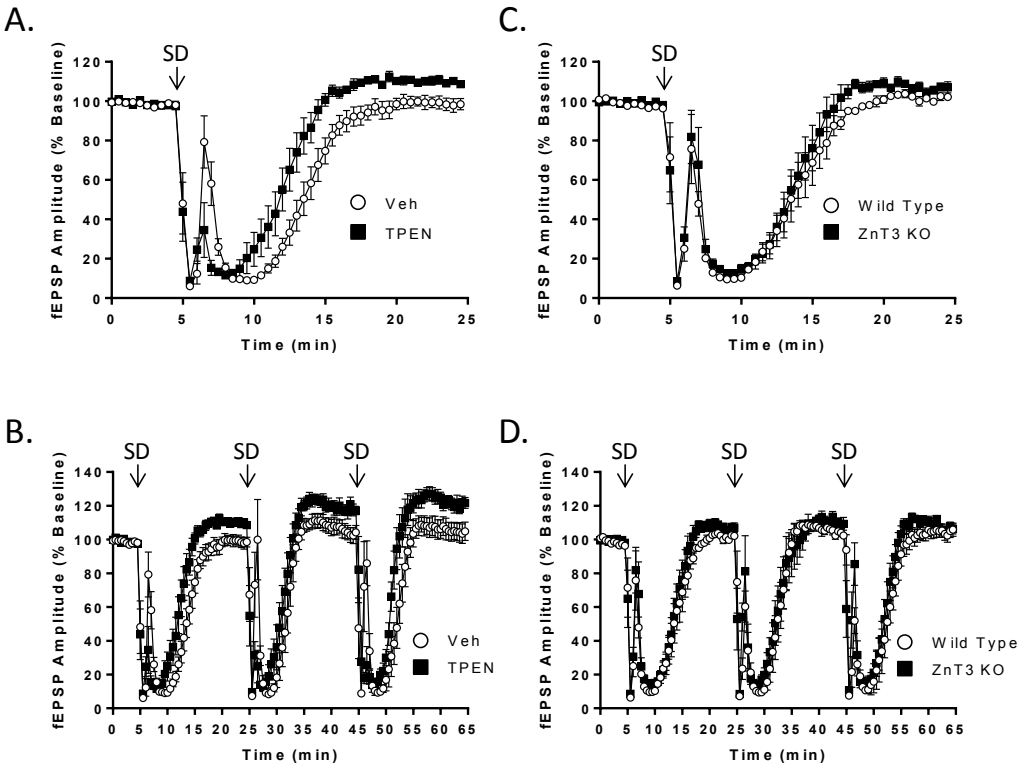
A.
C.
B.
D.
SD
fEPSP Amplitude (% Baseline)
Time (min)
Veh
TPEN
Wild Type
ZnT3 KO

Figure 4.7

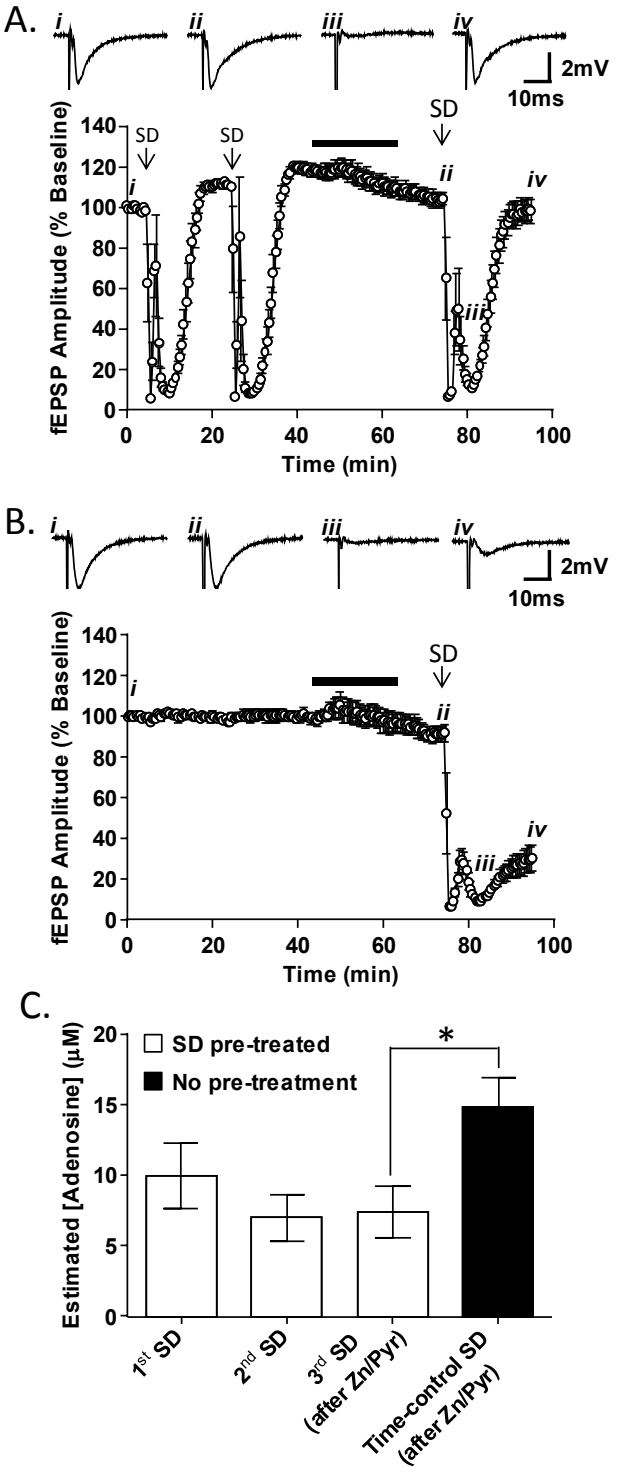
A.
i
ii
iii
iv
2mV
10ms
SD
SD
SD
fEPSP Amplitude (% Baseline)
Time (min)
B.
C.
Estimated [Adenosine] (μM)
SD pre-treated
No pre-treatment
*
1st SD
2nd SD
3rd SD (after Zn/Pyr)
Time-control SD (after Zn/Pyr)

Chapter 5: Fluorescence Detection of Synaptic Zn^{2+} Release during Spreading Depolarization *in vivo* and Implications for Ischemic Injury

Russell E. Carter[1], Andrew P. Carlson[2], Sava Sakadzic [3], Katharina Eikermann-Haerter [4], Cenk Ayata[4,5], Christian T. Sheline[6], Lee Anna Cunningham[1], and C. William Shuttleworth[1]

[1]Department of Neurosciences, University of New Mexico, Albuquerque, NM, USA

[2]Department of Neurological Surgery, University of New Mexico, Albuquerque, NM, USA

[3]Martinos Center for Biomedical Imaging, MGH, Harvard Medical School, Charlestown, Massachusetts, USA

[4]Stroke Service and Neuroscience Intensive Care Unit, Department of Neurology, MGH, Harvard Medical School, Charlestown, Massachusetts, USA

[5]Neurovascular Research Laboratory, Department of Radiology, MGH, Harvard Medical School, Charlestown, Massachusetts, USA

[6]Department of Ophthalmology and the Neuroscience Center of Excellence LSU, Health Sciences Center, New Orleans, LA, USA

(In Preparation for Submission)

5.1 Abstract

Excess Zn^{2+} accumulation contributes to ischemic injury, however, the source(s) of neurotoxic Zn^{2+} remain incompletely understood. We have previously shown large releases of synaptic Zn^{2+} during waves of spreading depolarization (SD) in hippocampal brain slice preparations. SD is a coordinated depolarizing event that occurs repetitively following ischemic insults. In the present study we investigated whether SD results in synaptic Zn^{2+} release in neocortical tissues *in vitro* and *in vivo*, and whether synaptic Zn^{2+} contributes to ischemic injury. Fluorescence detection of FluoZin-3, by single- and two-photon microscopy, revealed synaptic Zn^{2+} release during SD generated in normoxic conditions, in both neocortical brain slices, and in somatosensory cortex in anesthetized mice. Signals were abolished in tissues from mice lacking the transporter responsible for synaptic Zn^{2+} accumulation (ZnT3 KO). Focal ischemia was generated by distal middle cerebral artery occlusion (dMCAO), and resulted in SD events being generated around the infarct core. SDs generated by focal ischemia also produced significant synaptic Zn^{2+} release, which were absent in ZnT3 KO animals. Furthermore, ischemic infarcts generated by dMCAO were significantly smaller in ZnT3 KO animals. Together, these results provide the first visualization of synaptic Zn^{2+} release *in vivo*, and suggest that SD events following ischemia may be a significant source of neurotoxic zinc that contributes to injury progression.

5.2 Introduction

High levels of Zn^{2+} are present throughout the brain, bound to intracellular proteins and localized into a subset of glutamatergic synaptic nerve terminals by the Zn^{2+}

transporter ZnT3 (Palmiter et al., 1996b, Cole et al., 1999). While levels of Zn^{2+} are tightly maintained, excessive accumulation of Zn^{2+} is well known to be neurotoxic to both neurons and glia (Sensi et al., 2009). Prior work has shown that intracerebroventricular injections of a membrane impermeable Zn^{2+} chelator (CaEDTA) significantly reduced neuronal damage following ischemia (Koh et al., 1996, Calderone et al., 2004), suggesting that Zn^{2+} accumulated in the extracellular space can be neurotoxic under ischemic conditions. Subsequent *in vivo* microdialysis studies detected increased levels of extracellular Zn^{2+} accumulation following experimental stroke (Kitamura et al., 2006a, b). While accumulating evidence supports a toxic role for extracellular Zn^{2+} following ischemia, the source of this toxic Zn^{2+} has not been clearly identified. Synaptic Zn^{2+} can be released in an activity-dependent manner from hippocampal slices (Assaf and Chung, 1984, Howell et al., 1984), and recent work has utilized the high affinity fluorescent Zn^{2+} indicator FluoZin-3 to visualize synaptic Zn^{2+} release during electrical stimulation in hippocampal tissues (Qian and Noebels, 2005, 2006). While evidence exists for the capability of synaptic Zn^{2+} release in multiple brain regions, based on the localization of ZnT3 and synaptic Zn^{2+} by histochemical staining techniques (Lee et al., 2011), direct real-time fluorescence detection of release and quantification in brain regions other than the hippocampus is less understood.

Spreading depolarization (SD) is a coordinated depolarizing event that propagates through neuronal tissue in a feed-forward manner by the release of synaptic glutamate and the extracellular accumulation of K^+ (Somjen, 2001, Dreier, 2011, Lauritzen et al., 2011). While SD does not generally result in injury in healthy tissue (Nedergaard and Hansen, 1988), accumulating evidence, from both clinical and animal recordings,

suggests that repetitive SDs occur and are a contributing factor in the expansion of numerous brain injuries, including ischemic stroke (Hartings et al., 2003, Dohmen et al., 2008, Dreier, 2011, Lauritzen et al., 2011). As Zn^{2+} is co-stored with glutamate in synaptic vesicles and due to the sharply coordinated depolarization of large neuronal populations, these events provide an excellent model system to study synaptic Zn^{2+} release in brain tissues. We have recently exploited the phenomenon of SD to characterize significant synaptic Zn^{2+} release and postsynaptic accumulation in hippocampal tissues (Carter et al., 2011). As repetitive SDs can occur in neocortical tissues in the hours to days following the initial ischemic insult, we have considered the possibility that synaptic Zn^{2+} release during these events could be a significant contributor to the toxic extracellular Zn^{2+} accumulation previously reported.

In the current study, we tested whether synaptic Zn^{2+} release could be fluorescently detected in real-time during SD in neocortical tissues *in vitro* and *in vivo*. The studies utilize a selective Zn^{2+} fluorescence indicator (FluoZin-3), and mice lacking synaptic Zn^{2+} (ZnT3 KO mice). We also assessed the contribution of synaptic Zn^{2+} release to the progression of ischemic injury in a mouse model of distal middle cerebral artery occlusion (dMCAO). The results presented here show that there are sufficient levels of synaptic Zn^{2+} present in neocortical tissues to be released and fluorescently detected during SD both *in vitro* and *in vivo*. Following experimental stroke, synaptic Zn^{2+} significantly contributed to the progression of ischemic injury. These data suggest that targeting synaptic Zn^{2+} stores or release associated with SD events may be beneficial, even at relatively late time points following stroke onset.

5.3 Materials and Methods

Slice preparation and recording

All procedures were carried out in accordance with the National Institute of Health guidelines for the humane treatment of laboratory animals, and the protocol for these procedures was reviewed annually by the Institutional Animal Care and Use Committee at the University of New Mexico School of Medicine. Acute brain slices (350μm) were prepared from wild type C57Bl/6J and ZnT3 KO mice from either sex (4-8 weeks old). After cutting in ice-cold solution and then holding for 1 hour at 35^{o}C, artificial cerebrospinal fluid (ACSF) was changed, and slices were held at room temperature until used for recording. Individual slices were then transferred to the recording chamber, and were superfused with oxygenated artificial cerebrospinal fluid (ACSF) at 2 mL/min. Mice homozygous for deletion of the ZnT3 gene were originally obtained from Dr. Richard Palmiter (Cole et al., 1999) and backcrossed onto C57Bl/6 for >13 generations (LSUHSC). A homozygous breeding colony of ZnT3 KO animals was then established at the University of New Mexico.

Extracellular measurements of direct current (DC) potentials were made using borosilicate glass microelectrodes, filled with ACSF (~5MΩ) and placed in layer III ~50 μm below the surface of the slice. SD was generated by bath application of a high KCl modified ACSF (40mM KCl, equimolar reduction of NaCl), and was identified as a sharp negative deflection of the extracellular direct current (DC) potential. In some experiments, the spread of SD was monitored by using intrinsic optical signals, generated by transmission of red light (>575nm).

Brain Slice Zn^{2+} indicator measurements

Extracellular Zn^{2+} measurements were made using the charged form of the Zn^{2+}-sensitive indicator FluoZin-3, using approaches developed by others (Kay, 2003, Qian and Noebels, 2005, 2006) and utilized in our recent work (Dietz et al., 2008, Carter et al., 2011). FluoZin-3 was dissolved in ACSF at 1.5μM and superfused over the slice at 35^{o}C. Background fluorescence was then reduced by addition of CaEDTA (1mM) in all experiments, except where indicated otherwise. Responses are reported as (%$\Delta F/F_0$), as Zn^{2+} binds to multiple components of the recording buffer (Rumschik et al., 2009), making absolute calibration from addition of exogenous Zn^{2+} standards problematic. FluoZin-3 excitation at 495nm (150ms), and emission was detected at 535/50nm using a monochromator-based imaging system (Till Photonics). Images were acquired every 1.5 seconds and analyzed with TillVision software (Till Photonics).

Surgical preparation

Wild type C57Bl/6 and ZnT3 KO of either sex (3-6months old) were deeply anesthetized with 2.5% isoflurane in a mixture of 70% N_2O / 30% O_2. Mice were then placed into a stereotaxic frame and maintained with 1% isoflurane provided via nose cone. Body temperature was maintained at 37°C by a rectal feedback controlled heating blanket (Harvard Instruments). The skin above the skull was cut and removed and a cranial window (~1mm diameter) was created over the left somatosensory cortex (centered 2mm lateral and 1mm caudal to bregma). Care was taken to leave the dura intact. A ring of dental cement was placed around the craniotomy with a piece of polyethylene tubing (PE10) embedded in to allow the inflow of solutions. A burr hole

was created over the frontal bone, ~2mm rostral from the craniotomy for SD induction. Application of a piece of gel foam soaked in 1M KCl to the burr hole for 1-2s, followed by saline wash, was used to elicit a single SD.

Single-photon in vivo imaging

Tissue autofluorescence and FluoZin-3 imaging was performed at 490nm (350ms), with emission detected at 535/50nm using similar set up for slice work (Till Photonics), through the dura intact open cranial window. Images were collected at 2Hz, with 2x2 binning, resulting in an image with pixel dimensions of 320x240. Fluorescence data was collected using 4x air (NA 0.13) or 10x water immersion (NA 0.3) objective as indicated in text. Extracellular recordings of DC potential changes were via glass electrodes (~3-5MΩ) filled with ACSF, placed approximately 200µm below the cortical surface, using PowerLab software (PowerLab). FluoZin-3 (10µM) and CaEDTA (1mM) were applied together in normal saline over the cortical surface via a syringe pump. Initial wash-in was applied at 200µL/min for 2min, followed by 1µL/min for 10min prior to any recording session. Unless indicated otherwise, FluoZin-3 and CaEDTA were continually superfused over the cortex throughout the entire experiment.

Two-photon in vivo imaging

Two-photon imaging utilized a Ti:Sapphire femtosecond mode-locked IR laser (Spectra Physics Tsunami) connected to a Prairie Ultima two-photon upright microscope. Images were acquired using Prairie View software at 810nm and a 4µs pixel dwell time. A 20x WI (NA 0.5) objective was used to acquire images, with a final image size of

512x512 pixels. For time series acquisition of FluoZin-3 wash in, images where acquired every 10s. Z-stacks were acquired at 10µm steps starting 50µm above the surface of the dura to 150µm into the brain. In studies were SD was monitored, images were acquired every 1.5s for a duration of 5min. SD induction and FluoZin-3 (10uM) and CaEDTA (1mM) superfusion was as described for single-photon imaging.

For electrical stimulation, procedures for animal preparation and cranial window placement were the same as for CSD recordings. A custom made parallel bipolar stimulating electrode was inserted into the neocortex at the caudal edge of the craniotomy. One second square pulses of 500µA, 200µs at 20, 50, and 100Hz were delivered through a stimulation box (Isoflex) connected to a Master8 control box. Two-photon images were acquired using a 20x WI (NA 0.5) objective at 2Hz with a final image size of 256x256 pixels and were analyzed using ImageJ (NIH), or imported and analyzed in TillVision (Till Photonics). For all *in vivo* FluoZin-3 responses (single- and two-photon), data are expressed as ($\%\Delta F/F_0$).

Distal Middle Cerebral Artery Occlusion Model

The procedure for distal middle cerebral artery occlusion (dMCAO) was modified from previously published studies (Chen et al., 1986, Kuraoka et al., 2009). Mice were anesthetized as above and placed in the stereotaxic frame, rotated to lay on their right side. An incision was made in the skin between the lateral portion of the left orbit and external auditory meatus. The temporalis muscle was separated and resected to reveal the distal portion of the MCA through the zygoma. A small rectangular craniotomy was made over the MCA and a loose square knot (8-0 suture) was created on the MCA to tie

off later during imaging. Care was taken to ensure that the suture was not occluding the vessel prior to imaging. Mice were then positioned in the stereotaxic frame in the prone position and a cranial window was created for FluoZin-3 imaging as described above for single-photon imaging.

For survival studies, the distal MCA was immediately tied off and Laser Doppler measurements were recorded in a subset of animals to ensure proper occlusion in both genotypes. A piece of bone wax was placed over the craniotomy, and following would closure, animals were placed back into their home cages, and were monitored for 1hr to ensure proper recovery from the surgery. All animals were supplied with soft food supplements following surgery.

Imaging was performed at low power (4x air) for visualization of a large portion of the cortical surface. FluoZin-3 (10μM) and CaEDTA (1mM) were superfused and imaged as described above for *in vivo* single-photon imaging. After image acquisition started the suture was tightened over the MCA to occlude the vessel. Care was taken to not sever the MCA during tie off, and animals in which this occurred were excluded from the analysis and data presented in this report.

Infarct volume measurements

Infarct volumes were measured 24hrs following permanent dMCAO by TTC staining. The brains were rapidly removed in ice-cold cutting solution and sectioned into 2mm thick slices and incubated in 1% TTC in ACSF for 1hr at 35°C. Slices were then fixed in 4% PFA overnight, and infarct volumes were subsequently quantified.

Reagents and solutions

Cutting solution contained (in mM): 3 KCl, 1.25 NaH_2PO_4, 6 $MgSO_4$, 26 $NaHCO_3$, 0.2 $CaCl_2$, 10 glucose, 220 sucrose and 0.43 ketamine. ACSF contained (in mM): 126 NaCl, 3 KCl, 1.25 NaH_2PO_4, 1 $MgSO_4$, 26 $NaHCO_3$, 2 $CaCl_2$, and 10 glucose and was equilibrated with 95%O_2 / 5%CO_2. Cutting and recording solutions were both 315-320 mOsm. FluoZin-3, prepared as a 10mM stock in water, was obtained from Invitrogen (Carlsbad, CA). All other reagents were obtained from Sigma (St. Louis, MO).

Statistical Analysis

Data are reported as mean ± standard error of the mean (S.E.M.). Significant differences between group data were evaluated using unpaired or paired Student's t-tests, with correction for multiple comparisons where appropriate.

5.4 Results

Fluorescence detection of synaptic Zn^{2+} release in neocortex during SD in vitro

To confirm that SD could be generated in the neocortex in our model, brain slices were superfused with 40mM KCl in ACSF for 2min to induce SD (see (Zhou et al., 2010a)). SD could be reliably generated by this stimulation, and Figure 1A shows the propagation of SD through the neocortex visualized from the intrinsic optical signals (IOS) (Andrew et al., 1999). Upon the passage of SD (arrows in Fig. 1A, mean propagation rate:4.56±0.35mm/min (n=7)), a sharp negative DC deflection occurred (bottom right trace of Fig. 1A) characteristic of SD.

To test for extracellular Zn^{2+} accumulation during SD, a separate set of slices were superfused with FluoZin-3 (1.5μM) in the presence of CaEDTA (1mM). In wild type slices, SD resulted in an increase in FluoZin-3 fluorescence (Fig. 1B), which followed a similar rate of propagation as the IOS signal (mean rate: 4.37±0.44mm/min, n=7). The peak FluoZin-3 signal (199.671±13.37 $\%\Delta F/F_0$) occurred coincident with the sharp negative DC deflection. In order to test whether synaptic Zn^{2+} contributed to the increase FluoZin-3 fluorescence during SD above, experiments were repeated in slices from ZnT3 KO animals. SD was still generated in ZnT3 KO tissues, however instead of an increased FluoZin-3 signal, there was a small decrease in fluorescence that propagated during SD (-15.59±4.27 $\%\Delta F/F_0$, propagation rate: 3.86±0.47mm/min, n=6). This decrease in fluorescence can be attributed to emission of intrinsic autofluorescence of flavoproteins at the wavelength used to excite FluoZin-3 (Qian and Noebels, 2005, Carter et al., 2011). A summary of the peak FluoZin-3 response during SD is provided in Figure 1D. Taken together, these results show that synaptic Zn^{2+} release can occur during SD in neocortical tissues *in vitro*.

Imaging of flavoprotein autofluorescence (in the absence of FluoZin-3) revealed similar responses in wild type and ZnT3 KO tissues (-6.64±0.48 vs. -5.80±0.23 $\%\Delta F/F_0$, wild type (n=7) vs. ZnT3 KO (n=5) respectively, p=0.19) during SD that propagated through the tissue at similar rates (4.27±0.79 vs. 4.41±0.50 mm/min, wild type (n=7) vs. ZnT3 KO (n=5) respectively, p=0.90). These results indicate that SD in the neocortex was similar in both genotypes, and that autofluorescence changes associated with SD cannot account for the differences in FlouZin-3 signals between wild type and ZnT3 KO tissues.

In vivo fluorescence detection of synaptic Zn^{2+} release during SD

We next assessed whether similar approaches used to visualize synaptic Zn^{2+} release *in vitro* could be adapted to evaluate synaptic Zn^{2+} release *in vivo*. SD was induced *in vivo* by a brief application of KCl to the cortical surface through a burr hole in isoflurane-anesthetized mice (see Materials and Methods). This procedure is well established to generate SDs, and the occurrence of SD was verified in the present study with optical propagation measurements and extracellular DC recordings. In the absence of FluoZin-3, the propagation of SD was accompanied by autofluorescence decreases in both wild type and ZnT3 KO animals (propagation rate: 3.14±0.42 vs. 2.58±0.63 mm/min, p=0.47; autofluorescence decrease: -12.40±1.37 vs. -11.34±1.53 $\%\Delta F/F_0$, p=0.62, n=5 WT, n=4 ZnT3 KO respectively).

In initial studies, FluoZin-3 (10μM) and CaEDTA (1mM) were continually superfused over the cortical surface (dura intact) and visualized with single-photon excitation (490nm) using a low power air objective (4X, NA 0.13), which permitted simultaneous recording of extracellular DC potential shifts associated with SD. SD induction resulted in a large FluoZin-3 fluorescence increase in wild type animals (Fig. 2A) coincident with the extracellular negative DC shift. Increased FluoZin-3 signals during SD were completely absent in ZnT3 KO animals (Fig. 2B). Instead, a decrease in fluorescence was detected with the electrical DC shift, similar to the fluorescence responses described in the slice experiments above (see Fig. 1C).

Subsequent studies were performed without electrical recordings and using the FluoZin-3 signal as an indicator for SD occurrence. Higher power imaging (10x water immersion objective, NA 0.3) was used to quantify FluoZin-3 changes, and showed that

the wave-like increase in FluoZin-3 fluorescence propagated at a rate of 2.81±0.14mm/min in wild type animals (n=5), while the decrease seen in ZnT3 KO animals propagated at 2.71±0.37mm/min (n=4). Repetitive SD challenges in the same animal were examined to determine if each event releases similar levels of synaptic Zn^{2+}. Little change in the peak fluorescence level was observed during repetitive challenges, consistent with our previous *in vitro* work (Carter et al., 2011), indicating similar release characteristics with each SD (Fig. 2C). The peak FluoZin-3 amplitude during the first SD in wild type animals and ZnT3 KO animals is shown in Figure 2D.

Source of fluorescence signals in vivo

We considered the possibility that FluoZin-3 signals acquired during single-photon excitation could be contributed to by Zn^{2+} diffusing away from the source of release and binding with indicator above the dura, in addition to signals generated close to release sites within the brain parenchyma. To address this issue, we utilized two-photon microscopy to image FluoZin-3 fluorescence (see Methods) at three levels of interest during the propagation of SD: 1) superfusion well (70µm above dura); 2) dura surface; and 3) within the brain parenchyma (50µm below the dura). FluoZin-3 and CaEDTA were applied continuously in the superfusion well above the dura, identically to the single-photon experiments above. During the passage of SD, the majority of the fluorescence increase was observed within the brain, with only a slight signal detectable above the dura surface (Fig. 3A). The average peak FluoZin-3 fluorescence increase during SD within the parenchyma was 1181.79±222.18 $\%\Delta F/F_0$ (n=4) in wild type animals and autofluorescence decreases (-38.94±10.54$\%\Delta F/F_0$, n=4) were seen in ZnT3

KO animals during the propagation of SD, consistent with our previous findings (see above).

Comparative amplitudes of FluoZin-3 responses in vivo

To determine if synaptic Zn^{2+} release could be detected *in vivo* during a less intense stimulus than SD, we used direct electrical stimulation of the cortex. Repetitive electrical stimulation (200μs pulse duration, 500μA, at 20, 50, or100Hz for 1s) was used to stimulate a region of the brain encompassing the somatosensory cortex, at the same coordinates as SD imaging. Figure 4A shows a representative trace following 50Hz stimulation from a wild type animal. In the absence of FluoZin-3, very little to no response was detected at the wavelength used for two-photon excitation (810nm). However, after the addition of FluoZin-3 (10μM) and CaEDTA (1mM), a robust signal was detected upon stimulation. In ZnT3 KO animals, no autofluorescence response was seen during electrical stimulation, and in contrast to wild type animals, no FluoZin-3 response was detected following stimulation (Fig. 4B). FluoZin-3 responses in wild type animals were frequency-dependent as shown in Figure 4C.

Synaptic Zn^{2+} release during SDs generated by distal MCAO

We used a distal focal ischemia technique to permanently occlude a portion of the left distal middle cerebral artery (dMCAO, see Materials and Methods). Confirmation of loss of blood flow following occlusion was imaged with laser speckle contrast imaging of the entire cerebral cortex (LSCI, Fig 5A). Shortly after occlusion, an SD event was detected (mean onset time 6.19±2.70min after occlusion), and could be visualized with

LSCI, with similar characteristics to the first SD reported in previous stroke models in rats and cats (Nakamura et al., 2010, Kumagai et al., 2011). We next tested whether synaptic Zn^{2+} was released during this SD event following ischemia by superfusing FluoZin-3 and CaEDTA over the exposed cortex of a different group of wild type and ZnT3 KO animals. Imaging with single-photon excitation allowed for a larger field of view with a low power objective, similar to that used in Figure 2. Following dMCAO in a wild type animal, a wave of increased FluoZin-3 fluorescence was detected (Fig. 5A), similar to that seen with SD induced by KCl (Fig 2A). The FluoZin-3 signal (232.1±67.43%$\Delta F/F_0$, n=4) propagated at a rate consistent with the SD (2.71±0.25mm/min). In ZnT3 KO animals, SD was still generated from dMCAO (2.52±0.09mm/min, n=4), however no increase in FluoZin-3 fluorescence was seen (Fig 5C). Like SD induced by KCl application, a decrease in fluorescence was detected (-22.78±5.19%$\Delta F/F_0$) in ZnT3 KO animals, again attributed to autofluorescence changes. These results suggest that synaptic Zn^{2+} release during SD could be a source of extracellular Zn^{2+} accumulation following ischemia *in vivo*.

Synaptic Zn^{2+} contributes to ischemic injury

To test the contribution of synaptic Zn^{2+} release to the progression of ischemic injury, permanent dMCAO, as described above, was induced in a separate set of wild type and ZnT3 KO mice. Laser Doppler measurements were recorded in both genotypes immediately following dMCAO and no difference in CBF reduction was seen (data not shown) indicating successful occlusion in both genotypes. Infarct volumes were measured 24hrs after dMCAO with TTC (see Materials and Methods). Representative

whole brain TTC staining revealed a robust infarct area in a wild type animal with a substantial reduction in infarct area in the ZnT3 KO animal (Figs. 6A&B). Correspondingly, brain slices stained with TTC showed an infarct restricted to the cortex in both genotypes, however, the infarct volume was significantly reduced in ZnT3 KO animals (10.46±2.72 vs. 3.22±0.93mm^3, wild type (n=12) vs. ZnT3 KO (n=11), p=.02, Figs. 6C,D,&E).

5.5 Discussion

General

This study investigated whether synaptic Zn^{2+} release could be detected in neocortical tissues and if synaptic Zn^{2+} could be neurotoxic in the post-ischemic period. Sufficient levels of synaptic Zn^{2+} were present in the neocortex to be detected during SD *in vitro*, and single- and two-photon microscopy confirmed fluorescence detection of synaptic Zn^{2+} release within the brain parenchyma during SD *in vivo*. Visualization of synaptic Zn^{2+} release during direct electrical stimulation could imply that synaptic Zn^{2+} release occurs during a wide range of stimuli *in vivo*. The large release of synaptic Zn^{2+} during SD following dMCAO, combined with the significant reduction in infarct volumes in ZnT3 KO mice, implicates synaptic Zn^{2+} release during SD as a major source of neurotoxic Zn^{2+} during ischemia.

Comparison between hippocampal and neocortical synaptic Zn^{2+} release in vitro

A large number of studies have examined characteristics of Zn^{2+} release and actions in hippocampal preparations. Zn^{2+} in synaptic vesicles is readily detectable in the

large mossy fiber boutons that terminate on CA3 pyramidal neurons, and release and actions in mossy fiber – CA3 plasticity have been identified (Li et al., 2001, Sensi et al., 2009). However, synaptic Zn^{2+} is also demonstrable with Timm's staining throughout the neocortex (Frederickson et al., 2000), and the results in the current study show that synaptic Zn^{2+} release during SD in neocortical slices was quantitatively comparable to our previous work in hippocampal tissues (Carter et al., 2011). The propagation rates and DC shifts associated with SD were also comparable between the two studies, indicating that the underlying characteristics of SD are also similar between hippocampal and neocortical tissues. While fluorescence visualization was only examined from layers II/III in neocortical slices encompassing the somatosensory cortex, it is possible that release characteristics may differ in different cortical regions. Staining for synaptic Zn^{2+} and ZnT3 has revealed a heterogeneous distribution throughout the cortical layers, with the highest levels present in layers I, II, III, and V (Lee et al., 2011). However, as synaptic Zn^{2+} is present throughout the entire neocortex (Frederickson et al., 2000), it is likely that synaptic Zn^{2+} release can occur throughout all neocortical regions. Therefore, synaptic Zn^{2+} release in the neocortex may be involved in similar physiological processes, such as synaptic plasticity, in the neocortex that have previously been described in hippocampal tissues (Li et al., 2001, Pan et al., 2011).

Technical issues imaging FluoZin-3 fluorescence in vivo

Utilizing single- and two-photon microscopy, we have demonstrated that it is possible to image FluoZin-3 through the intact mouse dura. Additionally, as CaEDTA has been previously utilized to increase the signal/noise of FluoZin-3 fluorescence (Qian

and Noebels, 2005, Carter et al., 2011), the apparent ability of this slow-acting chelator to also penetrate the dura aided in the detection of FluoZin-3 transients *in vivo*. In the absence of CaEDTA, relatively low basal FluoZin-3 fluorescence levels were seen with two-photon imaging within the parenchyma, indicating a relatively low extracellular concentration of Zn^{2+} *in vivo*. Previous *in vitro* work indicated the presence of a large source of extracellular Zn^{2+}, likely from contaminating Zn^{2+} from solution salts (Kay, 2004), or the proposed "Zn^{2+}-veneer" coating the extracellular surface of cells (Nydegger et al., 2012). In the current study, only contaminating Zn^{2+} signals were seen in the well above the dura (see supplemental Fig. 1), however, basal fluorescence signals decreased rapidly within the brain parenchyma. The maintenance of a relatively low level of extracellular Zn^{2+} during resting conditions, possibly mediated by membrane Zn^{2+} transporters such as the ZIP family of Zn^{2+} transporters (Qian et al., 2011), could indicate the importance of maintaining low extracellular levels of Zn^{2+} for normal brain function.

A large fluorescence increase was seen at the dura surface upon the addition of FluoZin-3. This signal was greatly reduced, but not completely by CaEDTA (see supplemental Fig 1), suggesting that a fraction of this fluorescence increase may not be due to Zn^{2+}. Additional increases in FlouZin-3 fluorescence not abolished by CaEDTA were apparent in surface blood vessel walls. It is possible that FluoZin-3 is sequestered or trapped in these structures, thus preventing CaEDTA from interacting with FluoZin-3 and decreasing the fluorescence. Similar residual FluoZin-3 signals were present in both wild type and ZnT3 KO animals suggesting that synaptic Zn^{2+} does not contribute to the generation of these potential artifacts.

FluoZin-3 signals obtained using single-photon epifluorescence excitation with low power (4x air) objectives had lower signal intensities compared with two-photon excitation, likely due to the higher signal/noise ratio with single-photon imaging. In addition, optical artifacts were more prevalent while imaging FluoZin-3 fluorescence with single-photon excitation. Amplification of tissue autofluorescence was observed in ZnT3 KO animals in the presence of FluoZin-3, indicating that the FluoZin-3 transients observed in wild type animals are likely to be underestimated using single-photon excitation.

Waves of synaptic Zn^{2+} release in vivo during SD

The present study demonstrates large waves of synaptic Zn^{2+} release, detectable through intact dura, during SD induced by KCl *in vivo* (Fig. 2). This observation may suggest a role for synaptic Zn^{2+} release during several pathological states where SDs are known to occur, such as migraine with aura (Hadjikhani et al., 2001), traumatic brain injury (Hartings et al., 2011b) and stroke (Dreier, 2011). In addition, as there was little run-down in FluoZin-3 signal observed following repetitive SDs in the same animal (Fig. 2C), it is possible that each event is capable of releasing large amounts of Zn^{2+} into the extracellular space.

Extracellular Zn^{2+} is well known to inhibit NMDA receptors (Paoletti et al., 1997), and NMDA receptors are essential for the propagation of SD through neuronal tissue (Somjen, 2001). Therefore, synaptic release of Zn^{2+} may serve as an intrinsic modulator of CSD propagation *in vivo*. Recent work has supported this notion, both in brain slices and *in vivo* (Aiba et al., 2012), suggesting a role for synaptic Zn^{2+} in limiting

the spread of SD. In the current study, CaEDTA was present in a majority of the studies to improve the signal/noise for FluoZin-3 measurements. Consistent with our prior work (Aiba et al., 2012), similar SD propagation rates were observed in wild type and ZnT3 KO tissues in the presence of CaEDTA.

Visualization of synaptic Zn^{2+} release during electrical stimulation

As mentioned above, SD is a large stimulus, providing an ideal model system to evaluate synaptic Zn^{2+} release in brain tissue. More moderate stimuli (electrical stimulation to the dura surface) also generated detectable FluoZin-3 signals, extending previous work with electrical stimuli in brain slices (Qian and Noebels, 2005, 2006, Carter et al., 2011). The characterization performed by Quian and Noebels suggests that imaging FluoZin-3 fluorescence could be used as a surrogate for glutamate release, and the present work implies that this could be utilized for studies of physiological activation *in vivo*. Immunohistochemical and immunofluorescence stains have shown the presence of synaptic Zn^{2+} and ZnT3 in the barrel cortex of mice (Liguz-Lecznar et al., 2005). In recent studies investigating experience dependent plasticity of the barrel cortex in mice, alterations in the levels of synaptic Zn^{2+} have been reported (Brown and Dyck, 2005, Nakashima and Dyck, 2010). It would be of interest to determine whether fluorescence visualization of synaptic Zn^{2+} release can be detected following whisker stimulation. It is important to note that due to the significant decrease in signal from SD to electrical stimulation with two-photon excitation, it may be technically difficult to visualize synaptic Zn^{2+} release during physiological activity.

Synaptic Zn^{2+} and ischemic injury

Recent reports have described the occurrence of SD in the neocortex in humans following a wide range of brain traumas (Dreier, 2011, Lauritzen et al., 2011). SDs are emerging as a potentially important and targetable causative factor in the enlargement of ischemic infarcts following stroke in animal models (Hartings et al., 2003), and in human patients (Dreier, 2011, Lauritzen et al., 2011). Previous microdialysis studies have detected increases in extracellular Zn^{2+} following forebrain ischemia *in vivo* (Kitamura et al., 2006b). However, due to the temporal resolution in sampling frequency it is difficult to determine whether a slow steady increase in extracellular Zn^{2+}, or pulsatile increases from SD contribute. The present results suggest that coordinated release from SD events following ischemia could significantly contribute to the increases in extracellular Zn^{2+} accumulation following ischemia. Thus, it is possible that Zn^{2+} release during SDs could be a significant contributor to metabolic compromise, and injury following repetitive SD in post-ischemic tissues. We have recently shown that intracellular Zn^{2+} loading prior to SD significantly worsens recovery of synaptic activity (Carter et al., 2013). Evidence for the worsened metabolic status under these conditions comes from increased duration of DC shifts associated with SD, and also significant increases in extracellular accumulation of the metabolic product adenosine (Carter et al., 2013).

The results with focal ischemia model provide support for the idea that Zn^{2+} released from synaptic vesicles during SD could contribute to the progression of stroke injury. SDs were demonstrated to propagate around the edge of the ischemic core, similar to previous reports in the middle cerebral artery occlusion model (Nakamura et al., 2010). Furthermore, waves of extracellular Zn^{2+} increases were verified as being of a

synaptic source based on the loss of signals in ZnT3 KO animals. These results imply synaptic Zn^{2+} release during these events, and identify a potentially large pulsatile source of Zn^{2+} in the post-ischemic period. Finally, infarct volumes were significantly reduced in ZnT3 KO animals, following the same ischemic challenges. This provides circumstantial evidence that the Zn^{2+} released during ischemic SDs contributed to infarct volume, as SD-induced Zn^{2+} release appears to be by far the largest possible source of Zn^{2+} detectable with these methods in the early post-ischemic phase. It is of course possible that other sources emerge and contribute to injury later in the time course of stroke progression, after the imaging sessions were terminated. However, the reports of numerous, repetitive SDs in the late post-stroke phase, in animals models (Hartings et al., 2003) and in clinical recordings (Dohmen et al., 2008) emphasize that SDs should be considered for these later times as well.

5.6 Figure Legends

Figure 5.1: Synaptic Zn^{2+} release in neocortical slices during SD. **A.** Intrinsic optical signal (IOS) depicting the propagation of SD. SD was induced by bath application of 40mM KCl, and in this representative slice propagated from the right to the left of the slice (arrows). (*top right*) Representative IOS trace showing the kinetics of the light transmission during and after the passage of SD. (*bottom right*) Extracellular DC potential recording showing the sharp negative deflection characteristic of SD. **B.** Fluorescence imaging of FluoZin-3 in a representative wild type slice with kinetic profile of a large extracellular FluoZin-3 signal coincident with the extracellular DC shift. **C.** Fluorescence imaging of FluoZin-3 in a representative ZnT3 KO slice depicting a small

decrease in the fluorescence signal coincident with the passage of SD. **D.** Summary data from wild type and ZnT3 KO slices showing the peak FluoZin-3 response during SD. Numbers in bars represent the number of slices used from each genotype.

Figure 5.2: Synaptic Zn^{2+} release during SD *in vivo* imaged with single-photon microscopy. **A.** Large FluoZin-3 fluorescence increases were observed during the passage of SD in a wild type animal. The kinetics of the FluoZin-3 response was plotted with the extracellular DC recording, and shows that the FluoZin-3 fluorescence increase occurs with the sharp negative DC shift. **B.** FluoZin-3 responses were completely abolished in a ZnT3 KO animal imaged under the same conditions as ***A***. Instead, an amplified autofluorescence decrease was observed, consistent with *in vitro* observations. **C.** Repetitive SDs generated in the same animal show similar FluoZin-3 peak increases with each event. Arrows indicate KCl application to induce SD. Data was collected with 10x water immersion objective. **D.** Summary data from 10x water immersion objectives showing the larger peak FluoZin-3 response to the first SD in wild type animals, and the small decreases attributed to autofluorescence in the ZnT3 KO animals. Numbers in bars represent the numbers of animals from each genotype.

Figure 5.3: Source of FluoZin-3 signals during two-photon microscopy *in vivo*. **A.** Raw fluorescence image from a wild type animal after FluoZin-3 and CaEDTA superfusion (20x water immersion objective). Three regions of interest are drawn to include: brain (-50μm, red), dura (0μm, blue), and well (+70μm, green). Scale bar 200μm. A series of images ($\Delta F/F_0$) acquired during the passage of SD show the vast majority of FluoZin-3

fluorescence detected occurred within the brain. A small response is seen in the well above the brain following the passage of SD. **B.** Two-photon imaging of FluoZin-3 fluorescence from a representative ZnT3 KO animal showed small fluorescence decreases during SD, in agreement with previous *in vitro* slice and *in vivo* single-photon work.

Figure 5.4: Detection of synaptic Zn^{2+} release during bipolar electrical stimulation. **A.** FluoZin-3 response from a wild type animal during a 50Hz stimulation train. Images at the top show raw FluoZin-3 fluorescence (left), baseline $\Delta F/F_0$ 1s before (middle), and 0.5s after stimulation (right). The dura surface is outlined for reference in the $\Delta F/F_0$ images. (*) indicates location of the bipolar stimulating electrode. Scale bar 200μm. Traces at bottom compares the autofluorescence response (in the absence of FluoZin-3, open circles) to the response generated in the presence of FluoZin-3 (filled squares) to a 50Hz stimulation train (grey bar). **B.** Representative images and traces from a ZnT3 KO animal to a 50Hz stimulation train, as in ***A***. **C.** Stimulation response curve showing greater FluoZin-3 signals to higher stimulation frequencies in wild type animals.

Figure 5.5: Synaptic Zn^{2+} release during SD generated by focal ischemia. **A.** Confirmation of loss of cerebral blood flow during dMCAO. (left) Baseline image of cerebral blood flow. (middle) Montage of images following dMCAO showing propagation of SD (arrows indicating leading edge of SD). (right) Kinetic trace of CBF during dMCAO. SD onset indicated by arrow. **B.** FluoZin-3 imaging in a representative wild type animal during dMCAO. (left) Low power (4X air) autofluorescence image of

cortical surface through open cranial window (dura intact). (middle) Series of FluoZin-3 fluorescence images (in the presence of CaEDTA) depicting the propagation of Zn^{2+} release during SD generated by dMCAO. (right) Kinetic profile of FluoZin-3 fluorescence during SD (indicated by arrow). **C.** FluoZin-3 imaging in a representative ZnT3 KO animal during dMCAO. (left) Low power (4X air) autofluorescence image of cortical surface through open cranial window (dura intact). (middle) Series of FluoZin-3 fluorescence images (in the presence of CaEDTA) showing a lack of increased FluoZin-3 fluorescence during SD generated by dMCAO. (right) Kinetic profile of FluoZin-3 fluorescence during SD (indicated by arrow).

Figure 5.6: Synaptic Zn^{2+} contributes to acute ischemic injury. **A.** Whole brain TTC stain from a wild type animal 24hrs following permanent dMCAO showing the cortical infarct area. **B.** Whole brain TTC stain from a ZnT3 KO animal 24hrs following dMCAO revealed a smaller surface cortical infarct. **C.** Wild type brain slices (2mm thickness) from a representative animal stained with TTC 24 hours after dMCAO show an infarct restricted to cortical tissues spread over several sections. **D.** Slices from a representative ZnT3 KO animal stained with TTC showed a reduced cortical infarct. **E.** Summary data of infarct volumes from wild type and ZnT3 KO animals 24hrs following permanent dMCAO. Numbers in bars represent the number of animals included in the analysis (*p=.024).

Supplemental Figure 5.1: Permeation of FluoZin-3 through the dura. **A.** Fluorescence intensity of FluoZin-3 was plotted as a function of time at a depth of 50μm below the

dura. Arrows indicate when agents were applied, and the durations of applications. A marked fluorescence increase was observed immediately following FluoZin-3 application to the cortical surface (200μL/min for 2min). Addition of CaEDTA reduced fluorescence levels to that of the tissue autofluorescence (indicated by dashed line). FluoZin-3 and CaEDTA were then both washed for an extended period of time (~80 min) from the imaging well. Subsequent application of $ZnCl_2$ caused a large fluorescence increase. This indicates that FluoZin-3 was still present in the brain parenchyma following application and subsequent wash-out. Letters in parentheses represent times where Z-stacks were obtained and plotted in (B). **B.** Fluorescence Z-stacks acquired at time intervals depicted in (A). Application of FluoZin-3 (open circles) showed a marked increase in fluorescence above the dura, with a rapid decrease to near autofluorescence levels (filled squares) around 50μm below the dura. Addition of 1mM CaEDTA (open triangles) resulted in the reduction of fluorescence above the dura. It is noted that there was still an increased signal at the dura surface in the presence of CaEDTA. After wash out of FluoZin-3 and CaEDTA, the signals obtained (open diamonds) were nearly identical to autofluorescence levels. Following the wash out period, $ZnCl_2$ was added to determine if any FluoZin-3 was still present. The addition of $ZnCl_2$ (asterisks) resulted in an increase both above and well below the dura, with clear increases evident to 100μm below the dura.

Figure 5.1

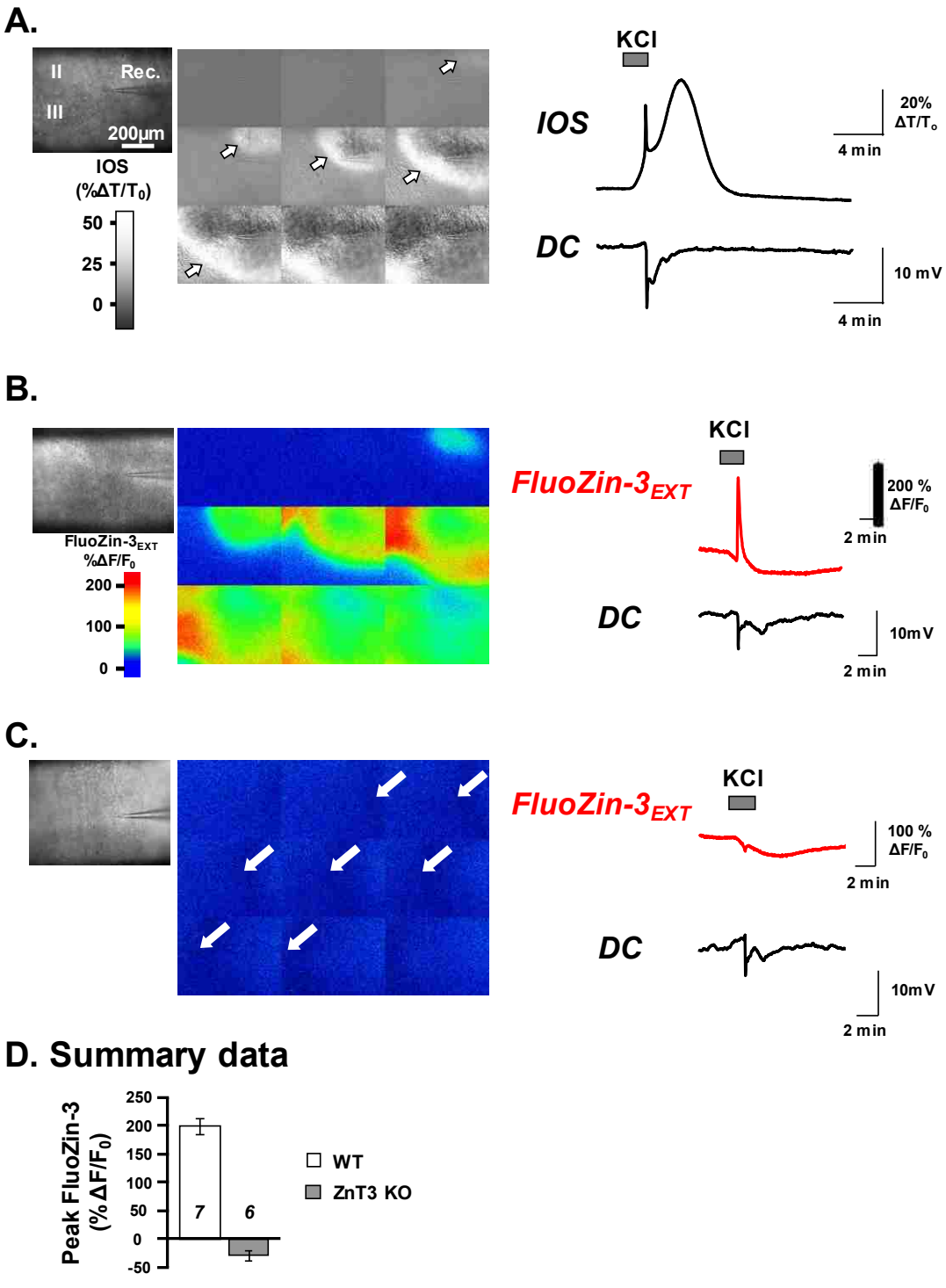
A.
II
III
Rec.
200µm
IOS
(%ΔT/T0)
50
25
0
KCl
IOS
20%
ΔT/To
4 min
DC
10 mV
4 min
B.
FluoZin-3EXT
%ΔF/F0
200
100
0
KCl
FluoZin-3EXT
200 %
ΔF/F0
2 min
DC
10mV
2 min
C.
KCl
FluoZin-3EXT
100 %
ΔF/F0
2 min
DC
10mV
2 min
D. Summary data
Peak FluoZin-3
(% ΔF/F0)
250
200
150
100
50
0
-50
7
6
WT
ZnT3 KO

Figure 5.2

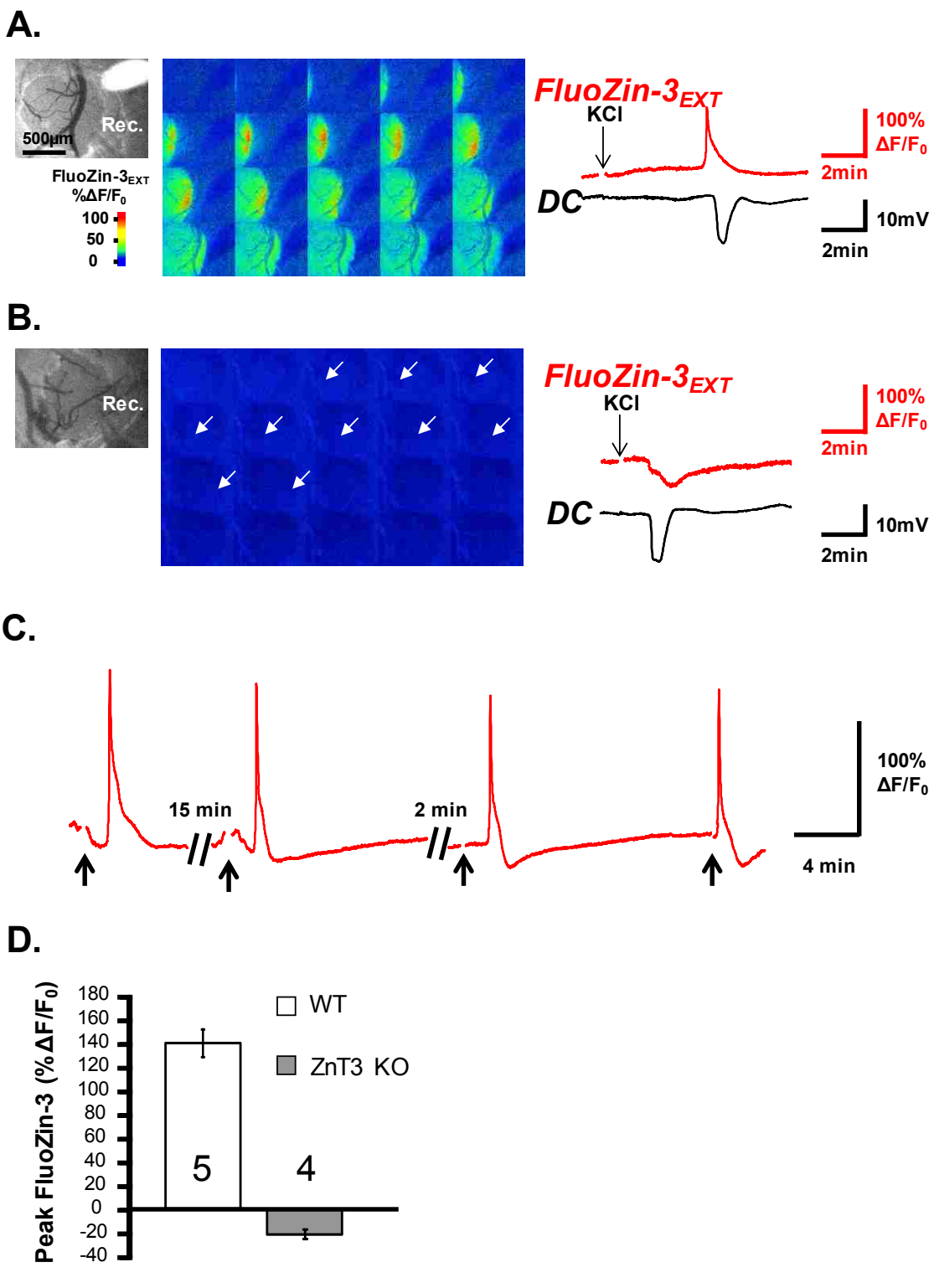
A.
Rec.
500μm
FluoZin-3EXT
%ΔF/F0
100
50
0
FluoZin-3EXT
KCl
DC
100%
ΔF/F0
2min
10mV
2min
B.
Rec.
FluoZin-3EXT
KCl
DC
100%
ΔF/F0
2min
10mV
2min
C.
15 min
2 min
100%
ΔF/F0
4 min
D.
Peak FluoZin-3 (%ΔF/F0)
180
160
140
120
100
80
60
40
20
0
-20
-40
WT
ZnT3 KO
5
4

Figure 5.3

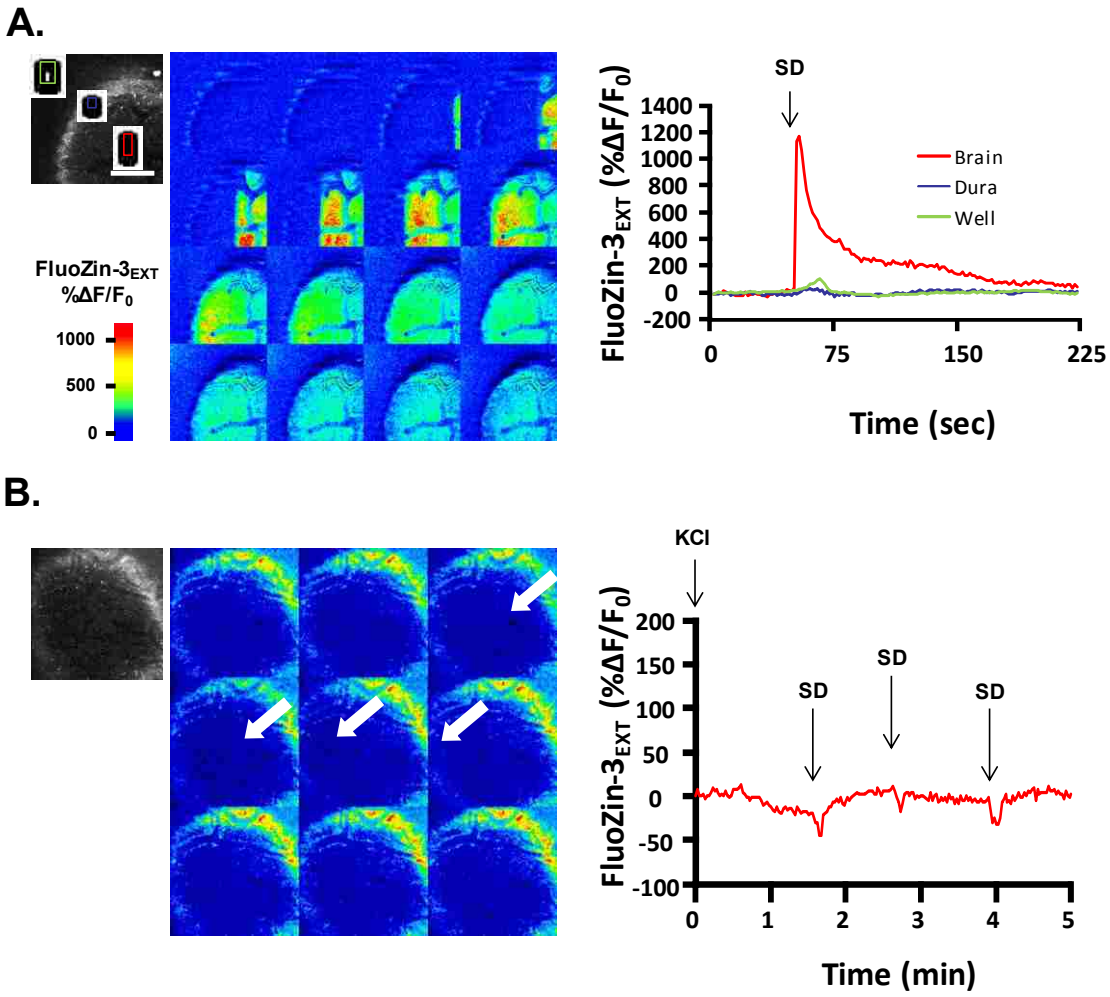
A.
FluoZin-3EXT
%ΔF/F0
1000
500
0
SD
1400
1200
1000
800
600
400
200
0
-200
FluoZin-3EXT (%ΔF/F0)
Brain
Dura
Well
0
75
150
225
Time (sec)
B.
KCl
SD
SD
SD
200
150
100
50
0
-50
-100
FluoZin-3EXT (%ΔF/F0)
0
1
2
3
4
5
Time (min)

Figure 5.4

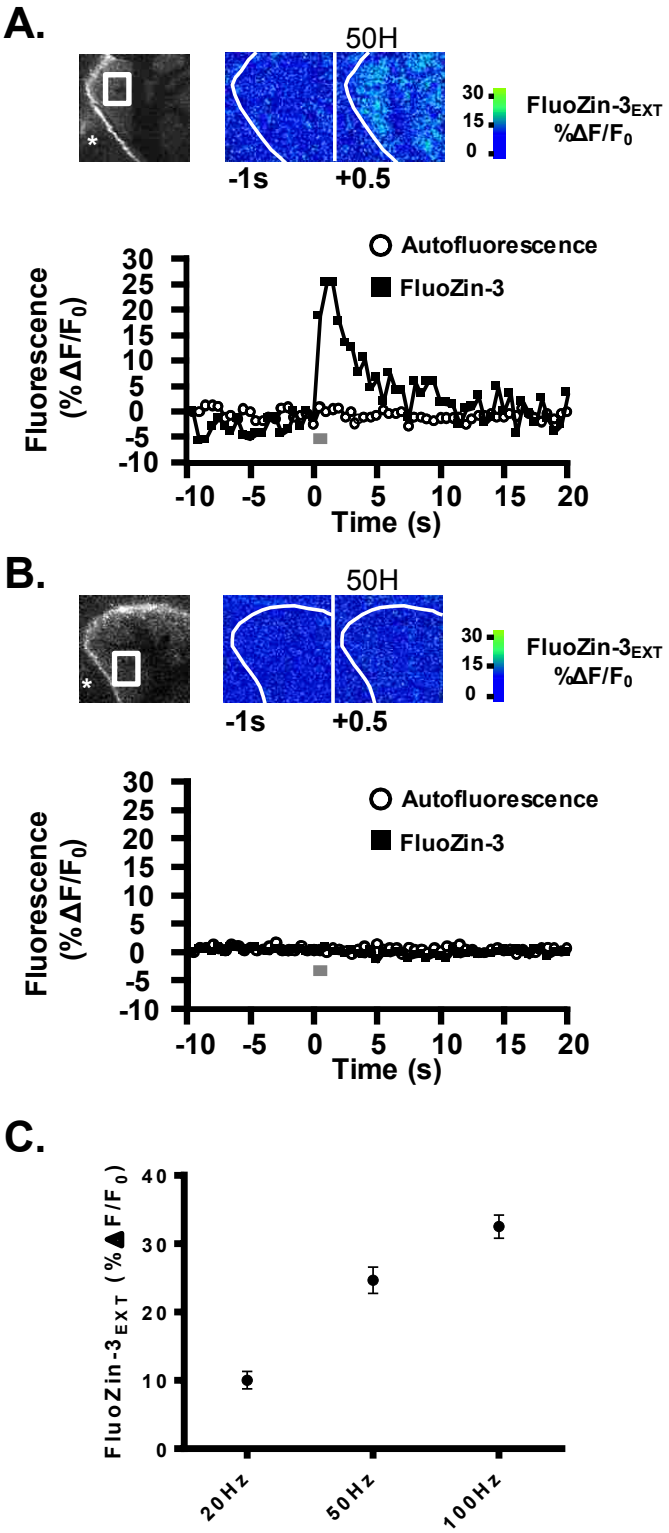
A.
50H
30
15
0
FluoZin-3EXT
%ΔF/F0
-1s
+0.5
Autofluorescence
FluoZin-3
Fluorescence
(%ΔF/F0)
Time (s)
B.
50H
30
15
0
FluoZin-3EXT
%ΔF/F0
-1s
+0.5
Autofluorescence
FluoZin-3
Fluorescence
(%ΔF/F0)
Time (s)
C.
FluoZin-3EXT (%ΔF/F0)
20Hz
50Hz
100Hz

Figure 5.5

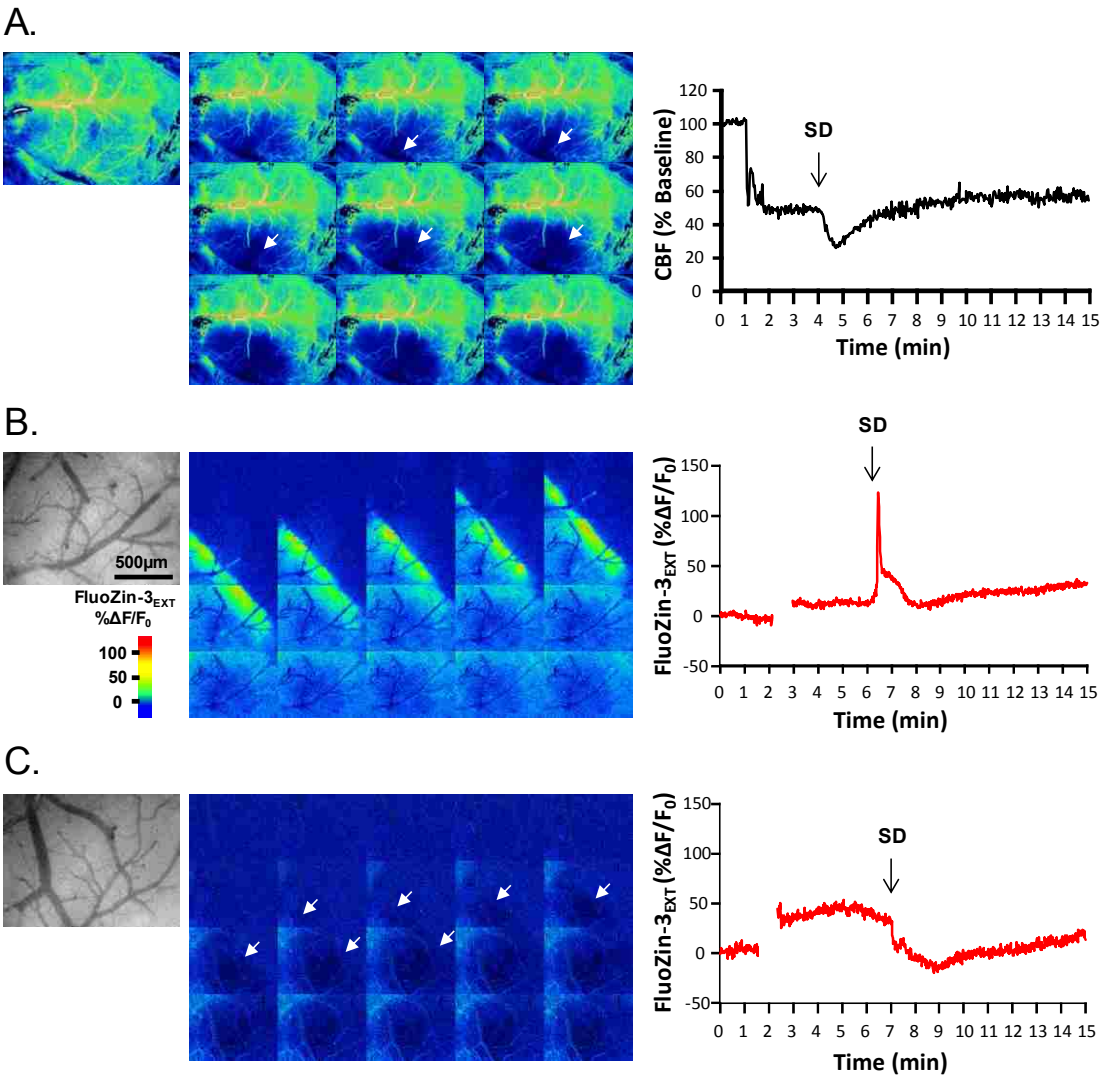
A.
CBF (% Baseline)
SD
Time (min)
B.
500µm
FluoZin-3EXT
%ΔF/F0
100
50
0
SD
FluoZin-3EXT (%ΔF/F0)
Time (min)
C.
SD
FluoZin-3EXT (%ΔF/F0)
Time (min)

Figure 5.6

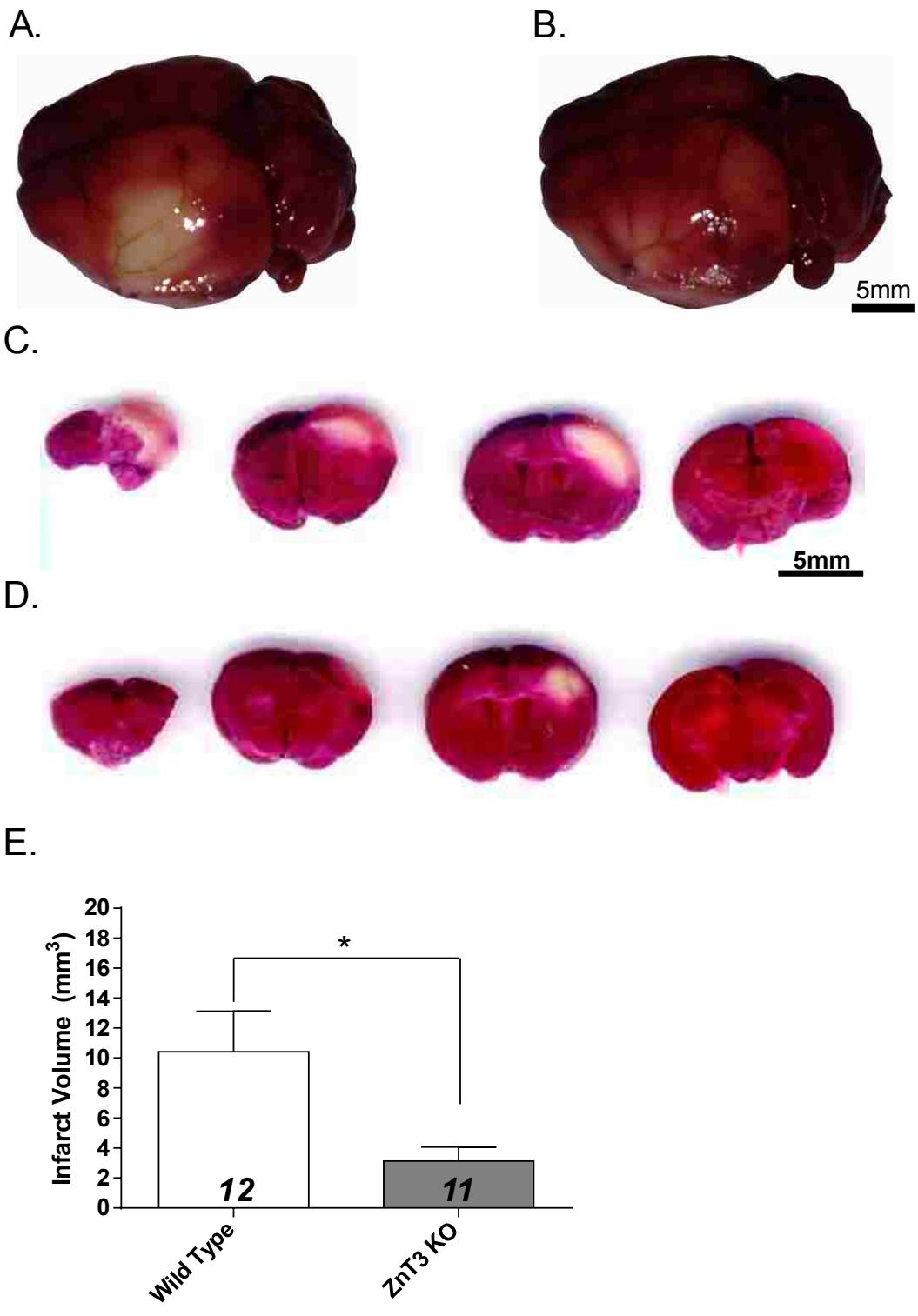
A.
B.
5mm
C.
5mm
D.
E.
Infarct Volume (mm3)
20
18
16
14
12
10
8
6
4
2
0
*
12
11
Wild Type
ZnT3 KO

Supplemental Figure 5.1

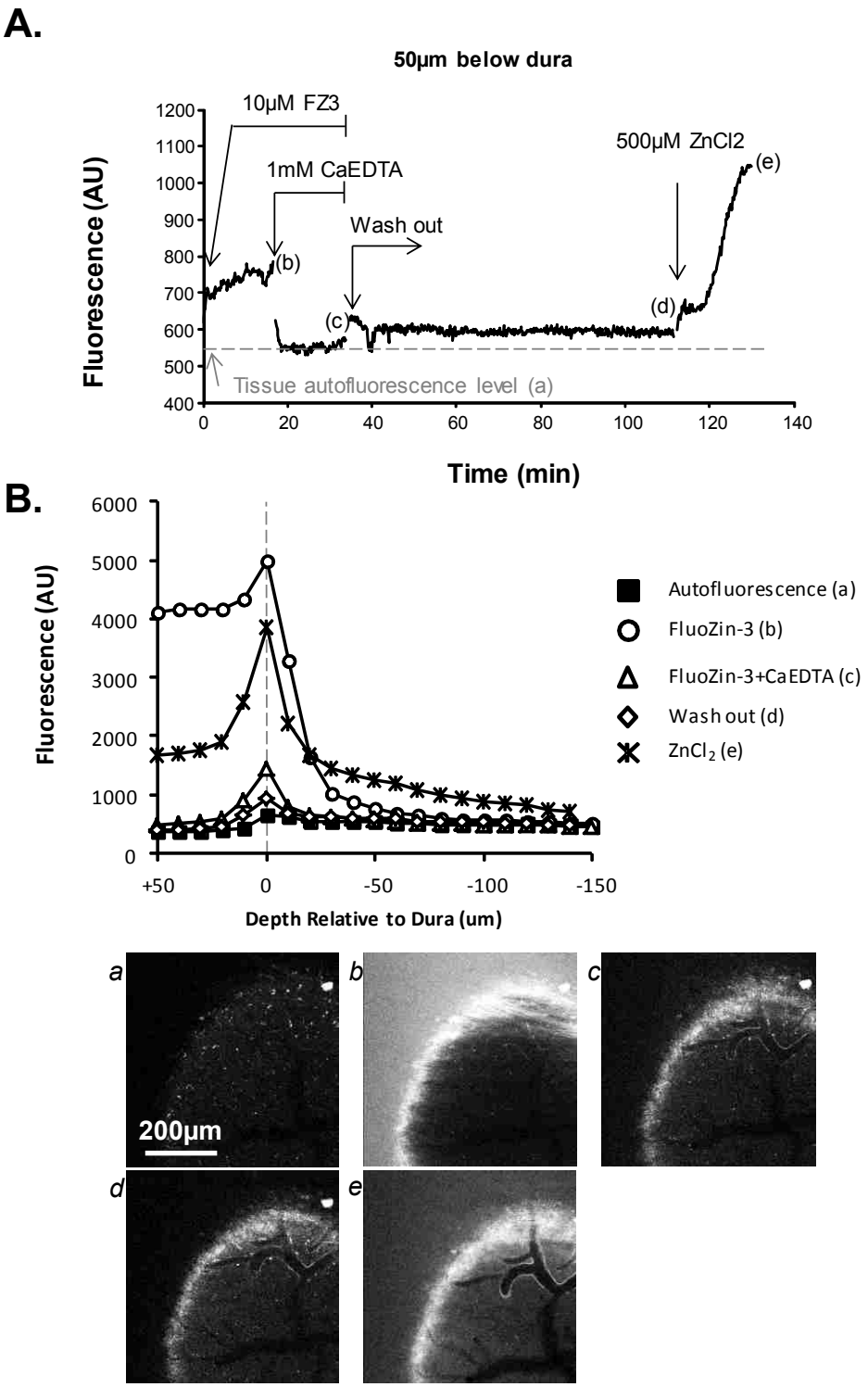

Chapter 6: Discussion

6.1 Summary of Dissertation Studies

The work presented here provides new insights into the sources of toxic Zn^{2+} accumulation relevant for ischemic injury. Studies from Chapter 2 provide the first evidence for large releases of synaptic Zn^{2+} during the passage of SD with little decrement in the levels of synaptic Zn^{2+} released with each event triggered by high K^+-SD. Further studies supported true synaptic release of Zn^{2+} and translocation into postsynaptic cells following SD through the use of intracellular indicators for, and extracellular chelators of, Zn^{2+}.

Results from Chapter 3 expanded on and clarified previously published work and provide evidence that Zn^{2+} chelation by a membrane permeable Zn^{2+} chelator, TPEN, was only protective by significantly delaying the onset of OGD-SD (Medvedeva et al., 2009). When slices were exposed to a defined length of OGD, in the presence of TPEN, where SD did not occur, there was complete neuronal recovery. However, even when OGD-SD occurred in the absence of Zn^{2+}, irrecoverable neuronal injury still occurred, which was mediated by Ca^{2+}. Thus, the current work suggests that the recovery seen previously was likely due to Zn^{2+} chelation delaying the onset of SD (Dietz et al., 2008), and sheds light on the importance for monitoring the time-course of experiments when testing new neuroprotective treatments.

The work presented in Chapter 4 provided evidence that Zn^{2+} accumulation can significantly impair the ability to recover from SD. Suppression of evoked synaptic potentials, DC shift durations, and extracellular adenosine accumulation were all

prolonged only when there was significant Zn^{2+} accumulation combined with SD. Additionally, there was a surprising finding that a rapid adaptation occurs following repetitive SDs that preconditions tissues to a subsequent Zn^{2+} challenge. This work suggests that not only can Zn^{2+} accumulation contribute to impaired recovery following SD, but that SD itself may have some significant short term beneficial effects that need to be further investigated.

In Chapter 5, the first fluorescence visualization of synaptic Zn^{2+} release *in vivo* is provided. Synaptic Zn^{2+} release was seen following three paradigms, electrical stimulation, SD in healthy tissue, and SD generated by distal middle cerebral artery occlusion (dMCAO). Both single- and two-photon microscopy were used to verify that synaptic Zn^{2+} release occurred within the brain parenchyma. Finally, this work also provides the strong evidence that synaptic Zn^{2+} significantly contributes to the progression of ischemic injury by measuring infarct volumes in wild-type and ZnT3 KO animals following dMCAO.

6.2 Imaging Synaptic Zn^{2+} Release

There has been a controversy in the Zn^{2+} field as to whether there is indeed synaptic Zn^{2+} release. Previous studies have utilized extracellular Zn^{2+} indicators, which may produce a false signal, as suggested by the works of Alan Kay's group (Kay, 2003). This point was addressed in the current studies by using the following approach. First, by using the extracellular Zn^{2+} chelator CaEDTA, all sources of extracellular Zn^{2+} were removed, including contaminating Zn^{2+} as well as any possibility of the presence of Zn^{2+} coating the extracellular surface of cells, before SD induction. Secondly, by combining

this with intracellular measurements from single cells loaded with FluoZin-3 (experiments performed by Isamu Aiba) any increases in intracellular fluorescence can be attributable to synaptic Zn^{2+} translocation. Increases in intracellular fluorescence were only seen following SD in wild-type animals and not in ZnT3 KO animals. This observation, combined with the large releases of synaptic Zn^{2+} following SD, supports the hypothesis that synaptic Zn^{2+} is released upon neuronal activation and translocates into postsynaptic cells.

The implication that synaptic Zn^{2+} release occurs *in vivo* is based on *in vitro* evidence for the presence of synaptic Zn^{2+} and the detection of release previously described in the Introduction (see section 1.2.1). By utilizing similar approaches used for imaging synaptic Zn^{2+} release in slice work, the results from Chapter 5 provide the first real-time fluorescence detection of synaptic Zn^{2+} release *in vivo*. The FluoZin-3 fluorescence signal seen during SD did not decrease following repetitive episodes of SD in the same tissue, both *in vitro* and *in vivo*. This could suggest that there is only a subpopulation of synaptic vesicles released during SD, that synaptic Zn^{2+} is completely re-filled between SD episodes, or a contribution of both mechanisms, contribute to this lack of decreased signal.

Little is known about synaptic vesicle dynamics during and following SD. Three pools of synaptic vesicles have been identified and their release characteristics depend on the intensity and duration of the stimulation. The readily releasable pool (RRP) and the recycling pool are released and can refill within seconds of the stimulation, while the reserve pool requires a more prolonged stimulation (seconds to minutes) to be released and is much slower, on the order of minutes, to refill (Rizzoli and Betz, 2005). Due to

the intense neuronal depolarization that can last for minutes during SD, it remains unclear if all available synaptic vesicles could be released during SD. Synaptic vesicle fusion is dependent on the influx of Ca^{2+} into the presynaptic terminal, predominantly through P/Q-type calcium channels (Pietrobon, 2005). These calcium channels show more sensitive voltage-dependent inactivation compared to L-type Ca^{2+} channels (Villarroya et al., 1999), which could suggest that, despite the prolonged neuronal depolarization during SD, complete synaptic vesicle release may not occur. In support of this, it was recently shown that immediately following the passage of SD, the frequency of spontaneous excitatory postsynaptic currents was significantly increased (Aiba and Shuttleworth, 2012), suggesting that at this time-point, sufficient amounts of synaptic vesicles are still present. It is not known if and how synaptic vesicle re-filling contributes to the refractory period of SD, but further study might indicate if it is possible to target this process to prevent the occurrence of these events selectively in ischemic tissue.

It is not yet known how Zn^{2+} is cleared from the synapse following normal neuronal activity or SD, and whether this clearance is similar to classical neurotransmitter clearance mechanisms. Astrocytes play a major role in glutamate clearance, mediated by both the glutamate transporter-1 (GLT-1) and the glutamate/aspartate transporter (GLAST) (Rothstein et al., 1996). Several Zn^{2+} transporters are expressed on the plasma membrane and could contribute to Zn^{2+} clearance, with the primary Zn^{2+} importer being ZIP1 (Gaither and Eide, 2001b). This transporter appears to play a role in the clearance of Zn^{2+} following seizure-like activity ((Qian et al., 2011) and see section 6.4 below), suggesting the presence of clearance mechanisms for extracellular Zn^{2+}. The mechanism(s) underlying ZnT3 transport of Zn^{2+} into synaptic vesicles also remains to be

elucidated. Studies conducted with bacterial analogues of Zn^{2+} transporters suggest that Zn^{2+} transport into vesicles is dependent on an electrochemical H^{+} gradient generated by a V-ATPase (MacDiarmid et al., 2002, Smidt and Rungby, 2012). Whether or not a similar mechanism exists for ZnT3 is not known, and how this relates to glutamate re-filling after SD could be assessed in future studies.

Utilizing the phenomenon of SD was an ideal starting model to investigate fluorescence detection of synaptic Zn^{2+} release. Having shown large, robust signals following not only SD, but direct electrical stimulation, leads to the question of whether synaptic Zn^{2+} release can be detected following normal physiological stimulation *in vivo*. Recent work utilizing whisker stimulation in rodents has revealed alterations in the levels of synaptic Zn^{2+}, assessed by histochemical stains, in the barrel cortex of mice (Brown and Dyck, 2002, 2005, Nakashima and Dyck, 2010). It should be noted that these studies utilized prolonged (up to 24hrs) whisker stimulation to see reductions in synaptic Zn^{2+} levels. This may result in adaptations to the constant stimulation by reducing the amount of postsynaptic glutamate receptors. Zn^{2+} can inhibit NMDA receptors (Paoletti et al., 1997) and act to modulate neuronal communication by influencing glutamate signaling. Therefore, the constant stimulation may result not in a depletion of synaptic Zn^{2+} due to constant release, but in a modulation of synaptic Zn^{2+} present in vesicle to decrease the postsynaptic inhibition on fewer receptors and allow for proper signaling. Nevertheless, from these studies, it would seem apparent that the barrel cortex could be an ideal region to test for synaptic Zn^{2+} release during physiological activation *in vivo*.

Pilot studies were conducted for the present dissertation work to investigate the possibility of imaging synaptic Zn^{2+} release during whisker stimulation in mice.

However, FluoZin-3 fluorescence signals could not be detected in those studies following whisker stimulation. It would seem appropriate to investigate this possibility further, for example by utilizing different anesthetics to optimize the stimulus conditions, using electrophysiological measures of effective activation. Isoflurane, the main anesthetic used in the current work, significantly inhibits evoked responses (Rojas et al., 2006) and could have significantly reduced the intensity of whisker stimulation-evoked cortical signals. Other anesthetics which are more suited for electrophysiology *in vivo* may be useful in re-examining this possibility. However, based on the relatively small FluoZin-3 signal amplitudes acquired from strong direct electrical stimulation of the cortex (Chapter 5), it still may be necessary to utilize higher power objectives to image a smaller portion of the cortex, and improve detection sensitivity for small events such as whisker stimulation. Additionally, the use of CaEDTA should be avoided here to allow for any synaptic Zn^{2+} release to interact solely with the indicator and remove the possibility of added Zn^{2+} chelation, and therefore decreased FluoZin-3 responses, during whisker stimulation.

Direct fluorescence detection of synaptic Zn^{2+} release *in vivo* (Chapter 5) further supports the possibility of using FluoZin-3 fluorescence as a surrogate for "imaging" synaptic glutamate release. This hypothesis was originally based on studies conducted in hippocampal slice preparations that found that the levels of extracellular FluoZin-3 fluorescence were positively correlated with the amplitudes of evoked excitatory postsynaptic potentials (Qian and Noebels, 2005, 2006). This has the potential for applications investigating either increased or decreased neurotransmitter release *in vivo*, such as during synaptic plasticity (LTP and/or LTD). Interestingly, certain mutations in

presynaptic P/Q-type Ca^{2+} channels have been implicated in migraine with aura, a condition which is thought to be mediated by SD. These mutations can result in increased Ca^{2+} conductance leading to enhanced neurotransmitter release, which is thought to facilitate the occurrence of SD (Tottene et al., 2009). Imaging synaptic Zn^{2+} release in these models could be another measure of increased neurotransmitter release.

6.3 Targets for Synaptically Released Zn^{2+}

While the present work does not directly address actions of synaptic Zn^{2+} release on postsynaptic targets, one of the more relevant targets for SD and ischemia would be the NMDA receptor. The NMDA receptor can be inhibited by extracellular Zn^{2+} interacting with the NR2A subunit (Paoletti et al., 1997). As described earlier, NMDA receptors are critical for the propagation of SD, and therefore it seems likely that the large amounts of synaptic Zn^{2+} released during SD may have an impact on NMDA receptor function. Indeed, studies from our lab conducted in parallel with the present work have indicated that synaptic Zn^{2+} release during SD acts as an intrinsic inhibitor on SD propagation *in vitro* and *in vivo* (Aiba et al., 2012), further supporting synaptic Zn^{2+} release but also implicating a physiological role for Zn^{2+} release *in vivo*. The inhibition of SD by synaptic Zn^{2+} could account for the increased numbers of SDs seen in ZnT3 KO animals in response to KCl applications in the previous (Aiba et al., 2012) and in the current studies (Chapter 5). However, whether this inhibition occurs under ischemic conditions is still unclear.

The experiments from Chapter 5 show that ZnT3 KO animals have significantly smaller infarcts compared to wild type animals. If the ZnT3 KOs are still experiencing a

greater number of SDs in the post-ischemic period, based on previous reports they should have larger infarcts with the increased occurrence of SDs (Back et al., 1996, Busch et al., 1996). Yet ZnT3 KO animals have smaller infarcts. The number of SDs occurring in these animals following dMCAO was not investigated in the current work and future studies should examine the frequency of SDs during longer recording sessions in these two genotypes to determine whether there is a difference. If there is still an increased number of SDs in ZnT3 KO animals, it could support the hypothesis that synaptic Zn^{2+} release and postsynaptic accumulation has a major role in limiting the recovery from SD (see Chapter 4) and contributes to the progression of ischemic injury.

Recently, an orphan G protein-coupled receptor was found to be sensitive to Zn^{2+} (GPR39/mZnR) and activation of this receptor in response to exogenous Zn^{2+} application results in release and accumulation of intracellular Ca^{2+} (Hershfinkel et al., 2001). This receptor was then identified within the hippocampus, where similar intracellular Ca^{2+} increases were observed in slices in response to exogenous applications of Zn^{2+}, as well as from the release of endogenous synaptic Zn^{2+} (Besser et al., 2009). Following electrical stimulation of the mossy fibers in hippocampal slices, increases in intracellular Ca^{2+} were seen in control animals, while Ca^{2+} increases were significantly reduced in ZnT3 KO animals (Besser et al., 2009). In addition, subsequent studies utilizing GPR39 KO mice found similar levels of synaptic Zn^{2+} release in hippocampal slices following similar mossy fiber stimulation, and subsequent postsynaptic Ca^{2+} increases were reduced in these animals (Chorin et al., 2011), supporting a role for synaptic Zn^{2+} release and postsynaptic interactions. Following SD there is an increase in postsynaptic $[Ca^{2+}]$ that can either be fully recoverable resulting in no injury in healthy conditions, or can be

irrecoverable leading to neuronal death depending on the metabolic status of the tissue (Dietz et al., 2008, Aiba and Shuttleworth, 2012). From the current work, the large levels of synaptic Zn^{2+} release during SD may activate postsynaptic mZnRs and contribute to the increased levels of intracellular Ca^{2+} following SD. Currently it is not known what the effects of knocking out the zinc-sensing receptor are on SD and ischemic injury and would be important to investigate in future studies.

6.4 Routes of Zn^{2+} Influx

Routes of Zn^{2+} influx may be important to investigate as potential targets to prevent neurotoxic accumulation of extracellular Zn^{2+} following ischemia. Several routes have been identified to allow Zn^{2+} entry, and not surprisingly, many of the pathways are routes originally found to be Ca^{2+} permeable. Voltage-gated Ca^{2+} channels have been found to be permeable to Zn^{2+}, as by blocking these channels with Gd^{3+}, Cd^{2+}, or nimodipine (an L-type Ca^{2+} channel blocker) reduced the uptake of Zn^{2+} into cultured neurons (Weiss et al., 1993, Kerchner et al., 2000, Sheline et al., 2002). It was also recently discovered that Zn^{2+} entry through L-type Ca^{2+} channels was an important trigger for the initiation of some forms of SD in slice preparations (Dietz et al., 2008). L-type Ca^{2+} channel blockers prevented Zn^{2+} uptake, and under certain conditions relevant for ischemia, was sufficient in blocking SD alltogether (Dietz et al., 2008).

Zn^{2+} can also enter through Ca^{2+}-permeable AMPA/kainate receptors. This was shown by applying exogenous extracellular kainite and Zn^{2+} to cultured cortical neurons in the absence of extracellular Na^{+}, to prevent depolarization induced Zn^{2+} entry, and found Zn^{2+} accumulation mediated by AMPA/kainate receptors (Yin and Weiss, 1995).

AMPA receptors that lack the GluR2 subunit are permeable to both Ca^{2+} and Zn^{2+} (Pellegrini-Giampietro et al., 1997). Interestingly, it was reported that GluR2-containing AMPA receptors are down-regulated in hippocampal CA1 neurons 72 hours following global ischemia in gerbils (Gorter et al., 1997). Blocking Ca^{2+}-permeable AMPA/kainate receptors with a compound that only recognizes GluR2 lacking AMPA receptors (Naspm), partially prevented toxic intracellular Zn^{2+} accumulation (assessed by TSQ staining) and subsequent neuronal death assessed at the same 72 hour mark after ischemia (Noh et al., 2005). Therefore, it is possible that synaptic Zn^{2+} release during SD could accumulate via Ca^{2+}-permeable AMPA/kainate receptors in the days following the initial ischemic event.

As noted above, a recent study has also suggested significant contributions of the plasma membrane Zn^{2+} transporters ZIP1 and ZIP3 to intracellular Zn^{2+} accumulation following seizure-like activity (Qian et al., 2011). Thus, knockouts of these transporters significantly reduced Zn^{2+} accumulation in hippocampal brain slices, and reduced neuronal damage following kainic acid induced seizures *in vivo* (Qian et al., 2011). The results from Chapter 2 suggest that the extracellular Zn^{2+} levels remain elevated for several minutes following SD. When other sources of Zn^{2+} flux may be blocked at this time, such as from voltage-dependent channel inactivation due to persistent membrane depolarization, Zn^{2+}-selective transporters may continue to import extracellular Zn^{2+} into cells. Future studies could investigate these routes of Zn^{2+} entry following SD to determine whether synaptic Zn^{2+} translocation can be prevented by ZIP inhibition.

6.5 Potential Mechanisms Linking Synaptic Zn^{2+} to Ischemic Damage

Metabolic Inhibition

The current work provides evidence for a novel mechanism that links Zn^{2+} to neuronal injury (Chapter 4). This study showed that intracellular Zn^{2+} accumulation was found to enhance the metabolic burden associated with SD. The prominent hypothesis in the SD field is that impaired metabolic activity following repetitive SDs in compromised tissue is the major mechanism behind the deleterious effects of SD (Dreier, 2011, Lauritzen et al., 2011). As mentioned in the Introduction, experimental recordings of SD found that these events can continuously cycle around ischemic infarcts and result in the expansion of infarct with each cycle (Nakamura et al., 2010, Kumagai et al., 2011). Additionally, clinical recordings have identified clusters of SDs, defined as repetitive SD events occurring within 2hrs from a previous event (Hartings et al., 2011b), to be associated with enhanced metabolic burden resulting in the expansion of injured tissue (Dreier, 2011, Hartings et al., 2011b, Sakowitz et al., 2013, Woitzik et al., 2013).

Enhanced metabolic challenges are associated with an increase in extracellular adenosine accumulation from a wide range of sources, including from the breakdown of ATP (Dunwiddie and Masino, 2001). This is thought to be neuroprotective, as adenosine can decrease the release of glutamate and therefore help prevent excessive glutamate signaling and excitotoxicity (Rudolphi et al., 1992b, Dunwiddie and Masino, 2001, Lovatt et al., 2012). It was recently found that SD results in a large extracellular adenosine accumulation, providing a mechanism that mediates the secondary synaptic suppression following SD (Lindquist and Shuttleworth, 2012). In the current study, when intracellular Zn^{2+} levels were increased, SD resulted in larger extracellular adenosine

accumulations and prolonged DC shift durations, both measureable indicators for an increase in metabolic burden (Rudolphi et al., 1992a, Masino et al., 1999, Hartings et al., 2011b). Therefore, the results of the current study suggest that the synaptic Zn^{2+} release and accumulation following repetitive SD events could be a potential link for the increased metabolic challenge associated with these events, under compromised conditions, leading to neuronal injury.

This raises the question as to whether additional, or alternative, metabolic substrate supplementation would enable tissues to better recover from elevated intracellular Zn^{2+} combined with SD. Following metabolic inhibition by toxic Zn^{2+} exposures, pyruvate supplementation was beneficial in limiting the amount of neuronal injury in culture (Sheline et al., 2000). Results from the current study suggested that metabolic inhibition, in slice experiments, occurred downstream of pyruvate utilization (Chapter 4), suggesting that metabolic supplementation would need to be provided at later stages. This warrants further study to elucidate the site(s) where Zn^{2+} inhibits metabolism to test whether metabolic supplementation could be a beneficial strategy to help tissues recover following SD.

In a previous report, following OGD exposures in slice, rapid Zn^{2+} accumulation into mitochondria significantly enhanced mitochondrial dysfunction leading to Ca^{2+} deregulation and impaired synaptic recovery, all of which was ameliorated by total Zn^{2+} chelation (Medvedeva et al., 2009). While it was suggested that Zn^{2+} was contributing to the majority of the effects reported, recent evidence (Dietz et al., 2008) and results from Chapter 3 support the hypothesis that SD is the major culprit behind neuronal injury in the slice OGD model. Zn^{2+} chelation with TPEN significantly delayed the onset of SD,

consistent with prior work (Dietz et al., 2008), however, even with Zn^{2+} chelation, OGD-SD could still be induced in the current study and resulted in irrecoverable neuronal injury. These observations are consistent with a model where under complete metabolic substrate removal, intracellular Zn^{2+} increases facilitate the generation of SD events and subsequent Ca^{2+} deregulation leading to neuronal injury (Dietz et al., 2008, Vander Jagt et al., 2008, Vander Jagt et al., 2009a). It could be possible that with repetitive rounds of SD during ischemia, synaptic Zn^{2+} release and accumulation in mitochondria may contribute to the initiation of subsequent SDs, furthering metabolic compromise and leading to neuronal injury.

Blood-Brain Barrier Disruption

Synaptic Zn^{2+} release was found to significantly contribute to ischemic injury progression *in vivo* (Chapter 5). One interesting possibility is the potential for synaptic Zn^{2+} to activate extracellular matrix metalloproteases (MMPs) and result in the breakdown of the extracellular matrix and components comprising the blood-brain barrier (BBB). MMPs, specifically MMP-9, have been implicated to lead to BBB disruption in brain pathologies, such as bacterial meningitis (Leppert et al., 2000) as well as following ischemia/reperfusion (Aoki et al., 2002). MMP-9 protein expression was found to be up-regulated starting at 3hrs and continued to increase for up to 24hrs following permanent MCAO in mice (Asahi et al., 2000). Furthermore, utilizing MMP-9 knockout mice, the same group showed a significant reduction in infarct volume in the MMP-9 KO mice compared to wild types (Asahi et al., 2000). A more recent study revealed that following 3 repetitive SDs in normally perfused tissue *in vivo*, MMP-9 levels increased in a fashion

similar to that described following ischemia above, steadily increasing and peaking at 24hrs (Gursoy-Ozdemir et al., 2004). Correspondingly, an increase in Evan's Blue leakage was seen in a similar manner to that of increased levels of MMP-9, and by either blocking SD, inhibiting MMPs, or using MMP-9 KO mice there was a significant reductions in Evan's Blue leakage (Gursoy-Ozdemir et al., 2004), suggesting that MMP-9 activation following SD results in BBB disruption. As MMPs require Zn^{2+} for catalytic activity, it seems very possible that the synaptic Zn^{2+} released during SD shown in the current studies contributes to the activation of MMP-9 and subsequent BBB disruption. This could provide a potential mechanism behind the enhanced BBB disruption and increased infarct volume reported in previous studies. Further looking at MMP-9 activation in ZnT3 KO animals could provide new insights into how synaptic Zn^{2+} may contribute to BBB disruption and ischemic injury.

Another potential mechanism for the decreased infarct size in ZnT3 KO animals seen in Chapter 5 could result from an interesting effect that brain endothelial cells have in response to Zn^{2+} depletion. Di Cello et al. tested the transendothelial electrical resistance (TEER) across a film of cultured human brain microvascular endothelial cells (HBMEC) as a measure of the strength of the tight junctions created by these cells in culture (Di Cello et al., 2005). They found that in response to Zn^{2+} removal, TEER decreased in non-brain endothelial cells indicating disruption of the tight junctions, however, brain endothelial cells displayed an increase in TEER in response to Zn^{2+} removal, indicating an enhancement of tight junctions (Di Cello et al., 2005). This process could strengthen the BBB and help resist against breakdown and leakage following SD and ischemia. An exchangeable pool of Zn^{2+} was found in the

cerebrovascular wall of mice (Friedlich et al., 2004). The source of this Zn^{2+} appeared to originate from synaptic stores, as this pool was not detected in ZnT3 KO mice (Friedlich et al., 2004). Therefore, one explanation of reduced infarct volumes in ZnT3 KO mice could be from preventing BBB disruption by the lack of synaptic Zn^{2+} strengthening tight junctions. Another important contributor to the BBB function is from pericytes. Pericytes are located mainly on the abluminal side of capillaries, express tight junction markers, and can contribute to capillary constriction (Sa-Pereira et al., 2012). Specifically, it was found that regardless of reperfusion following ischemia, contraction of pericytes can still impair blood flow through capillaries (Yemisci et al., 2009). It is unclear what role, if any, Zn^{2+} has on pericytes, but the presence of an exchangeable pool of Zn^{2+} within the cerebrovascular space could suggest that synaptic Zn^{2+} might interact with pericytes. Whether or not enhanced cerebral blood flow could contribute to the reduction in infarct volume in ZnT3 KO mice remains an open question.

Inflammation

Inflammation also plays a major role in injury mechanisms following ischemia (Yenari et al., 2010). It was recently observed that extracellular Zn^{2+} can activate microglial cells (Kauppinen et al., 2008), likely by Zn^{2+} uptake via ZIP1, and subsequent signaling cascades (including PARP-1 and NADPH oxidase activation, reactive oxygen species (ROS) generation, and ATP secretion) resulting in microglial activation (Kauppinen et al., 2008, Higashi et al., 2011). Activated microglial cells can secrete pro-inflammatory cytokines, MMPs, and generate ROS, all of which could impair recovery following ischemia (Yenari et al., 2010). It would seem possible that synaptic Zn^{2+}

release contributes to microglia activation following ischemia, as injections of CaEDTA immediately following transient 20min global ischemia in mice decreased the number of activated microglia (Kauppinen et al., 2008). As inflammation was thought to be one of the major mechanisms for the expansions of some lesions at later times following ischemia (Dirnagl et al., 1999), it seems important to investigate the possibility of synaptic Zn^{2+} to this process.

6.6 Beneficial Effects of Spreading Depolarizations

Synaptic Zn^{2+} Release

As discussed above, numerous studies have investigated the deleterious roles Zn^{2+} plays following ischemia. However, there is a possibility that synaptic Zn^{2+} may provide some protection. Endogenous synaptic Zn^{2+} release may limit the occurrence of SDs, as described above (Aiba et al., 2012). Synaptic Zn^{2+} release may also contribute to an ischemic preconditioning effect in healthy and nominally healthy tissue surrounding the penumbra and ischemic core. A recent report investigated the potential for Zn^{2+} to contribute to preconditioning effects in cell culture and found that a sub-lethal exposure to Zn^{2+} conferred neuroprotection to a later lethal challenge (Aras et al., 2009). The observed Zn^{2+}-induced preconditioning effect in that study was mediated by PKC signaling, which has been implicated in other neuronal preconditioning paradigms (Li et al., 2005, Sivaswamy et al., 2010).

Following ischemia, an increase in neurogenesis can occur that directs new neuronal precursors to the injured areas and is thought to contribute to the repair process (Ohira, 2011). The mechanism(s) of this increased neurogenesis remains unclear, but

recent experimental evidence suggests that SD might play a role. Inducing SD in the neocortex *in vivo* led to an increase in neurogenesis in the dentate gyrus (Urbach et al., 2008) and new immature neurons found in the cortex (Xue et al., 2009). In these studies, neurogenesis was assessed days to weeks following a repetitive SD stimulation paradigm ranging from hours to days. It was also recently found that by either chelating Zn^{2+} or using ZnT3 KO mice, there was a reduction in neurogenesis at basal conditions (in the absence of SD) and following hypoglycemia (Suh et al., 2009), a condition found to transiently influence hippocampal neurogenesis (Suh et al., 2005). Therefore, it is possible that synaptic Zn^{2+} released during repetitive SDs following ischemia could be a potential mechanism for the increased neurogenesis reported following ischemia.

Reactive Oxygen Species Signaling

One interesting hypothesis of intracellular Zn^{2+} accumulation combined with SD described in the discussion section of Chapter 4 is the possibility for the enhanced generation of reactive oxygen species (ROS). The recovery of fEPSPs was enhanced in the presence of DMSO following Zn/Pyr exposure with SD, and recently it was reported that DMSO has antioxidant properties (Sanmartin-Suarez et al., 2011). As mentioned in the Introduction, Zn^{2+} accumulation into mitochondria can lead to the generation of ROS, likely due to inhibition of the electron transport chain. This effect could account in part for the decreased recovery of fEPSPs seen following Zn/Pyr exposure combined with SD. Interestingly, ROS are not thought to solely be involved in neuronal injury processes. There has been accumulating evidence that ROS can act as a signaling molecule.

Originally, ROS were found to be an important mediator in the formation of LTP in the hippocampus in a series of studies by Eric Klann's group, whereby application of exogenous ROS scavengers or the overexpression of endogenous ROS scavengers greatly decreased LTP formation (Klann, 1998, Klann et al., 1998, Thiels et al., 2000). Following repetitive SDs, a potentiation of fEPSPs was observed, akin to LTP, and this LTP-like effect was observed in the current studies (Chapter 4), as well as in rat (Footitt and Newberry, 1998) and human tissues (Berger et al., 2008). It is not known whether ROS plays a role in this LTP-like effect following SD. In a set of supplementary studies in the presence of DMSO, the LTP-like effect was decreased following repetitive SDs (see Appendix Figure A1). Additionally, in these same supplementary studies, the protective effect (metabolic adaptation) of SD was lost when these slices were subsequently exposed to the Zn/Pyr challenge combined with SD (see Appendix Figure A1). If DMSO is indeed acting as an ROS scavenger, it would seem that ROS not only play a role in the observed LTP-like effect following SD, but can be neuroprotective following SD. Consistent with this idea is the observation that ROS can mediate preconditioning effects to subsequent noxious stimuli, and this preconditioning effect was attenuated by the antioxidant vitamin E (Ravati et al., 2000). Additional studies with widely used antioxidants, such as the vitamin E or its analog trolox, will be useful to confirm the possibility of neuroprotective ROS signaling following SD.

6.7 Differing Effects of Extracellular and Intracellular Zn^{2+}

The development of new therapeutic targets for preventing the spread of ischemic damage is greatly needed, especially if they can be given, and are effective, at time-points

later than the only current FDA approved drug, t-PA. Blocking the occurrence of SD following ischemia is potentially one such target that could have profound effects. These events continuously occur for days following the initial ischemic event and can significantly contribute to the evolution of the ischemic core. However, finding specific blockers for SD has been challenging, and only one such drug has been identified to have some clinical benefit, ketamine (Sakowitz et al., 2009). An adjunct approach would be to target and limit the deleterious consequences following SD. Synaptic Zn^{2+} significantly contributed to ischemic injury in the current study and prompts the question as to whether this source of Zn^{2+} can be selectively targeted following ischemia.

There is a potential for a dual role of synaptic Zn^{2+} following ischemia. In the current study, it was shown to be neurotoxic under ischemic conditions, however, as mentioned above, synaptic Zn^{2+} can limit the occurrence of SDs *in vivo* under normal conditions (Aiba et al., 2012). One hypothesis is that synaptic Zn^{2+} release is beneficial while it remains in the extracellular space, but once it enters the postsynaptic cell it becomes neurotoxic. Therefore, chelating intracellular Zn^{2+} might be more beneficial than chelating either extracellular or all Zn^{2+}. While the extracellular Zn^{2+} chelator CaEDTA has been shown to be neuroprotective, the slow kinetics of the chelator make it so that it may not be able to chelate all extracellular Zn^{2+} released during SD before it can enter postsynaptic cells (see Chapters 2 and 5). Further understanding of the roles of synaptic Zn^{2+} release during SD and ischemia are needed to determine if drugs that can interfere with the activity of ZnT3, or that can selectively chelate intracellular Zn^{2+}, will be better suited to provide protection following ischemia and other disorders involving excess Zn^{2+} accumulation.

Recent experimental and clinical trials using a newly synthesized metal chelator has utilized this approach and had some successful results. This chelator, DP-b99, is a lipophilic chelator that integrates within the plasma membrane with the metal binding domain facing the intracellular compartment (Barkalifa et al., 2009). The affinity is such that it will not affect normal intracellular Zn^{2+} binding, but should help prevent toxic Zn^{2+} surges within the cell that are often seen following ischemia. DP-b99 has been shown to prevent neuronal injury induced by Zn^{2+} in cell culture models (Barkalifa et al., 2009), and has been tested in several phase II clinical trials, some of which have shown beneficial effects on recovery rate within 9hrs of stroke onset (Diener et al., 2008). However, subsequent major clinical trials failed to find any benefit of DP-b99 (Lees et al., 2013). This does not suggest that the concept of chelating intracellular Zn^{2+} is futile, as there may be some issues with using membrane associated chelators following ischemia. Membrane integrity can become disrupted under ischemic conditions and following SD (Tanaka et al., 1999), therefore potentially allowing dissociation and removal of the metal chelator from the membrane. One other confound of the study was that the chelator also bound Ca^{2+}, and could therefore compete with Zn^{2+} chelation, potentially allowing for toxic levels of Zn^{2+} to be attained. Nevertheless, the preliminary results of this chelator are encouraging and the technical aspects of chelating intracellular Zn^{2+} are one the right track. With future developments and research it seems possible to build on these findings and create more effective intracellular Zn^{2+} chelators.

6.8 Critiques of the Current Work

Slice Preparations

The propagation of SD requires the close association of neurons to allow for extracellular levels of K^+ and glutamate to reach threshold and allow for the feed-forward nature of the event. Therefore, studies of SD are restricted to slice (acute or organotypic) or *in vivo* preparations, and cannot be accurately studied in dissociated cell culture models. Slice preparations are extremely useful as experimental conditions can be greatly controlled and manipulated, such as temperature, flow rate, and drug applications. However, it is worth noting that due to the lack of perfusion throughout the slice from the vasculature, the delivery of metabolic substrates (O_2 and glucose) is limited by diffusion and the concentration of these substrates in the superfusate. To compensate for this, slices are usually superfused with high concentrations of glucose (10mM) and saturated with O_2 (typically 95%). These levels are necessary to keep relatively normal neuronal functions within the slice. However, there may be a steep drop off in O_2 levels within slice preparations, despite saturating levels in the superfusate, and this needs to be taken into consideration when interpreting results that may be influenced by O_2 levels.

When trying to assess studies of ischemia in slice, it is technically challenging to reproduce the gradient of ischemia seen *in vivo*. Typically, entire slice preparations are exposed to either hypoxia or OGD to assess the effects of ischemia, which limits the interpretation of the results to either the corresponding hypoxic or ischemic core *in vivo*. A recent study utilized focal applications of OGD solution to try and address this important issue and found that they could create an ischemic core and surrounding penumbra (Richard et al., 2010). This may be an important model to adapt for studying

SD mechanisms in slice preparations in the future. Another important aspect of slice preparations is that the temperatures used for recordings are lower than that *in vivo*. Most studies in the current work was performed at either 32°C or 35°C, lower than the 37°C maintained for *in vivo* preparations. This is typical for *in vitro* slice recordings as slice viability is maintained longer at lower temperatures.

In vivo Preparations

Studies of *in vivo* brain function in healthy and pathological states are critically important for scientific research, as they maintain all aspects of biological function. There are some limitations when using *in vivo* preparations, however, some of which have great impact on aspects of studying SD. Cerebral blood flow measurements seem to be dependent on species, with pronounced hypoperfusion in mice and a transient hyperemia in rats (Ayata et al., 2004). This may be influenced by the craniotomy procedure used, as blood volume responses were more similar in intact skull preparations compared to the exposed cortex (Chang et al., 2010). Both craniotomy techniques (intact skull and open window) were used in Chapter 5, however blood flow measurements were restricted to intact skull preparations to minimize the effects of exposed cortex previously described.

The ability for FluoZin-3, CaEDTA, and Zn^{2+} to permeate the dura was an additional surprise in the current studies. Therefore the technical challenge of removing the dura was absent in the present work. Severe brain swelling can occur following the removal of the dura in mice (personal observation) and requires the use of a closed cranial window setup to preserve intracranial pressure. By leaving the dura intact in the

current studies detailed in Chapter 5, drugs in the superfusate were able to diffuse into the parenchyma, thereby leaving the system intact. The ability of FluoZin-3 to permeate the dura is similar to that of *in vivo* applications of SR101 to label cortical astrocytes (Nimmerjahn et al., 2004), and speculates as to whether other fluorescent dyes can be topically applied to dura intact *in vivo* preparations, in order to reduce not only technical but physiological issues in dura free preparations.

The anesthetic used for *in vivo* procedures may also influence SD. The impact of several anesthetics on the occurrence of SDs has been investigated to test whether they can inhibit or limit SDs to better understand which anesthetics to use for experimental settings and which could have a beneficial impact following neurosurgical procedures (Piper and Lambert, 1996, Kitahara et al., 2001, Kudo et al., 2008, Hertle et al., 2012). In a set of studies that was conducted in parallel with the current work, it was found that SDs can occur in mice under simulated neurosurgical anesthesia commonly used in humans (Carlson et al., 2012). Therefore, when studying mechanisms of SD *in vivo*, it is important to address which anesthetic should be used.

FluoZin-3 Measurements

The fluorescent Zn^{2+} indicator used throughout the current work (FluoZin-3) is only a single wavelength indicator and therefore ratiometric measurements cannot be made. This makes it very difficult to calibrate fluorescence signals and generate exact or estimated Zn^{2+} concentrations. Genetically-encoded ratiometric Zn^{2+} indicators have been developed for use in studying intracellular Zn^{2+} homeostasis in organelles (Miranda et al., 2012). Future development of ratiometric indicators that can be exogenously

applied extracellularly would greatly enhance our understanding of the levels that extracellular Zn^{2+} can reach during SD.

Due to the existence of "contaminating Zn^{2+}" in salt solutions and from plastic tubing (Kay, 2004), an extracellular Zn^{2+} chelator, CaEDTA, was used in the majority of the current studies. CaEDTA greatly reduces background fluorescence of FluoZin-3 to almost autofluorescence levels. This makes reporting signals as $\%\Delta F/F_0$ potentially complicating as after background subtraction, F_0 reaches very small values, potentially leading to an overestimate of fluorescence signals. This was noticed when using two-photon imaging of FluoZin-3 and comparing fluorescence signals acquired from single-photon imaging. FluoZin-3 signals obtained from two-photon imaging were almost 10 times larger than single-photon signals, presumably due to the extremely small background fluorescence of FluoZin-3 from two-photon excitation. As such, it has been suggested that FluoZin-3 measurements be internally calibrated to maximal FluoZin-3 fluorescence intensity with applications of saturating exogenous Zn^{2+} (Kiedrowski, 2011). All FluoZin-3 responses were reported as $\%\Delta F/F_0$ in the current studies to maintain consistency throughout and with previous studies. However, future studies utilizing FluoZin-3 should adopt this as the new standard for reporting fluorescence signals.

6.9 Concluding Remarks

The major findings of the current dissertation studies is that synaptic Zn^{2+} release occurs following SD *in vitro* and *in vivo* and that this source of Zn^{2+} is neurotoxic in the post-ischemic period. While the mechanism(s) of how synaptic Zn^{2+} contributes to

neuronal injury following ischemia remains unclear, several possibilities exist and require further investigation. This could lead to the development of new therapeutics targeting synaptic Zn^{2+} and subsequent actions to potentially provide better outcomes following stroke.

Appendix

Appendix Figure A1

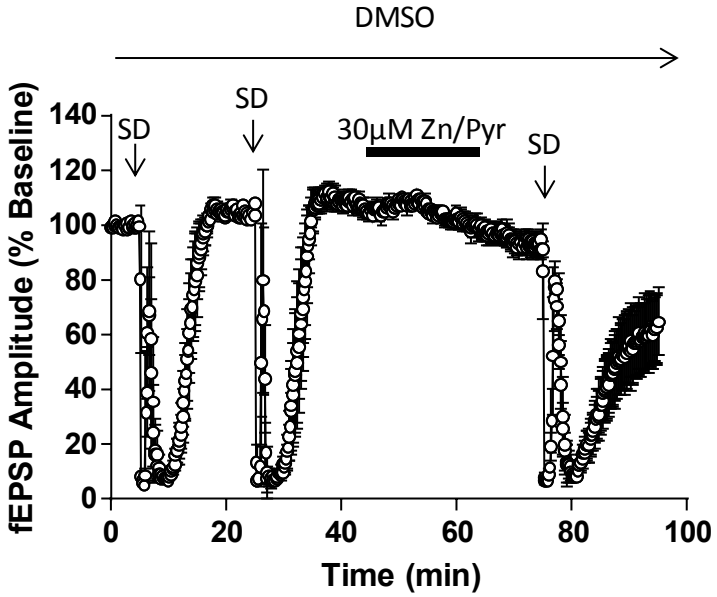

Figure A1: Preconditioning effect of SD lost in the presence of DMSO. Slices were exposed to 2 SDs before loading with 30µM Zn/Pyr exposure (black bar). In the presence of 0.1% DMSO, fEPSPs remained suppressed following a subsequent SD challenge after Zn/Pyr exposure, and the metabolic adaptation effect (see Chapter 4) was lost.

Abbreviations Used

A1R	adenosine A1 receptor
ACSF	artificial cerebral spinal fluid
Ado	adenosine
AIF	apoptosis inducing factor
AMPA	α-amino-3-hydroxy-5-methylisoxazole-4-propionic acid
ATP	adenosine triphosphate
BBB	blood-brain barrier
CA1	Cornu Ammonis 1
CA3	Cornu Ammonis 3
CBF	cerebral blood flow
COSBID	Co-operative study on brain ischemic depolarizations
CNS	central nervous system
CT	computed tomography
DC	direct current
dMCAO	distal middle cerebral artery occlusion
DMSO	dimethyl sulfoxide
DPCPX	8-cyclopentyl-1,3-dipropylxanthine
DPQ	3,4-dihydro-5-[4-(1-piperidinyl)butoxyl]-1(2H)-isoquinolinone
EDTA	ethylenediaminetetraacetic acid
EEG	electroencephalogram
ECoG	electrocorticography
fEPSP	field excitatory post-synaptic potential

GAPDH	glyceraldehyde-3-phosphate dehydrogenase
IOS	intrinsic optical signal
KGDHC	α-ketoglutarate dehydrogenase complex
KO	knockout
LSCI	laser speckle contrast imaging
LTD	long-term depression
LTP	long-term potentiation
mPTP	mitochondrial permeability transition pore
MT	metallothioneins
NMDA	N-methyl-D-aspartic acid
OGD	oxygen/glucose deprivation
PARP-1	poly(ADP-ribose) polymerase 1
PFK	phosphofructokinase
Pyr	pyrithione
SD	spreading depolarization
SEM	standard error of the mean
slm	stratum lacunosum moleculare
so	stratum oriens
sp	stratum pyramidale
sr	stratum radiatum
t-PA	tissue plasminogen activator
TCA cycle	tricarboxylic acid cycle
TPEN	*N,N,N',N'*-tetrakis(2-pyridylmethyl)-ethylenediamine

TSQ	6-methoxy-8-*p*-toluene sulfonamide quinolone
TTC	2,3,5-triphenyltetrazolium chloride
TTX	tetrodotoxin
$[Zn^{2+}]_i$	intracellular Zn^{2+}
Zn/Pyr	$ZnCl_2$ together with pyrithione

References

Adam-Vizi V (2005) Production of reactive oxygen species in brain mitochondria: contribution by electron transport chain and non-electron transport chain sources. Antioxidants & redox signaling 7:1140-1149.

Adlard PA, Parncutt JM, Finkelstein DI, Bush AI (2010) Cognitive loss in zinc transporter-3 knock-out mice: a phenocopy for the synaptic and memory deficits of Alzheimer's disease? J Neurosci 30:1631-1636.

Aiba I, Carlson AP, Sheline CT, Shuttleworth CW (2012) Synaptic release and extracellular actions of Zn2+ limit propagation of spreading depression and related events in vitro and in vivo. Journal of neurophysiology 107:1032-1041.

Aiba I, Shuttleworth CW (2012) Sustained NMDA receptor activation by spreading depolarizations can initiate excitotoxic injury in metabolically compromised neurons. The Journal of physiology 590:5877-5893.

Aizenman E, Stout AK, Hartnett KA, Dineley KE, McLaughlin B, Reynolds IJ (2000) Induction of neuronal apoptosis by thiol oxidation: putative role of intracellular zinc release. Journal of neurochemistry 75:1878-1888.

Andrew RD, Jarvis CR, Obeidat AS (1999) Potential sources of intrinsic optical signals imaged in live brain slices. Methods (San Diego, Calif 18:185-196, 179.

Aoki T, Sumii T, Mori T, Wang X, Lo EH (2002) Blood-brain barrier disruption and matrix metalloproteinase-9 expression during reperfusion injury: mechanical versus embolic focal ischemia in spontaneously hypertensive rats. Stroke; a journal of cerebral circulation 33:2711-2717.

Aras MA, Hara H, Hartnett KA, Kandler K, Aizenman E (2009) Protein kinase C regulation of neuronal zinc signaling mediates survival during preconditioning. Journal of neurochemistry 110:106-117.

Arslan P, Di Virgilio F, Beltrame M, Tsien RY, Pozzan T (1985) Cytosolic Ca2+ homeostasis in Ehrlich and Yoshida carcinomas. A new, membrane-permeant chelator of heavy metals reveals that these ascites tumor cell lines have normal cytosolic free Ca2+. The Journal of biological chemistry 260:2719-2727.

Asahi M, Asahi K, Jung JC, del Zoppo GJ, Fini ME, Lo EH (2000) Role for matrix metalloproteinase 9 after focal cerebral ischemia: effects of gene knockout and enzyme inhibition with BB-94. J Cereb Blood Flow Metab 20:1681-1689.

Assaf SY, Chung SH (1984) Release of endogenous Zn2+ from brain tissue during activity. Nature 308:734-736.

Astrup J, Symon L, Branston NM, Lassen NA (1977) Cortical evoked potential and extracellular K+ and H+ at critical levels of brain ischemia. Stroke; a journal of cerebral circulation 8:51-57.

Attwell D, Buchan AM, Charpak S, Lauritzen M, Macvicar BA, Newman EA (2010) Glial and neuronal control of brain blood flow. Nature 468:232-243.

Ayata C, Shin HK, Salomone S, Ozdemir-Gursoy Y, Boas DA, Dunn AK, Moskowitz MA (2004) Pronounced hypoperfusion during spreading depression in mouse cortex. J Cereb Blood Flow Metab 24:1172-1182.

Back T, Ginsberg MD, Dietrich WD, Watson BD (1996) Induction of spreading depression in the ischemic hemisphere following experimental middle cerebral

artery occlusion: effect on infarct morphology. J Cereb Blood Flow Metab 16:202-213.
Back T, Kohno K, Hossmann KA (1994) Cortical negative DC deflections following middle cerebral artery occlusion and KCl-induced spreading depression: effect on blood flow, tissue oxygenation, and electroencephalogram. J Cereb Blood Flow Metab 14:12-19.
Bai S, Sheline CR, Zhou Y, Sheline CT (2013) A reduced zinc diet or zinc transporter 3 knockout attenuate light induced zinc accumulation and retinal degeneration. Experimental eye research 108:59-67.
Baird AE, Benfield A, Schlaug G, Siewert B, Lovblad KO, Edelman RR, Warach S (1997) Enlargement of human cerebral ischemic lesion volumes measured by diffusion-weighted magnetic resonance imaging. Annals of neurology 41:581-589.
Barkalifa R, Hershfinkel M, Friedman JE, Kozak A, Sekler I (2009) The lipophilic zinc chelator DP-b99 prevents zinc induced neuronal death. European journal of pharmacology 618:15-21.
Berger M, Speckmann EJ, Pape HC, Gorji A (2008) Spreading depression enhances human neocortical excitability in vitro. Cephalalgia : an international journal of headache 28:558-562.
Besser L, Chorin E, Sekler I, Silverman WF, Atkin S, Russell JT, Hershfinkel M (2009) Synaptically released zinc triggers metabotropic signaling via a zinc-sensing receptor in the hippocampus. J Neurosci 29:2890-2901.
Bonanni L, Chachar M, Jover-Mengual T, Li H, Jones A, Yokota H, Ofengeim D, Flannery RJ, Miyawaki T, Cho CH, Polster BM, Pypaert M, Hardwick JM, Sensi SL, Zukin RS, Jonas EA (2006) Zinc-dependent multi-conductance channel activity in mitochondria isolated from ischemic brain. J Neurosci 26:6851-6862.
Branston NM, Strong AJ, Symon L (1977) Extracellular potassium activity, evoked potential and tissue blood flow. Relationships during progressive ischaemia in baboon cerebral cortex. Journal of the neurological sciences 32:305-321.
Brown AM, Kristal BS, Effron MS, Shestopalov AI, Ullucci PA, Sheu KF, Blass JP, Cooper AJ (2000) Zn2+ inhibits alpha-ketoglutarate-stimulated mitochondrial respiration and the isolated alpha-ketoglutarate dehydrogenase complex. The Journal of biological chemistry 275:13441-13447.
Brown CE, Dyck RH (2002) Rapid, experience-dependent changes in levels of synaptic zinc in primary somatosensory cortex of the adult mouse. J Neurosci 22:2617-2625.
Brown CE, Dyck RH (2005) Modulation of synaptic zinc in barrel cortex by whisker stimulation. Neuroscience 134:355-359.
Busch E, Gyngell ML, Eis M, Hoehn-Berlage M, Hossmann KA (1996) Potassium-induced cortical spreading depressions during focal cerebral ischemia in rats: contribution to lesion growth assessed by diffusion-weighted NMR and biochemical imaging. J Cereb Blood Flow Metab 16:1090-1099.
Cai AL, Zipfel GJ, Sheline CT (2006) Zinc neurotoxicity is dependent on intracellular NAD levels and the sirtuin pathway. The European journal of neuroscience 24:2169-2176.

Calderone A, Jover T, Mashiko T, Noh KM, Tanaka H, Bennett MV, Zukin RS (2004) Late calcium EDTA rescues hippocampal CA1 neurons from global ischemia-induced death. J Neurosci 24:9903-9913.
Carlson AP, Carter RE, Shuttleworth CW (2012) Vascular, electrophysiological, and metabolic consequences of cortical spreading depression in a mouse model of simulated neurosurgical conditions. Neurological research 34:223-231.
Carter RE, Aiba I, Dietz RM, Sheline CT, Shuttleworth CW (2011) Spreading depression and related events are significant sources of neuronal Zn2+ release and accumulation. J Cereb Blood Flow Metab 31:1073-1084.
Carter RE, Seidel JL, Lindquist BE, Sheline CT, Shuttleworth CW (2013) Intracellular Zn accumulation enhances suppression of synaptic activity following spreading depolarization. Journal of neurochemistry.
Chang JC, Shook LL, Biag J, Nguyen EN, Toga AW, Charles AC, Brennan KC (2010) Biphasic direct current shift, haemoglobin desaturation and neurovascular uncoupling in cortical spreading depression. Brain 133:996-1012.
Chen ST, Hsu CY, Hogan EL, Maricq H, Balentine JD (1986) A model of focal ischemic stroke in the rat: reproducible extensive cortical infarction. Stroke; a journal of cerebral circulation 17:738-743.
Cheng C, Reynolds IJ (1998) Calcium-sensitive fluorescent dyes can report increases in intracellular free zinc concentration in cultured forebrain neurons. Journal of neurochemistry 71:2401-2410.
Chinopoulos C, Connor JA, Shuttleworth CW (2007) Emergence of a spermine-sensitive, non-inactivating conductance in mature hippocampal CA1 pyramidal neurons upon reduction of extracellular Ca2+: dependence on intracellular Mg2+ and ATP. Neurochem Int 50:148-158.
Choi DW, Koh JY (1998) Zinc and brain injury. Annual review of neuroscience 21:347-375.
Choi DW, Yokoyama M, Koh J (1988) Zinc neurotoxicity in cortical cell culture. Neuroscience 24:67-79.
Chorin E, Vinograd O, Fleidervish I, Gilad D, Herrmann S, Sekler I, Aizenman E, Hershfinkel M (2011) Upregulation of KCC2 Activity by Zinc-Mediated Neurotransmission via the mZnR/GPR39 Receptor. J Neurosci 31:12916-12926.
Cole TB, Martyanova A, Palmiter RD (2001) Removing zinc from synaptic vesicles does not impair spatial learning, memory, or sensorimotor functions in the mouse. Brain research 891:253-265.
Cole TB, Robbins CA, Wenzel HJ, Schwartzkroin PA, Palmiter RD (2000) Seizures and neuronal damage in mice lacking vesicular zinc. Epilepsy research 39:153-169.
Cole TB, Wenzel HJ, Kafer KE, Schwartzkroin PA, Palmiter RD (1999) Elimination of zinc from synaptic vesicles in the intact mouse brain by disruption of the ZnT3 gene. Proceedings of the National Academy of Sciences of the United States of America 96:1716-1721.
Czeh G, Aitken PG, Somjen GG (1992) Whole-cell membrane current and membrane resistance during hypoxic spreading depression. Neuroreport 3:197-200.
D'Amours D, Desnoyers S, D'Silva I, Poirier GG (1999) Poly(ADP-ribosyl)ation reactions in the regulation of nuclear functions. The Biochemical journal 342 (Pt 2):249-268.

Dale N, Frenguelli BG (2009) Release of adenosine and ATP during ischemia and epilepsy. Current neuropharmacology 7:160-179.
Dale N, Pearson T, Frenguelli BG (2000) Direct measurement of adenosine release during hypoxia in the CA1 region of the rat hippocampal slice. The Journal of physiology 526 Pt 1:143-155.
Danscher G, Jo SM, Varea E, Wang Z, Cole TB, Schroder HD (2001) Inhibitory zinc-enriched terminals in mouse spinal cord. Neuroscience 105:941-947.
del Zoppo GJ, Sharp FR, Heiss WD, Albers GW (2011) Heterogeneity in the penumbra. J Cereb Blood Flow Metab 31:1836-1851.
Devinney MJ, 2nd, Reynolds IJ, Dineley KE (2005) Simultaneous detection of intracellular free calcium and zinc using fura-2FF and FluoZin-3. Cell calcium 37:225-232.
Di Cello F, Siddharthan V, Paul-Satyaseela M, Kim KS (2005) Divergent effects of zinc depletion in brain vs non-brain endothelial cells. Biochemical and biophysical research communications 335:373-376.
Diener HC, Schneider D, Lampl Y, Bornstein NM, Kozak A, Rosenberg G (2008) DP-b99, a membrane-activated metal ion chelator, as neuroprotective therapy in ischemic stroke. Stroke; a journal of cerebral circulation 39:1774-1778.
Dietz RM, Weiss JH, Shuttleworth CW (2008) Zn2+ influx is critical for some forms of spreading depression in brain slices. J Neurosci 28:8014-8024.
Dietz RM, Weiss JH, Shuttleworth CW (2009) Contributions of Ca2+ and Zn2+ to spreading depression-like events and neuronal injury. Journal of neurochemistry 109 Suppl 1:145-152.
Dineley KE, Brocard JB, Reynolds IJ (2002) Elevated intracellular zinc and altered proton homeostasis in forebrain neurons. Neuroscience 114:439-449.
Dineley KE, Devinney MJ, 2nd, Zeak JA, Rintoul GL, Reynolds IJ (2008) Glutamate mobilizes [Zn2+] through Ca2+ -dependent reactive oxygen species accumulation. J Neurochem 106:2184-2193.
Dineley KE, Richards LL, Votyakova TV, Reynolds IJ (2005) Zinc causes loss of membrane potential and elevates reactive oxygen species in rat brain mitochondria. Mitochondrion 5:55-65.
Dineley KE, Votyakova TV, Reynolds IJ (2003) Zinc inhibition of cellular energy production: implications for mitochondria and neurodegeneration. J Neurochem 85:563-570.
Dirnagl U, Iadecola C, Moskowitz MA (1999) Pathobiology of ischaemic stroke: an integrated view. Trends in neurosciences 22:391-397.
Dohmen C, Sakowitz OW, Fabricius M, Bosche B, Reithmeier T, Ernestus RI, Brinker G, Dreier JP, Woitzik J, Strong AJ, Graf R (2008) Spreading depolarizations occur in human ischemic stroke with high incidence. Annals of neurology 63:720-728.
Dreier JP (2011) The role of spreading depression, spreading depolarization and spreading ischemia in neurological disease. Nature medicine 17:439-447.
Dunwiddie TV, Masino SA (2001) The role and regulation of adenosine in the central nervous system. Annual review of neuroscience 24:31-55.
Fabricius M, Fuhr S, Bhatia R, Boutelle M, Hashemi P, Strong AJ, Lauritzen M (2006) Cortical spreading depression and peri-infarct depolarization in acutely injured human cerebral cortex. Brain 129:778-790.

Fabricius M, Jensen LH, Lauritzen M (1993) Microdialysis of interstitial amino acids during spreading depression and anoxic depolarization in rat neocortex. Brain research 612:61-69.
Footitt DR, Newberry NR (1998) Cortical spreading depression induces an LTP-like effect in rat neocortex in vitro. Brain research 781:339-342.
Frederickson CJ, Kasarskis EJ, Ringo D, Frederickson RE (1987) A quinoline fluorescence method for visualizing and assaying the histochemically reactive zinc (bouton zinc) in the brain. Journal of neuroscience methods 20:91-103.
Frederickson CJ, Koh JY, Bush AI (2005) The neurobiology of zinc in health and disease. Nature reviews 6:449-462.
Frederickson CJ, Suh SW, Koh JY, Cha YK, Thompson RB, LaBuda CJ, Balaji RV, Cuajungco MP (2002) Depletion of intracellular zinc from neurons by use of an extracellular chelator in vivo and in vitro. J Histochem Cytochem 50:1659-1662.
Frederickson CJ, Suh SW, Silva D, Frederickson CJ, Thompson RB (2000) Importance of zinc in the central nervous system: the zinc-containing neuron. The Journal of nutrition 130:1471S-1483S.
Friedlich AL, Lee JY, van Groen T, Cherny RA, Volitakis I, Cole TB, Palmiter RD, Koh JY, Bush AI (2004) Neuronal zinc exchange with the blood vessel wall promotes cerebral amyloid angiopathy in an animal model of Alzheimer's disease. J Neurosci 24:3453-3459.
Gaither LA, Eide DJ (2001a) Eukaryotic zinc transporters and their regulation. Biometals 14:251-270.
Gaither LA, Eide DJ (2001b) The human ZIP1 transporter mediates zinc uptake in human K562 erythroleukemia cells. The Journal of biological chemistry 276:22258-22264.
Galarreta M, Solis JM, Menendez N, Conejero C, Martin del Rio R (1993) Nicotinamide adenine dinucleotides mimic adenosine inhibition on synaptic transmission by decreasing glutamate release in rat hippocampal slices. Neuroscience letters 159:55-58.
Galasso SL, Dyck RH (2007) The role of zinc in cerebral ischemia. Mol Med 13:380-387.
Gee KR, Zhou ZL, Qian WJ, Kennedy R (2002) Detection and imaging of zinc secretion from pancreatic beta-cells using a new fluorescent zinc indicator. Journal of the American Chemical Society 124:776-778.
Gorter JA, Petrozzino JJ, Aronica EM, Rosenbaum DM, Opitz T, Bennett MV, Connor JA, Zukin RS (1997) Global ischemia induces downregulation of Glur2 mRNA and increases AMPA receptor-mediated Ca2+ influx in hippocampal CA1 neurons of gerbil. J Neurosci 17:6179-6188.
Grafstein B (1956) Mechanism of spreading cortical depression. Journal of neurophysiology 19:154-171.
Grynkiewicz G, Poenie M, Tsien RY (1985) A new generation of Ca2+ indicators with greatly improved fluorescence properties. The Journal of biological chemistry 260:3440-3450.
Gursoy-Ozdemir Y, Qiu JH, Matsuoka N, Bolay H, Bermpohl D, Jin HW, Wang XY, Rosenberg GA, Lo EH, Moskowitz MA (2004) Cortical spreading depression

activates and upregulates MMP-9. Journal of Clinical Investigation 113:1447-1455.
Hadjikhani N, Sanchez Del Rio M, Wu O, Schwartz D, Bakker D, Fischl B, Kwong KK, Cutrer FM, Rosen BR, Tootell RB, Sorensen AG, Moskowitz MA (2001) Mechanisms of migraine aura revealed by functional MRI in human visual cortex. Proc Natl Acad Sci U S A 98:4687-4692.
Halassa MM, Haydon PG (2010) Integrated brain circuits: astrocytic networks modulate neuronal activity and behavior. Annual review of physiology 72:335-355.
Hansen AJ, Zeuthen T (1981) Extracellular ion concentrations during spreading depression and ischemia in the rat brain cortex. Acta physiologica Scandinavica 113:437-445.
Hartings JA, Bullock MR, Okonkwo DO, Murray LS, Murray GD, Fabricius M, Maas AI, Woitzik J, Sakowitz O, Mathern B, Roozenbeek B, Lingsma H, Dreier JP, Puccio AM, Shutter LA, Pahl C, Strong AJ (2011a) Spreading depolarisations and outcome after traumatic brain injury: a prospective observational study. Lancet neurology.
Hartings JA, Rolli ML, Lu XC, Tortella FC (2003) Delayed secondary phase of peri-infarct depolarizations after focal cerebral ischemia: relation to infarct growth and neuroprotection. J Neurosci 23:11602-11610.
Hartings JA, Watanabe T, Bullock MR, Okonkwo DO, Fabricius M, Woitzik J, Dreier JP, Puccio A, Shutter LA, Pahl C, Strong AJ (2011b) Spreading depolarizations have prolonged direct current shifts and are associated with poor outcome in brain trauma. Brain 134:1529-1540.
Haug FM (1967) Electron microscopical localization of the zinc in hippocampal mossy fibre synapses by a modified sulfide silver procedure. Histochemie Histochemistry Histochimie 8:355-368.
Hershfinkel M, Moran A, Grossman N, Sekler I (2001) A zinc-sensing receptor triggers the release of intracellular Ca2+ and regulates ion transport. Proceedings of the National Academy of Sciences of the United States of America 98:11749-11754.
Hertle DN, Dreier JP, Woitzik J, Hartings JA, Bullock R, Okonkwo DO, Shutter LA, Vidgeon S, Strong AJ, Kowoll C, Dohmen C, Diedler J, Veltkamp R, Bruckner T, Unterberg AW, Sakowitz OW (2012) Effect of analgesics and sedatives on the occurrence of spreading depolarizations accompanying acute brain injury. Brain 135:2390-2398.
Higashi Y, Segawa S, Matsuo T, Nakamura S, Kikkawa Y, Nishida K, Nagasawa K (2011) Microglial zinc uptake via zinc transporters induces ATP release and the activation of microglia. Glia 59:1933-1945.
Hossmann KA (1996) Periinfarct depolarizations. Cerebrovascular and brain metabolism reviews 8:195-208.
Howell GA, Welch MG, Frederickson CJ (1984) Stimulation-induced uptake and release of zinc in hippocampal slices. Nature 308:736-738.
Huang YZ, Pan E, Xiong ZQ, McNamara JO (2008) Zinc-mediated transactivation of TrkB potentiates the hippocampal mossy fiber-CA3 pyramid synapse. Neuron 57:546-558.
Hulsmann S, Greiner C, Kohling R, Wolfer J, Moskopp D, Riemann B, Lucke A, Wassmann H, Speckmann EJ (1999) Dimethyl sulfoxide increases latency of

anoxic terminal negativity in hippocampal slices of guinea pig in vitro. Neuroscience letters 261:1-4.
Iijima T, Mies G, Hossmann KA (1992) Repeated negative DC deflections in rat cortex following middle cerebral artery occlusion are abolished by MK-801: effect on volume of ischemic injury. J Cereb Blood Flow Metab 12:727-733.
Ikeda T, Kimura K, Morioka S, Tamaki N (1980) Inhibitory effects of Zn2+ on muscle glycolysis and their reversal by histidine. Journal of nutritional science and vitaminology 26:357-366.
Jiang D, Sullivan PG, Sensi SL, Steward O, Weiss JH (2001) Zn(2+) induces permeability transition pore opening and release of pro-apoptotic peptides from neuronal mitochondria. The Journal of biological chemistry 276:47524-47529.
Johansson B, Halldner L, Dunwiddie TV, Masino SA, Poelchen W, Gimenez-Llort L, Escorihuela RM, Fernandez-Teruel A, Wiesenfeld-Hallin Z, Xu XJ, Hardemark A, Betsholtz C, Herlenius E, Fredholm BB (2001) Hyperalgesia, anxiety, and decreased hypoxic neuroprotection in mice lacking the adenosine A1 receptor. Proceedings of the National Academy of Sciences of the United States of America 98:9407-9412.
Karonen JO, Vanninen RL, Liu Y, Ostergaard L, Kuikka JT, Nuutinen J, Vanninen EJ, Partanen PL, Vainio PA, Korhonen K, Perkio J, Roivainen R, Sivenius J, Aronen HJ (1999) Combined diffusion and perfusion MRI with correlation to single-photon emission CT in acute ischemic stroke. Ischemic penumbra predicts infarct growth. Stroke; a journal of cerebral circulation 30:1583-1590.
Kass IS, Lipton P (1982) Mechanisms involved in irreversible anoxic damage to the in vitro rat hippocampal slice. J Physiol 332:459-472.
Kauppinen TM, Higashi Y, Suh SW, Escartin C, Nagasawa K, Swanson RA (2008) Zinc triggers microglial activation. J Neurosci 28:5827-5835.
Kay AR (2003) Evidence for chelatable zinc in the extracellular space of the hippocampus, but little evidence for synaptic release of Zn. J Neurosci 23:6847-6855.
Kay AR (2004) Detecting and minimizing zinc contamination in physiological solutions. BMC physiology 4:4.
Kerchner GA, Canzoniero LM, Yu SP, Ling C, Choi DW (2000) Zn2+ current is mediated by voltage-gated Ca2+ channels and enhanced by extracellular acidity in mouse cortical neurones. The Journal of physiology 528 Pt 1:39-52.
Kiedrowski L (2011) Cytosolic zinc release and clearance in hippocampal neurons exposed to glutamate--the role of pH and sodium. Journal of neurochemistry 117:231-243.
Kim TY, Hwang JJ, Yun SH, Jung MW, Koh JY (2002) Augmentation by zinc of NMDA receptor-mediated synaptic responses in CA1 of rat hippocampal slices: mediation by Src family tyrosine kinases. Synapse 46:49-56.
Kim YH, Koh JY (2002) The role of NADPH oxidase and neuronal nitric oxide synthase in zinc-induced poly(ADP-ribose) polymerase activation and cell death in cortical culture. Experimental neurology 177:407-418.
Kitahara Y, Taga K, Abe H, Shimoji K (2001) The effects of anesthetics on cortical spreading depression elicitation and c-fos expression in rats. Journal of neurosurgical anesthesiology 13:26-32.

Kitamura Y, Iida Y, Abe J, Mifune M, Kasuya F, Ohta M, Igarashi K, Saito Y, Saji H (2006a) In vivo measurement of presynaptic Zn2+ release during forebrain ischemia in rats. Biological & pharmaceutical bulletin 29:821-823.
Kitamura Y, Iida Y, Abe J, Mifune M, Kasuya F, Ohta M, Igarashi K, Saito Y, Saji H (2006b) Release of vesicular Zn2+ in a rat transient middle cerebral artery occlusion model. Brain research bulletin 69:622-625.
Kitamura Y, Iida Y, Abe J, Ueda M, Mifune M, Kasuya F, Ohta M, Igarashi K, Saito Y, Saji H (2006c) Protective effect of zinc against ischemic neuronal injury in a middle cerebral artery occlusion model. Journal of pharmacological sciences 100:142-148.
Klann E (1998) Cell-permeable scavengers of superoxide prevent long-term potentiation in hippocampal area CA1. Journal of neurophysiology 80:452-457.
Klann E, Roberson ED, Knapp LT, Sweatt JD (1998) A role for superoxide in protein kinase C activation and induction of long-term potentiation. The Journal of biological chemistry 273:4516-4522.
Koh JY, Suh SW, Gwag BJ, He YY, Hsu CY, Choi DW (1996) The role of zinc in selective neuronal death after transient global cerebral ischemia. Science (New York, NY 272:1013-1016.
Koumura A, Hamanaka J, Shimazawa M, Honda A, Tsuruma K, Uchida Y, Hozumi I, Satoh M, Inuzuka T, Hara H (2009) Metallothionein-III knockout mice aggravates the neuronal damage after transient focal cerebral ischemia. Brain research 1292:148-154.
Krotkiewska B, Banas T (1992) Interaction of Zn2+ and Cu2+ ions with glyceraldehyde-3-phosphate dehydrogenase from bovine heart and rabbit muscle. The International journal of biochemistry 24:1501-1505.
Kudo C, Nozari A, Moskowitz MA, Ayata C (2008) The impact of anesthetics and hyperoxia on cortical spreading depression. Experimental neurology 212:201-206.
Kumagai T, Walberer M, Nakamura H, Endepols H, Sue M, Vollmar S, Adib S, Mies G, Yoshimine T, Schroeter M, Graf R (2011) Distinct spatiotemporal patterns of spreading depolarizations during early infarct evolution: evidence from real-time imaging. J Cereb Blood Flow Metab 31:580-592.
Kunkler PE, Hulse RE, Schmitt MW, Nicholson C, Kraig RP (2005) Optical current source density analysis in hippocampal organotypic culture shows that spreading depression occurs with uniquely reversing currents. J Neurosci 25:3952-3961.
Kunkler PE, Kraig RP (2004) P/Q Ca2+ channel blockade stops spreading depression and related pyramidal neuronal Ca2+ rise in hippocampal organ culture. Hippocampus 14:356-367.
Kuraoka M, Furuta T, Matsuwaki T, Omatsu T, Ishii Y, Kyuwa S, Yoshikawa Y (2009) Direct experimental occlusion of the distal middle cerebral artery induces high reproducibility of brain ischemia in mice. Experimental animals / Japanese Association for Laboratory Animal Science 58:19-29.
Lauritzen M, Dreier JP, Fabricius M, Hartings JA, Graf R, Strong AJ (2011) Clinical relevance of cortical spreading depression in neurological disorders: migraine, malignant stroke, subarachnoid and intracranial hemorrhage, and traumatic brain injury. J Cereb Blood Flow Metab 31:17-35.

Lauritzen M, Hansen AJ (1992) The effect of glutamate receptor blockade on anoxic depolarization and cortical spreading depression. J Cereb Blood Flow Metab 12:223-229.
Lauritzen M, Jorgensen MB, Diemer NH, Gjedde A, Hansen AJ (1982) Persistent oligemia of rat cerebral cortex in the wake of spreading depression. Annals of neurology 12:469-474.
Leao AA (1947) Further observations on the spreading depression of activity in the cerebral cortex. Journal of neurophysiology 10:409-414.
Leao AAP (1944a) Pial circulation and spreading depression of activity in the cerebral cortex. Journal of neurophysiology 7:391-396.
Leao AAP (1944b) Spreading depression of activity in the cerebral cortex. J Neurophysiol 7:359-390.
Leao AAP (1944c) Spreading depression of activity in the cerebral cortex. Journal of neurophysiology 7:359-390.
Lee JM, Zipfel GJ, Park KH, He YY, Hsu CY, Choi DW (2002) Zinc translocation accelerates infarction after mild transient focal ischemia. Neuroscience 115:871-878.
Lee JY, Cole TB, Palmiter RD, Koh JY (2000) Accumulation of zinc in degenerating hippocampal neurons of ZnT3-null mice after seizures: evidence against synaptic vesicle origin. J Neurosci 20:RC79.
Lee JY, Kim JS, Byun HR, Palmiter RD, Koh JY (2011) Dependence of the histofluorescently reactive zinc pool on zinc transporter-3 in the normal brain. Brain research 1418:12-22.
Lees KR, Bornstein N, Diener HC, Gorelick PB, Rosenberg G, Shuaib A (2013) Results of Membrane-activated Chelator Stroke Intervention Randomized Trial of DP-b99 in Acute Ischemic Stroke. Stroke; a journal of cerebral circulation 44:580-584.
Leppert D, Leib SL, Grygar C, Miller KM, Schaad UB, Hollander GA (2000) Matrix metalloproteinase (MMP)-8 and MMP-9 in cerebrospinal fluid during bacterial meningitis: association with blood-brain barrier damage and neurological sequelae. Clinical infectious diseases : an official publication of the Infectious Diseases Society of America 31:80-84.
Li J, Niu C, Han S, Zu P, Li H, Xu Q, Fang L (2005) Identification of protein kinase C isoforms involved in cerebral hypoxic preconditioning of mice. Brain research 1060:62-72.
Li Y, Hough CJ, Frederickson CJ, Sarvey JM (2001) Induction of mossy fiber --> Ca3 long-term potentiation requires translocation of synaptically released Zn2+. J Neurosci 21:8015-8025.
Liguz-Lecznar M, Nowicka D, Czupryn A, Skangiel-Kramska J (2005) Dissociation of synaptic zinc level and zinc transporter 3 expression during postnatal development and after sensory deprivation in the barrel cortex of mice. Brain research bulletin 66:106-113.
Lindquist BE, Shuttleworth CW (2012) Adenosine receptor activation is responsible for prolonged depression of synaptic transmission after spreading depolarization in brain slices. Neuroscience 223:365-376.
Lipton P (1999) Ischemic cell death in brain neurons. Physiol Rev 79:1431-1568.

Lloyd-Jones D, Adams R, Carnethon M, De Simone G, Ferguson TB, Flegal K, Ford E, Furie K, Go A, Greenlund K, Haase N, Hailpern S, Ho M, Howard V, Kissela B, Kittner S, Lackland D, Lisabeth L, Marelli A, McDermott M, Meigs J, Mozaffarian D, Nichol G, O'Donnell C, Roger V, Rosamond W, Sacco R, Sorlie P, Stafford R, Steinberger J, Thom T, Wasserthiel-Smoller S, Wong N, Wylie-Rosett J, Hong Y (2009) Heart disease and stroke statistics--2009 update: a report from the American Heart Association Statistics Committee and Stroke Statistics Subcommittee. Circulation 119:480-486.

Lo EH (2008) A new penumbra: transitioning from injury into repair after stroke. Nature medicine 14:497-500.

Lovatt D, Xu Q, Liu W, Takano T, Smith NA, Schnermann J, Tieu K, Nedergaard M (2012) Neuronal adenosine release, and not astrocytic ATP release, mediates feedback inhibition of excitatory activity. Proceedings of the National Academy of Sciences of the United States of America 109:6265-6270.

MacDiarmid CW, Milanick MA, Eide DJ (2002) Biochemical properties of vacuolar zinc transport systems of Saccharomyces cerevisiae. The Journal of biological chemistry 277:39187-39194.

Masino SA, Mesches MH, Bickford PC, Dunwiddie TV (1999) Acute peroxide treatment of rat hippocampal slices induces adenosine-mediated inhibition of excitatory transmission in area CA1. Neuroscience letters 274:91-94.

Maske H (1955) Uber den topchemischen Natchweis von Zink in Ammonshorn vershieder Saugetieve. Naturwissenschaften 42:424.

Matsushima K, Hogan MJ, Hakim AM (1996) Cortical spreading depression protects against subsequent focal cerebral ischemia in rats. J Cereb Blood Flow Metab 16:221-226.

Matsushima K, Schmidt-Kastner R, Hogan MJ, Hakim AM (1998) Cortical spreading depression activates trophic factor expression in neurons and astrocytes and protects against subsequent focal brain ischemia. Brain research 807:47-60.

Medvedeva YV, Lin B, Shuttleworth CW, Weiss JH (2009) Intracellular Zn2+ accumulation contributes to synaptic failure, mitochondrial depolarization, and cell death in an acute slice oxygen-glucose deprivation model of ischemia. J Neurosci 29:1105-1114.

Mies G, Iijima T, Hossmann KA (1993) Correlation between peri-infarct DC shifts and ischaemic neuronal damage in rat. Neuroreport 4:709-711.

Mies G, Paschen W (1984) Regional changes of blood flow, glucose, and ATP content determined on brain sections during a single passage of spreading depression in rat brain cortex. Experimental neurology 84:249-258.

Miranda JG, Weaver AL, Qin Y, Park JG, Stoddard CI, Lin MZ, Palmer AE (2012) New alternately colored FRET sensors for simultaneous monitoring of Zn(2)(+) in multiple cellular locations. PloS one 7:e49371.

Morris GF, Bullock R, Marshall SB, Marmarou A, Maas A, Marshall LF (1999) Failure of the competitive N-methyl-D-aspartate antagonist Selfotel (CGS 19755) in the treatment of severe head injury: results of two phase III clinical trials. The Selfotel Investigators. Journal of neurosurgery 91:737-743.

Nakamura H, Strong AJ, Dohmen C, Sakowitz OW, Vollmar S, Sue M, Kracht L, Hashemi P, Bhatia R, Yoshimine T, Dreier JP, Dunn AK, Graf R (2010)

Spreading depolarizations cycle around and enlarge focal ischaemic brain lesions. Brain 133:1994-2006.
Nakashima AS, Dyck RH (2010) Dynamic, experience-dependent modulation of synaptic zinc within the excitatory synapses of the mouse barrel cortex. Neuroscience 170:1015-1019.
Nedergaard M, Astrup J (1986) Infarct rim: effect of hyperglycemia on direct current potential and [14C]2-deoxyglucose phosphorylation. J Cereb Blood Flow Metab 6:607-615.
Nedergaard M, Hansen AJ (1988) Spreading depression is not associated with neuronal injury in the normal brain. Brain research 449:395-398.
Nimmerjahn A, Kirchhoff F, Kerr JN, Helmchen F (2004) Sulforhodamine 101 as a specific marker of astroglia in the neocortex in vivo. Nature methods 1:31-37.
NINDS Study Group (1997) Intracerebral hemorrhage after intravenous t-PA therapy for ischemic stroke. Stroke 28:2109-2118.
Noh KM, Yokota H, Mashiko T, Castillo PE, Zukin RS, Bennett MV (2005) Blockade of calcium-permeable AMPA receptors protects hippocampal neurons against global ischemia-induced death. Proceedings of the National Academy of Sciences of the United States of America 102:12230-12235.
Nydegger I, Rumschik SM, Zhao J, Kay AR (2012) Evidence for an Extracellular Zinc-Veneer in Rodent Brains from Experiments with Zn-Ionophores and ZnT3 Knockouts. ACS chemical neuroscience 3:761-766.
Obeidat AS, Jarvis CR, Andrew RD (2000) Glutamate does not mediate acute neuronal damage after spreading depression induced by O2/glucose deprivation in the hippocampal slice. J Cereb Blood Flow Metab 20:412-422.
Ohira K (2011) Injury-induced neurogenesis in the mammalian forebrain. Cellular and molecular life sciences : CMLS 68:1645-1656.
Oliveira-Ferreira AI, Milakara D, Alam M, Jorks D, Major S, Hartings JA, Luckl J, Martus P, Graf R, Dohmen C, Bohner G, Woitzik J, Dreier JP (2010) Experimental and preliminary clinical evidence of an ischemic zone with prolonged negative DC shifts surrounded by a normally perfused tissue belt with persistent electrocorticographic depression. J Cereb Blood Flow Metab.
Olivot JM, Mlynash M, Thijs VN, Purushotham A, Kemp S, Lansberg MG, Wechsler L, Gold GE, Bammer R, Marks MP, Albers GW (2009) Geography, structure, and evolution of diffusion and perfusion lesions in Diffusion and perfusion imaging Evaluation For Understanding Stroke Evolution (DEFUSE). Stroke; a journal of cerebral circulation 40:3245-3251.
Palmiter RD, Cole TB, Findley SD (1996a) ZnT-2, a mammalian protein that confers resistance to zinc by facilitating vesicular sequestration. The EMBO journal 15:1784-1791.
Palmiter RD, Cole TB, Quaife CJ, Findley SD (1996b) ZnT-3, a putative transporter of zinc into synaptic vesicles. Proc Natl Acad Sci U S A 93:14934-14939.
Palmiter RD, Findley SD, Whitmore TE, Durnam DM (1992) MT-III, a brain-specific member of the metallothionein gene family. Proceedings of the National Academy of Sciences of the United States of America 89:6333-6337.

Pan E, Zhang XA, Huang Z, Krezel A, Zhao M, Tinberg CE, Lippard SJ, McNamara JO (2011) Vesicular zinc promotes presynaptic and inhibits postsynaptic long-term potentiation of mossy fiber-CA3 synapse. Neuron 71:1116-1126.

Paoletti P, Ascher P, Neyton J (1997) High-affinity zinc inhibition of NMDA NR1-NR2A receptors. J Neurosci 17:5711-5725.

Parsons MW, Barber PA, Chalk J, Darby DG, Rose S, Desmond PM, Gerraty RP, Tress BM, Wright PM, Donnan GA, Davis SM (2002) Diffusion- and perfusion-weighted MRI response to thrombolysis in stroke. Annals of neurology 51:28-37.

Pellegrini-Giampietro DE, Gorter JA, Bennett MV, Zukin RS (1997) The GluR2 (GluR-B) hypothesis: Ca(2+)-permeable AMPA receptors in neurological disorders. Trends in neurosciences 20:464-470.

Petzold GC, Windmuller O, Haack S, Major S, Buchheim K, Megow D, Gabriel S, Lehmann TN, Drenckhahn C, Peters O, Meierkord H, Heinemann U, Dirnagl U, Dreier JP (2005) Increased extracellular K+ concentration reduces the efficacy of N-methyl-D-aspartate receptor antagonists to block spreading depression-like depolarizations and spreading ischemia. Stroke; a journal of cerebral circulation 36:1270-1277.

Pietrobon D (2005) Function and dysfunction of synaptic calcium channels: insights from mouse models. Current opinion in neurobiology 15:257-265.

Piper RD, Lambert GA (1996) Inhalational anesthetics inhibit spreading depression: relevance to migraine. Cephalalgia : an international journal of headache 16:87-92.

Prasad AS (2012) Discovery of human zinc deficiency: 50 years later. J Trace Elem Med Biol 26:66-69.

Prasad AS, Halsted JA, Nadimi M (1961) Syndrome of iron deficiency anemia, hepatosplenomegaly, hypogonadism, dwarfism and geophagia. The American journal of medicine 31:532-546.

Qian J, Noebels JL (2005) Visualization of transmitter release with zinc fluorescence detection at the mouse hippocampal mossy fibre synapse. The Journal of physiology 566:747-758.

Qian J, Noebels JL (2006) Exocytosis of vesicular zinc reveals persistent depression of neurotransmitter release during metabotropic glutamate receptor long-term depression at the hippocampal CA3-CA1 synapse. J Neurosci 26:6089-6095.

Qian J, Xu K, Yoo J, Chen TT, Andrews G, Noebels JL (2011) Knockout of Zn transporters Zip-1 and Zip-3 attenuates seizure-induced CA1 neurodegeneration. J Neurosci 31:97-104.

Ravati A, Ahlemeyer B, Becker A, Krieglstein J (2000) Preconditioning-induced neuroprotection is mediated by reactive oxygen species. Brain research 866:23-32.

Richard MJ, Saleh TM, El Bahh B, Zidichouski JA (2010) A novel method for inducing focal ischemia in vitro. Journal of neuroscience methods 190:20-27.

Rizzoli SO, Betz WJ (2005) Synaptic vesicle pools. Nature reviews 6:57-69.

Rojas MJ, Navas JA, Rector DM (2006) Evoked response potential markers for anesthetic and behavioral states. American journal of physiology Regulatory, integrative and comparative physiology 291:R189-196.

Rosenberg PA, Dichter MA (1989) Extracellular cAMP accumulation and degradation in rat cerebral cortex in dissociated cell culture. J Neurosci 9:2654-2663.
Rothstein JD, Dykes-Hoberg M, Pardo CA, Bristol LA, Jin L, Kuncl RW, Kanai Y, Hediger MA, Wang Y, Schielke JP, Welty DF (1996) Knockout of glutamate transporters reveals a major role for astroglial transport in excitotoxicity and clearance of glutamate. Neuron 16:675-686.
Rudolphi KA, Schubert P, Parkinson FE, Fredholm BB (1992a) Adenosine and brain ischemia. Cerebrovascular and brain metabolism reviews 4:346-369.
Rudolphi KA, Schubert P, Parkinson FE, Fredholm BB (1992b) Neuroprotective role of adenosine in cerebral ischaemia. Trends in pharmacological sciences 13:439-445.
Rumschik SM, Nydegger I, Zhao J, Kay AR (2009) The interplay between inorganic phosphate and amino acids determines zinc solubility in brain slices. Journal of neurochemistry 108:1300-1308.
Sa-Pereira I, Brites D, Brito MA (2012) Neurovascular unit: a focus on pericytes. Molecular neurobiology 45:327-347.
Sakowitz OW, Kiening KL, Krajewski KL, Sarrafzadeh AS, Fabricius M, Strong AJ, Unterberg AW, Dreier JP (2009) Preliminary evidence that ketamine inhibits spreading depolarizations in acute human brain injury. Stroke; a journal of cerebral circulation 40:e519-522.
Sakowitz OW, Santos E, Nagel A, Krajewski KL, Hertle DN, Vajkoczy P, Dreier JP, Unterberg AW, Sarrafzadeh AS (2013) Clusters of spreading depolarizations are associated with disturbed cerebral metabolism in patients with aneurysmal subarachnoid hemorrhage. Stroke; a journal of cerebral circulation 44:220-223.
Salazar G, Craige B, Love R, Kalman D, Faundez V (2005) Vglut1 and ZnT3 co-targeting mechanisms regulate vesicular zinc stores in PC12 cells. Journal of cell science 118:1911-1921.
Sandstead HH, Prasad AS, Schulert AR, Farid Z, Miale A, Jr., Bassilly S, Darby WJ (1967) Human zinc deficiency, endocrine manifestations and response to treatment. The American journal of clinical nutrition 20:422-442.
Sanmartin-Suarez C, Soto-Otero R, Sanchez-Sellero I, Mendez-Alvarez E (2011) Antioxidant properties of dimethyl sulfoxide and its viability as a solvent in the evaluation of neuroprotective antioxidants. Journal of pharmacological and toxicological methods 63:209-215.
Sebastiao AM, de Mendonca A, Moreira T, Ribeiro JA (2001) Activation of synaptic NMDA receptors by action potential-dependent release of transmitter during hypoxia impairs recovery of synaptic transmission on reoxygenation. J Neurosci 21:8564-8571.
Seidel JL, Shuttleworth CW (2011) Contribution of astrocyte glycogen stores to progression of spreading depression and related events in hippocampal slices. Neuroscience 192:295-303.
Selman WR, Lust WD, Pundik S, Zhou Y, Ratcheson RA (2004) Compromised metabolic recovery following spontaneous spreading depression in the penumbra. Brain research 999:167-174.
Sensi SL, Paoletti P, Bush AI, Sekler I (2009) Zinc in the physiology and pathology of the CNS. Nature reviews 10:780-791.

Sensi SL, Paoletti P, Koh JY, Aizenman E, Bush AI, Hershfinkel M (2011) The Neurophysiology and Pathology of Brain Zinc. J Neurosci 31:16076-16085.
Sensi SL, Yin HZ, Carriedo SG, Rao SS, Weiss JH (1999) Preferential Zn2+ influx through Ca2+-permeable AMPA/kainate channels triggers prolonged mitochondrial superoxide production. Proc Natl Acad Sci U S A 96:2414-2419.
Sensi SL, Yin HZ, Weiss JH (2000) AMPA/kainate receptor-triggered Zn2+ entry into cortical neurons induces mitochondrial Zn2+ uptake and persistent mitochondrial dysfunction. The European journal of neuroscience 12:3813-3818.
Seo SR, Chong SA, Lee SI, Sung JY, Ahn YS, Chung KC, Seo JT (2001) Zn2+-induced ERK activation mediated by reactive oxygen species causes cell death in differentiated PC12 cells. Journal of neurochemistry 78:600-610.
Sharpley MS, Hirst J (2006) The inhibition of mitochondrial complex I (NADH:ubiquinone oxidoreductase) by Zn2+. The Journal of biological chemistry 281:34803-34809.
Sheline CT, Behrens MM, Choi DW (2000) Zinc-induced cortical neuronal death: contribution of energy failure attributable to loss of NAD(+) and inhibition of glycolysis. J Neurosci 20:3139-3146.
Sheline CT, Ying HS, Ling CS, Canzoniero LM, Choi DW (2002) Depolarization-induced 65zinc influx into cultured cortical neurons. Neurobiology of disease 10:41-53.
Shinohara M, Dollinger B, Brown G, Rapoport S, Sokoloff L (1979) Cerebral glucose utilization: local changes during and after recovery from spreading cortical depression. Science (New York, NY 203:188-190.
Shuttleworth CW, Brennan AM, Connor JA (2003) NAD(P)H fluorescence imaging of postsynaptic neuronal activation in murine hippocampal slices. J Neurosci 23:3196-3208.
Shuttleworth CW, Weiss JH (2011) Zinc: new clues to diverse roles in brain ischemia. Trends in pharmacological sciences 32:480-486.
Sick TJ, Solow EL, Roberts EL, Jr. (1987) Extracellular potassium ion activity and electrophysiology in the hippocampal slice: paradoxical recovery of synaptic transmission during anoxia. Brain research 418:227-234.
Sivaswamy S, Neafsey EJ, Collins MA (2010) Neuroprotective preconditioning of rat brain cultures with ethanol: potential transduction by PKC isoforms and focal adhesion kinase upstream of increases in effector heat shock proteins. The European journal of neuroscience 32:1800-1812.
Sloviter RS (1985) A selective loss of hippocampal mossy fiber Timm stain accompanies granule cell seizure activity induced by perforant path stimulation. Brain research 330:150-153.
Smidt K, Rungby J (2012) ZnT3: a zinc transporter active in several organs. Biometals 25:1-8.
Somjen GG (2001) Mechanisms of spreading depression and hypoxic spreading depression-like depolarization. Physiological reviews 81:1065-1096.
Somjen GG, Aitken PG, Czeh GL, Herreras O, Jing J, Young JN (1992) Mechanism of spreading depression: a review of recent findings and a hypothesis. Canadian journal of physiology and pharmacology 70 Suppl:S248-254.

Stork CJ, Li YV (2006) Intracellular zinc elevation measured with a "calcium-specific" indicator during ischemia and reperfusion in rat hippocampus: a question on calcium overload. J Neurosci 26:10430-10437.
Stork CJ, Li YV (2009) Rising zinc: a significant cause of ischemic neuronal death in the CA1 region of rat hippocampus. J Cereb Blood Flow Metab.
Strong AJ, Fabricius M, Boutelle MG, Hibbins SJ, Hopwood SE, Jones R, Parkin MC, Lauritzen M (2002) Spreading and synchronous depressions of cortical activity in acutely injured human brain. Stroke; a journal of cerebral circulation 33:2738-2743.
Strong AJ, Hartings JA, Dreier JP (2007) Cortical spreading depression: an adverse but treatable factor in intensive care? Current opinion in critical care 13:126-133.
Strong AJ, Smith SE, Whittington DJ, Meldrum BS, Parsons AA, Krupinski J, Hunter AJ, Patel S, Robertson C (2000) Factors influencing the frequency of fluorescence transients as markers of peri-infarct depolarizations in focal cerebral ischemia. Stroke; a journal of cerebral circulation 31:214-222.
Strong AJ, Venables GS, Gibson G (1983) The cortical ischaemic penumbra associated with occlusion of the middle cerebral artery in the cat: 1. Topography of changes in blood flow, potassium ion activity, and EEG. J Cereb Blood Flow Metab 3:86-96.
Suh SW (2009) Detection of zinc translocation into apical dendrite of CA1 pyramidal neuron after electrical stimulation. J Neurosci Methods 177:1-13.
Suh SW, Fan Y, Hong SM, Liu Z, Matsumori Y, Weinstein PR, Swanson RA, Liu J (2005) Hypoglycemia induces transient neurogenesis and subsequent progenitor cell loss in the rat hippocampus. Diabetes 54:500-509.
Suh SW, Frederickson CJ, Danscher G (2006) Neurotoxic zinc translocation into hippocampal neurons is inhibited by hypothermia and is aggravated by hyperthermia after traumatic brain injury in rats. J Cereb Blood Flow Metab 26:161-169.
Suh SW, Won SJ, Hamby AM, Yoo BH, Fan Y, Sheline CT, Tamano H, Takeda A, Liu J (2009) Decreased brain zinc availability reduces hippocampal neurogenesis in mice and rats. J Cereb Blood Flow Metab 29:1579-1588.
Takano T, Tian GF, Peng W, Lou N, Lovatt D, Hansen AJ, Kasischke KA, Nedergaard M (2007) Cortical spreading depression causes and coincides with tissue hypoxia. Nature neuroscience 10:754-762.
Tanaka E, Yamamoto S, Inokuchi H, Isagai T, Higashi H (1999) Membrane dysfunction induced by in vitro ischemia in rat hippocampal CA1 pyramidal neurons. Journal of neurophysiology 81:1872-1880.
Thiels E, Urban NN, Gonzalez-Burgos GR, Kanterewicz BI, Barrionuevo G, Chu CT, Oury TD, Klann E (2000) Impairment of long-term potentiation and associative memory in mice that overexpress extracellular superoxide dismutase. J Neurosci 20:7631-7639.
Timm F (1958) [Histochemistry of heavy metals; the sulfide-silver procedure]. Deutsche Zeitschrift fur die gesamte gerichtliche Medizin 46:706-711.
Tobiasz C, Nicholson C (1982) Tetrodotoxin resistant propagation and extracellular sodium changes during spreading depression in rat cerebellum. Brain research 241:329-333.

Tottene A, Conti R, Fabbro A, Vecchia D, Shapovalova M, Santello M, van den Maagdenberg AM, Ferrari MD, Pietrobon D (2009) Enhanced excitatory transmission at cortical synapses as the basis for facilitated spreading depression in Ca(v)2.1 knockin migraine mice. Neuron 61:762-773.

Urbach A, Redecker C, Witte OW (2008) Induction of neurogenesis in the adult dentate gyrus by cortical spreading depression. Stroke; a journal of cerebral circulation 39:3064-3072.

Van Harreveld A (1959) Compounds in brain extracts causing spreading depression of cerebral cortical activity and contraction of crustacean muscle. Journal of neurochemistry 3:300-315.

Van Harreveld A (1978) Two mechanisms for spreading depression in the chicken retina. Journal of neurobiology 9:419-431.

Vander Jagt TA, Connor JA, Shuttleworth CW (2008) Localized loss of Ca2+ homeostasis in neuronal dendrites is a downstream consequence of metabolic compromise during extended NMDA exposures. J Neurosci 28:5029-5039.

Vander Jagt TA, Connor JA, Weiss JH, Shuttleworth CW (2009a) Intracellular Zn2+ increases contribute to the progression of excitotoxic Ca2+ increases in apical dendrites of CA1 pyramidal neurons. Neuroscience 159:104-114.

Vander Jagt TA, Connor JA, Weiss JH, Shuttleworth CW (2009b) Intracellular Zn(2+) increases contribute to the progression of excitotoxic Ca(2+) increases in apical dendrites of CA1 pyramidal neurons. Neuroscience 159:104-114.

Villarroya M, Olivares R, Ruiz A, Cano-Abad MF, de Pascual R, Lomax RB, Lopez MG, Mayorgas I, Gandia L, Garcia AG (1999) Voltage inactivation of Ca2+ entry and secretion associated with N- and P/Q-type but not L-type Ca2+ channels of bovine chromaffin cells. The Journal of physiology 516 (Pt 2):421-432.

Wang X, Tsuji K, Lee SR, Ning M, Furie KL, Buchan AM, Lo EH (2004) Mechanisms of hemorrhagic transformation after tissue plasminogen activator reperfusion therapy for ischemic stroke. Stroke; a journal of cerebral circulation 35:2726-2730.

Wei G, Hough CJ, Li Y, Sarvey JM (2004) Characterization of extracellular accumulation of Zn2+ during ischemia and reperfusion of hippocampus slices in rat. Neuroscience 125:867-877.

Weiss JH, Hartley DM, Koh JY, Choi DW (1993) AMPA receptor activation potentiates zinc neurotoxicity. Neuron 10:43-49.

Weiss JH, Sensi SL, Koh JY (2000) Zn(2+): a novel ionic mediator of neural injury in brain disease. Trends in pharmacological sciences 21:395-401.

Woitzik J, Hecht N, Pinczolits A, Sandow N, Major S, Winkler MK, Weber-Carstens S, Dohmen C, Graf R, Strong AJ, Dreier JP, Vajkoczy P (2013) Propagation of cortical spreading depolarization in the human cortex after malignant stroke. Neurology 80:1095-1102.

Xie X, Hider RC, Smart TG (1994) Modulation of GABA-mediated synaptic transmission by endogenous zinc in the immature rat hippocampus in vitro. The Journal of physiology 478 (Pt 1):75-86.

Xiong ZQ, Stringer JL (2000) Sodium pump activity, not glial spatial buffering, clears potassium after epileptiform activity induced in the dentate gyrus. Journal of neurophysiology 83:1443-1451.

Xue JH, Yanamoto H, Nakajo Y, Tohnai N, Nakano Y, Hori T, Iihara K, Miyamoto S (2009) Induced spreading depression evokes cell division of astrocytes in the subpial zone, generating neural precursor-like cells and new immature neurons in the adult cerebral cortex. Stroke; a journal of cerebral circulation 40:e606-613.

Yanamoto H, Hashimoto N, Nagata I, Kikuchi H (1998) Infarct tolerance against temporary focal ischemia following spreading depression in rat brain. Brain research 784:239-249.

Yemisci M, Gursoy-Ozdemir Y, Vural A, Can A, Topalkara K, Dalkara T (2009) Pericyte contraction induced by oxidative-nitrative stress impairs capillary reflow despite successful opening of an occluded cerebral artery. Nature medicine 15:1031-1037.

Yenari MA, Kauppinen TM, Swanson RA (2010) Microglial activation in stroke: therapeutic targets. Neurotherapeutics : the journal of the American Society for Experimental NeuroTherapeutics 7:378-391.

Yin HZ, Sensi SL, Ogoshi F, Weiss JH (2002) Blockade of Ca2+-permeable AMPA/kainate channels decreases oxygen-glucose deprivation-induced Zn2+ accumulation and neuronal loss in hippocampal pyramidal neurons. J Neurosci 22:1273-1279.

Yin HZ, Weiss JH (1995) Zn(2+) permeates Ca(2+) permeable AMPA/kainate channels and triggers selective neural injury. Neuroreport 6:2553-2556.

Yokoyama M, Koh J, Choi DW (1986) Brief exposure to zinc is toxic to cortical neurons. Neuroscience letters 71:351-355.

Zalewski PD, Forbes IJ, Betts WH (1993) Correlation of apoptosis with change in intracellular labile Zn(II) using zinquin [(2-methyl-8-p-toluenesulphonamido-6-quinolyloxy)acetic acid], a new specific fluorescent probe for Zn(II). The Biochemical journal 296 (Pt 2):403-408.

Zhou N, Gordon GR, Feighan D, MacVicar BA (2010a) Transient swelling, acidification, and mitochondrial depolarization occurs in neurons but not astrocytes during spreading depression. Cereb Cortex 20:2614-2624.

Zhou N, Gordon GR, Feighan D, Macvicar BA (2010b) Transient Swelling, Acidification, and Mitochondrial Depolarization Occurs in Neurons but not Astrocytes during Spreading Depression. Cereb Cortex.